MASTER'S THESIS

FORCE DISTRIBUTION AND CONNECTION STRENGTH IN TIMBER LOCK GATES

FINAL REPORT

Author: J.R. van Otterloo
Date: 20 March 2013

TU Delft Delft University of Technology

Source of the right photograph on the front page: Wijma Kampen B.V. (2012a)

Delft University of Technology
Faculty of Civil Engineering and Geosciences
Section of Steel and Timber Structures
CIE5060-09 Graduation Work

Members thesiscommittee

prof. dr. ir. J.W.G. van de Kuilen	(TU Delft, Civil Engineering and Geosciences, GCC / TU München, Holzforschung)
ir. G.J.P. Ravenshorst	(TU Delft, Civil Engineering and Geosciences, GCC)
ir. P. de Vries	(TU Delft, Civil Engineering and Geosciences, GCC)
dr. ir. M.A.N. Hendriks	(TU Delft, Civil Engineering and Geosciences, CM)
ir. V.L. Raadschelders	(Raadschelders Bouwadvies B.V.)

Advisor and wood supplier
Wijma Kampen B.V.

Student

J.R. van Otterloo student number: 1354272

PREFACE

In completion of the Master Civil Engineering at the University of Technology Delft the Master's Thesis "Force distribution and connection strength in timber lock gates" is presented in this report. The report presents research to the calculation en verification of strength of the mortise and tenon joint in timber lock gates. Currently construction companies are not able to verify the joint's strength while in practice the mortise and tenon joint performs well.

In this research many subjects which have my interest came together. Firstly a wooden mitre gate is a beautiful example of traditional craftsmanship in timber. Timber structures in general have much of my interest and for this research this interest came together with the Dutch pride hydraulic engineering. Although the finite element modelling part took more time relative to the other parts than I preferred, all research aspects which I enjoy, such as analytical derivation, carrying out experiments and analysing test results, came forward during the research.

The coming about of this Master's Thesis is firstly thanks to my daily supervisors Geert Ravenshorst and Peter de Vries who supported the research greatly and with which I've had many meetings, of which some took a large amount of time during difficult parts of the research. I am also grateful to the section of Steel and Timber Structures because I could use a workplace at the Stevin II laboratory during a large period of my research work. Working at this office definitely made working more pleasant, sociable and made perseverance of work better possible.

Thirdly I want to thank my other thesiscommittee members Jan-Willem van de Kuilen, Max Hendriks and Vincent Raadschelders for their enthusiasm on the subject and feedback on my work. I want to thank Wijma Kampen B.V. which contributed to the research as well by supplying the wood used for testing and giving much information on - and insight into the construction of wooden mitre gates. Further all persons involved from various companies are thanked.

Fourthly I want to thank my fiancée Santosha for her uninterrupted support during the coming about of this Master's Thesis. I also want to thank my family and friends for their support with special reference to Gerben and Simon with whom I frequently had lunch and who were a great support as well. Finally, but with emphasis, I want to thank God from Whom I received my talents, many blessings and Who belongs all honour, including the honour for this thesis (Luke 2: 14).

J.R. (Jorick) van Otterloo
20 March 2013
Delft

SUMMARY

IMMEDIATE CAUSE OF RESEARCH

Many lock gates in the Netherlands are equipped with mitre gates made of hardwood. These gates are still built with real craftsmanship and according traditional design, perfected during the last hundreds of years. Construction companies are recently obliged by building authorities to prove the structure satisfies safety standards on e.g. strength more extensive than formerly. However, construction companies are not able to prove whether the mortise and tenon joint between the crossbeams and posts in such a wooden mitre gate satisfies strength requirements. Experience from practice reveals no loss or damage in relation with these connections though.

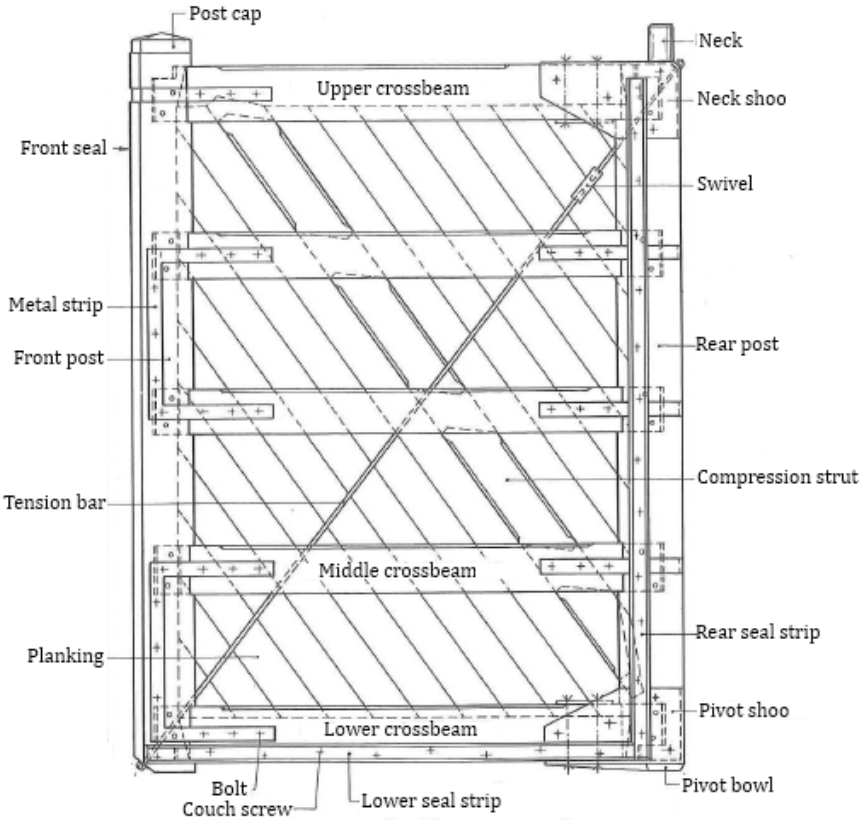

Figure 1: Common design wooden mitre gate with specialist terms (Van Leusen (1991), fig. 52.3)

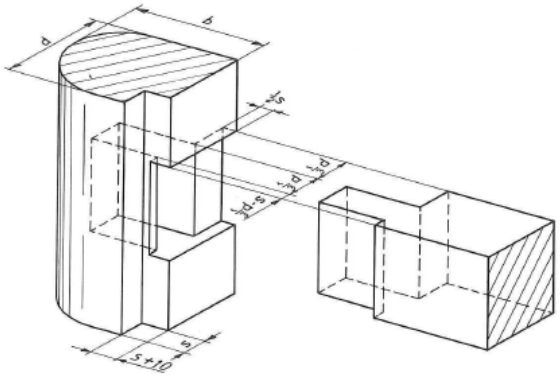

Figure 2: Design mortise and tenon joint (Van Leusen (1991), fig. 63.16)

Calculations on the mortise and tenon joint, common in practice, assume a simple force distribution, as is illustrated in Figure 3. Bending in the crossbeam, caused by water

pressure acting normal to the beam axis, introduces shear stresses in the beam. The shear force at the rear end of the beam is transferred through the tenon to the rear post at the location of the seal strip. Compression in the crossbeam due to the pointing shape of the two doors is transferred through the rear post to the support at the back of the rear post. Note the fibre direction of the crossbeam is set square on the fibre direction of the post and seal strip. How the load is actually transferred through the joint is unknown up to now though.

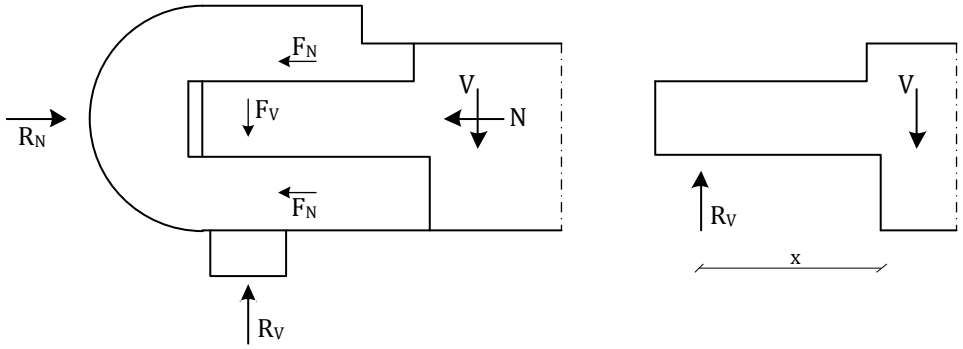

Figure 3: Commonly assumed force distribution within mortise and tenon joint

To take into account spitting at the pit of the tenon calculation rules for notched beams from paragraph 6.5.2 from Eurocode 5 (NEN-EN 1995-1-1, 2005) are often used by construction companies. According this standard the maximum shear stress in a notch needs to be compared with a reduced shear strength:

$$\tau_d = \frac{1.5V}{bh_{ef}} \leq k_v f_{v,d}$$

where

$$k_v = \frac{k_n\left(1 + \frac{1.1i^{1.5}}{\sqrt{h}}\right)}{\sqrt{h}\left(\sqrt{\alpha(1-\alpha)} + 0.8\frac{x}{h}\sqrt{\frac{1}{\alpha} - \alpha^2}\right)},$$

k_n depends on the wood product: LVL, solid timber or glued laminated timber , $\alpha = h_{ef}/h$ and other variables are depicted in Figure 28.

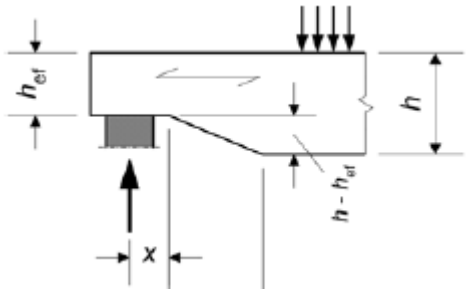

Figure 4: Variables notch strength formula EC5 (NEN-EN 1995-1-1 (2005), Figure 6.11)

The unity check for the mortise and tenon joint, designed according traditional design and where h_{eff} is taken to be equal to the height of the tenon, often returns values several times higher than 1.0. To make it possible for construction companies to satisfy building authorities' demands the mortise and tenon joint's strength needs to be researched.

RESEARCH SPECIFICATION

The main goal of this thesis is to obtain the strength of the mortise and tenon joint in a mitre gate made of hardwood and to provide means to calculate this strength in practice in order to keep traditional wooden mitre gates competitive to the use of other materials.

From the main goal the following main questions are formulated:

- How are the forces distributed in a mortise and tenon joint in a hardwood mitre gate and does this connection satisfy the demands from standards and regulations?
- Can the strength of a tenon be expressed in a formula and do the calculation rules for the strength of a notch from Eurocode 5 have to be supplemented for hardwoods?

Literature is studied to investigate common design and building practice of wooden mitre gates and the background of calculation rules from standards. Finite element modelling is applied to investigate the force distribution in a wooden mitre gate and its mortise and tenon joint. Notch and tenon strength for soft- and hardwoods is researched analytically after which finally an experimental program is set up to judge the result of the analytical research on notch and tenon strength.

PERFORMED RESEARCH

The remarkable case of the mortise and tenon joint not fulfiling the ultimate limit state can be addressed to three main issues of the calculation: the assumed force distribution, material properties of hardwood and use of the calculation rules for notched beams from Eurocode 5. These three main issues return in two main parts of this research: the force distribution within the mortise and tenon joint and the strength of tenonned Azobé beams.

Part on the force distribution within the mortise and tenon joint

Calculations common in practice assume a simple force distribution as is explained above. However, the specific geometry of the joint including its specific supports and its loading by compression, shear force and bending moment, make that a very different load transfer could actually occur.

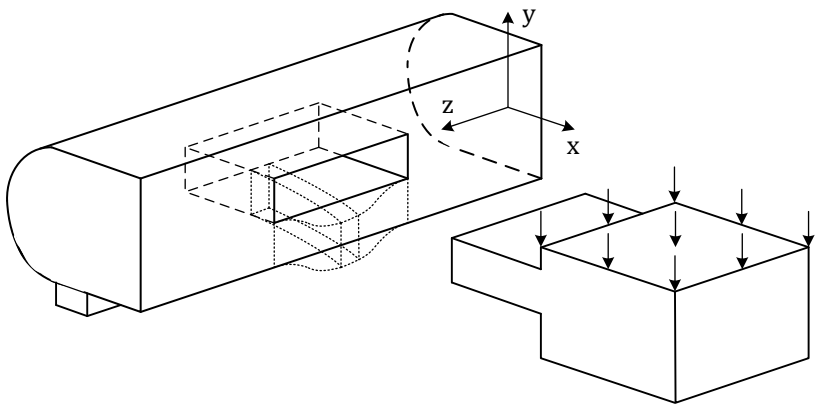

Figure 5: Exploded 3D view of a simplified mortise and tenon joint including magnified deformations. Note the fibre direction of the rear post and seal strip runs along the z-axis and the fibre direction of the crossbeam runs along the x-axis.

As deformation of the mortise in the rear post in Figure 5 indicates, applied forces from the crossbeam can be transferred in two directions. Firstly, the load can be transferred in the x-direction until its line of action meets the line of action of the support at the seal strip. In the x-direction the stiffness of the rear post is relatively low and therefore, when the analysis is restricted to the x-y plane, most of the load is transferred through the tenon until the support's line of action is reached.

Secondly, the load can be transferred in the relatively stiff z-direction after which the forces need to be transferred to the seal strip support within the full section of the rear post next to the mortise. An important condition for the load to be transferred along this route is that the rear post needs to resist rotation to make it possible for the applied force, when it is first transferred in the z-direction to the full-section rear post, to shift along the x-axis to the seal strip support. In fact, a negative moment needs to develop in the rear post if the line of action of the reaction force on the tenon would move in the positive x-direction. As a large compression force is present in the crossbeam and friction at the back of the rear post can develop, the rear post could be considered to be clamped for a certain amount. Note that next to the mortise the full section of the rear post is very stiff. Figure 6 illustrates the mentioned phenomenon.

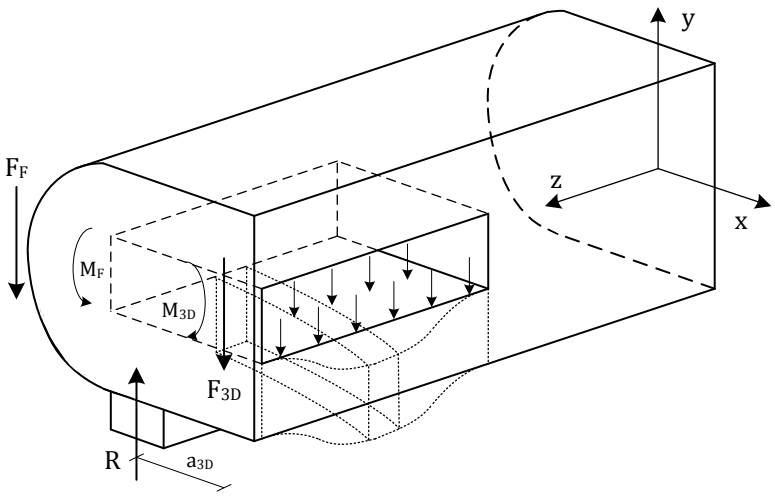

Figure 6: A negative moment in the rear post must develop when (a part of) the shear force from the crossbeam is not transferred from the tenon to the rear post at the line of action of the seal strip support

Using finite element modelling the force distribution is researched in detail using a 2D FE-model. The 3D effect is taken into account by adding an elastic support to the lower part of the rear post. Conclusions on the results are presented further on within this summary.

Part on the strength of tenonned Azobé beams
The Eurocode 5 expression for the strength of notched beams is used today for the calculation of the strength of the mortise and tenon joint. Without further notice this seems reasonable since the indicative failure mechanism for notched beams, splitting of the wood at the pit of the notch, is indicative for tenonned beams too.

The theoretical basic expression for notched beams (TEN) is derived by Gustafsson (1988):

$$\frac{V_f}{b\alpha d} = \frac{\sqrt{\frac{G_{f,y}}{d}}}{\sqrt{\frac{0.6(\alpha-\alpha^2)}{G_{xy}}} + \beta\sqrt{\frac{6\left(\frac{1}{\alpha}-\alpha^2\right)}{E_x}}}$$

where b is the width of the beam, $G_{f,y}$ is the fracture energy in pure tensile spitting perpendicular to the grain (mode 1), G_{xy} is the shear modulus and E_x is the modulus of elasticity parallel to the grain. In Figure 7 α, β and d are indicated.

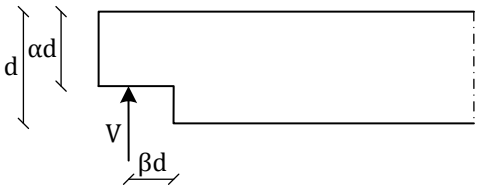

Figure 7: Variables notched beam

In TEN the influence of notch geometry on stresses and strains near the transition from tenon to beam is included. To obtain the expression given by Eurocode 5, the expression is reformulated and material parameters for softwood are included. Therefore the Eurocode 5 expression for the strength of notched beams assumes the considered beam is notched and the wood species used is softwood.

For tenonned beams a theoretical basic expression for tenonned beams (TET) is derived within this research:

$$\frac{V_f}{\mathrm{b}\alpha\mathrm{d}} = \sqrt{2}\sqrt{\frac{G_{f,y}}{b\alpha^2 d\left(\frac{1.2\left(\frac{1}{b\alpha}-\frac{1}{b}\right)}{G} + 2c\beta d^2 + \frac{12\beta^2\left(\frac{1}{\alpha^3}-1\right)}{Eb}\right)}}$$

where V_f [N] is the shear force, b [m] is the width of the beam, $G_{f,y}$ [N/m] is the fracture energy in pure tensile spitting perpendicular to the grain, G_{xy} [N/m²] is the shear modulus and E_x [N/m²] is the modulus of elasticity parallel to the grain. In Figure 8 α [-], β [-] and d [m] are indicated.

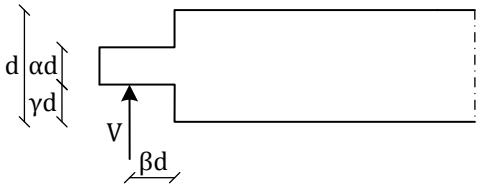

Figure 8: Variables tenonned beam

The fracture energy for softwoods is researched extensively by Larsen and Gustaffson (1990). A similar research project has not (yet) been performed for hardwood. In fact, very little, to nothing, is known about the fracture energy of hardwoods. Therefore several expressions are assumed for the determination of the fracture energy of hardwoods:

- The regression line found by Larsen and Gustaffson (1990) for European softwoods;
- An approximation of the fracture energy of softwoods by Larsen and Gustafsson (1992);
- An expression for the fracture energy of Azobé modeled using test results.

All three equations TEN, TET and the Eurocode 5 expression are compared with test results from two experimental programs. Conclusions on this analysis are presented further on within this summary.

CONCLUSIONS AND RECOMMENDATIONS

For a wooden mitre gate designed according traditional design the most important conclusions relating to the force distribution in the mortise and tenon joint are:

- The shear force from the crossbeam is transferred to the rear post for the largest part through the tenon. A 3D effect is present in the joint whereby the shear force from the tenon is transferred to the sides of the mortise and is then transferred to the seal strip via the full section of the rear post.

- Due to the 3D effect the line of action of the reaction force on the tenon lies closer to the pit of the tenon than the line of action of the reaction force at the seal strip support does. Therefore a negative moment is present in the rear post which is counteracted by a frictional force at the back of the rear post.

- Appearing stresses throughout the joint satisfy design strength values.

For notched and tenonned beams the following conclusions relating to today's standards can be made:

- The Eurocode 5 expression for the strength of notched beams, given in paragraph 6.5.2 from NEN-EN 1995-1-1 (2005), is specifically derived for notched softwood beams and is not applicable for notched Azobé and tenonned Spruce and Azobé beams. When the expression is yet applied for these beams, conservative results are obtained.

- The shear strength parameter $f_{v,k}$, present in the Eurocode 5 expression for the strength of notched beams, is not related to the strength of notched beams. This strength parameter is added to the expression to obtain a practical unity check, useful for engineers in practice.

For notched and tenonned beams the following conclusions relating to their strength can be made which are subscribed by test results:

- The strength of a notched beam is described by the theoretical basic expression for notched beams (TEN) which is derived by Gustafsson (1988):

$$\frac{V_f}{b\alpha d} = \frac{\sqrt{\frac{G_{f,y}}{d}}}{\sqrt{\frac{0.6(\alpha-\alpha^2)}{G_{xy}} + \beta\sqrt{\frac{6\left(\frac{1}{\alpha}-\alpha^2\right)}{E_x}}}}$$

where V_f [N] is the shear force, b [m] is the width of the beam, $G_{f,y}$ [N/m] is the fracture energy in pure tensile spitting perpendicular to the grain, G_{xy} [N/m²] is the shear modulus and E_x [N/m²] is the modulus of elasticity parallel to the grain. In Figure 9 α [-], β [-] and d [m] are indicated.

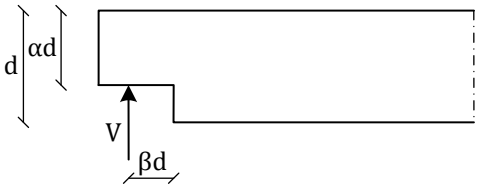

Figure 9: Variables notched beam

- TEN is not applicable to determine the strength of tenonned beams.

- The strength of a tenonned beam is described by the theoretical basic expression for tenonned beams (TET) which is derived within this thesis:

$$\frac{V_f}{b\alpha d} = \sqrt{2}\sqrt{\frac{G_{f,y}}{b\alpha^2 d\left(\frac{1.2\left(\frac{1}{b\alpha}-\frac{1}{b}\right)}{G} + 2c\beta d^2 + \frac{12\beta^2\left(\frac{1}{\alpha^3}-1\right)}{Eb}\right)}}$$

where V_f [N] is the shear force, b [m] is the width of the beam, c is a factor which introduces the influence of the tenon geometry on stresses and strains near the transition from tenon to beam, $G_{f,y}$ [N/m] is the fracture energy in pure tensile spitting perpendicular to the grain, G [N/m²] is the shear modulus and E [N/m²] is the modulus of elasticity parallel to the grain. In Figure 10 α [-], β [-] and d [m] are indicated.

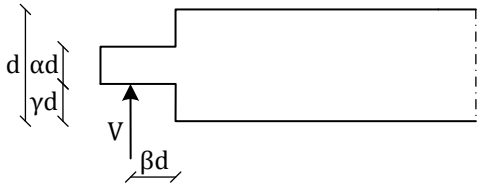

Figure 10: Variables tenonned beam

- The factor *c* depends on α, γ, E and G and introduces the influence of the tenon geometry on stresses and strains near the transition from tenon to beam. For a tenon it is not managed to obtain an analytical expression.

- TET can determine the influence of tenon cantilever length on the strength but the influence of different tenon geometries, present in test results, is not taken into account by TET (yet).

The following recommendations are made for continuation of the research:

- A three dimensional finite element model of the mortise and tenon joint should be built to confirm or adapt the statements on the 3D effect. Preferably different joint designs, other than only the traditional should also be researched.

- As the Eurocode 5 expression is only valid for notched Spruce beams, firstly the paragraph concerned should mention this fact and secondly expressions valid for notched hardwood beams and tenonned softwood and hardwood beams should be derived and added to a standard.

- Performing more tests is an important requirement to confirm the conclusions on the test results on tenonned beams. The test series performed within this research is too small to make definite conclusions. Wood species, tenon geometry and tenon cantilever length should be varied to research tenon strength fully.

- TET, and especially the factor c, should be researched further to obtain a theoretically completely correct expression.

- The fracture energy in pure tensile spitting perpendicular to the grain, in pure parallel splitting to the grain and their combination should be researched for hardwoods.

TABLE OF CONTENTS

1 INTRODUCTION

1.1 OUTLINE OF THE PROBLEM

The rivers and canals in the Netherlands contain a large number of locks. A significant part of these locks contain mitre gates made of wood. These gates are built with real craftsmanship and are still build according traditional design. In contrast to common perception wooden mitre gates are very durable; it is not uncommon for a gate to function well for 40 years in practice. A big advantage is that maintenance costs are low compared with e.g. steel mitre gates.

Wooden mitre gates consist of two vertical members (front and rear post) and horizontal cross members which are covered by planks. Figure 11 gives an impression of a lock gate in function and Figure 12 illustrates a common design for a wooden mitre gate. The crossbeams are connected to the posts by a mortise and tenon joint, depicted in Figure 13.

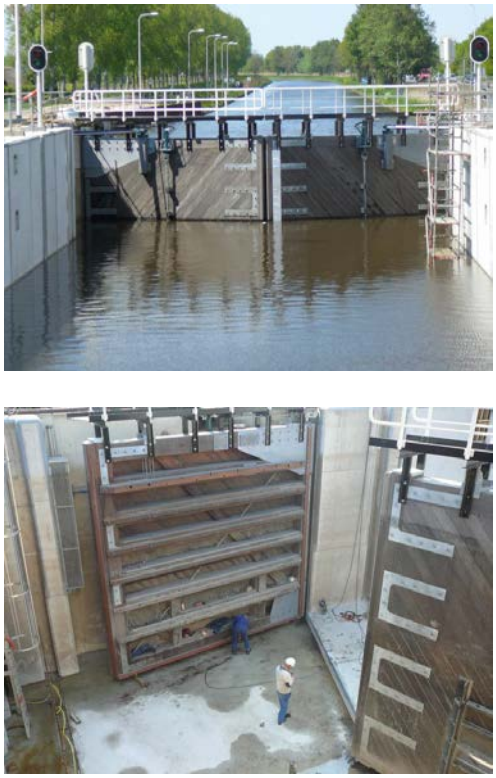

Figure 11: Lock gate Zuid-Willemsvaart (Wijma Kampen B.V., 2012b)

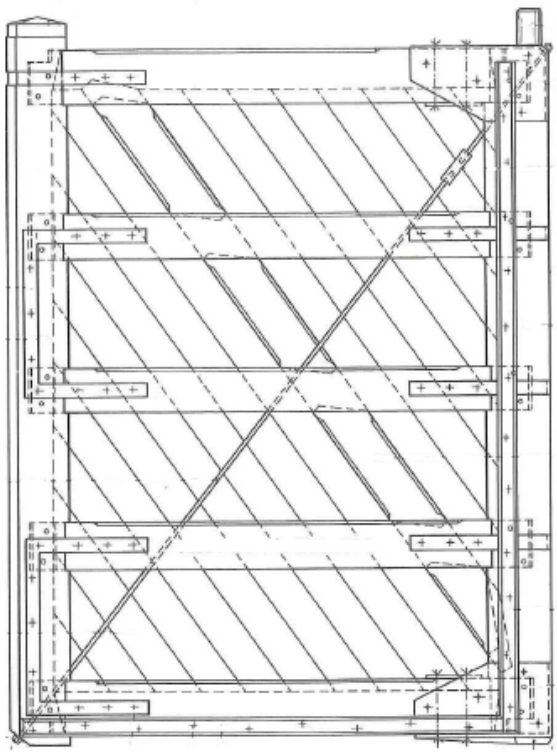

Figure 12: Common design wooden mitre gate (Van Leusen (1991), fig. 52.3)

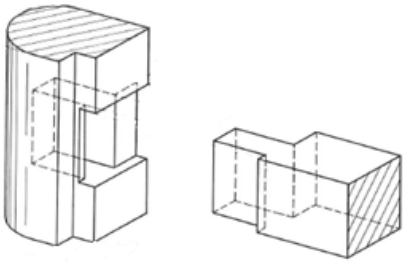

Figure 13: Design mortise and tenon joint (Van Leusen (1991), fig. 63.16)

Recently building authorities imposed construction companies to check more extensively than formerly whether new (to be build) lock gates fulfil the limit states set by the Eurocode.

It turned out that according to the additional calculations the mortise and tenon joint should fail at a much lower load level than which is usual in practice. However in practice the joints perform well, thus obviously there is a flaw in the calculation. Recently a BSc thesis (Vermeij, 2011) was written about the subject which indicated that the calculation rules from Eurocode 5 (NEN-EN 1995-1-1, 2005) are not applicable for this connection. Unfortunately the applied solution in practice often is to adapt the traditional design by changing its geometry or adding steel reinforcement to the connection. The problem is then circumvented instead of dealt with at its root.

Figure 14 illustrates the immediate cause for this master's thesis.

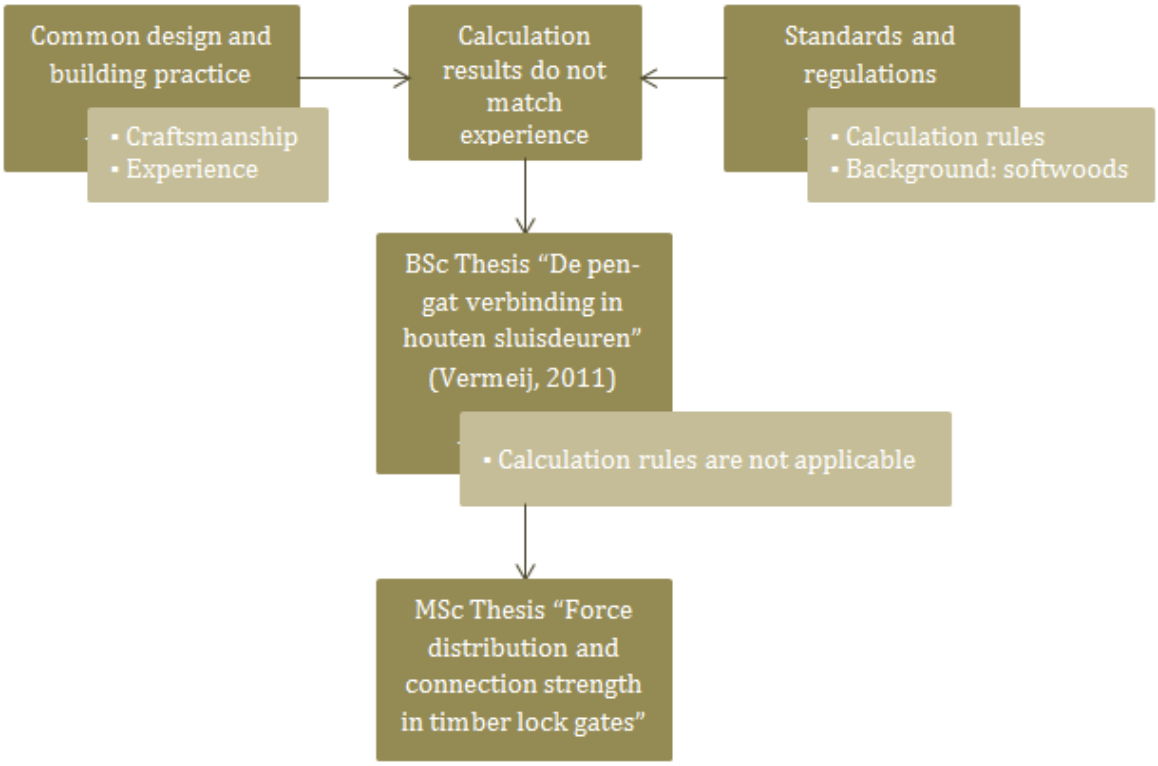

Figure 14: Immediate cause for this master's thesis

An important question following the outline of the problem is why does the traditional design of the mortise and tenon joint not satisfy today's standards while the joint has proven itself the last hundreds of years?

The main goal of this thesis is to obtain the strength of the mortise and tenon joint in a mitre gate of hardwood and to provide means to calculate this strength in practice in order to keep traditional wooden mitre gates competitive to the use of other materials.

1.2 Research questions

For this research the following main questions are formulated:

- How are the forces distributed in a mortise and tenon joint in a hardwood mitre gate and does this connection satisfy the demands from standards and regulations?
- Can the strength of a tenon be expressed in a formula and do the calculation rules for the strength of a notch from Eurocode 5 have to be supplemented for hardwoods?
- Could the connection, based on the research results, be optimized?

From the main questions the following sub questions are formulated:

- What is the actual force distribution in the mortise and tenon joint taking the actual loading into account?
- How can the strength of a mortise and tenon joint be calculated?
- What are the material properties of hardwoods which are indicative for the occurring failure mechanisms of the mortise and tenon joint and for a separate tenon/notch?
- Can a formula be derived that expresses tenon strength depending on the tenon height and length which takes account of the material properties of hardwoods?
- Does the formula for notch strength from Eurocode 5 need to be changed or supplemented for hardwoods based on the material properties obtained by experiments?
- Do the results point to an optimized design for the connection between the crossbeam and posts in a wooden mitre gate?

1.3 Structure of the report

Chapter 2 gives an introduction to the ins and outs of traditional design of wooden mitre gates and which problem construction companies actually face when constructing wooden mitre gates. The main issues concerning the calculation of the mortise and tenon joint are identified and the background of calculation rules concerning notched beams are elaborately explained. In chapter 3 an indicative analytical analysis of the first main issue, the force distribution in a wooden mitre gate and especially within the mortise and tenon joint, is performed and already some characteristics of the finite element model are determined qualitatively. The design and characteristics of the finite element model are explained in chapter 4 and input data for the model is determined quantitatively. Chapter 5 discusses results from the finite element model on the force distribution. In chapter 6 the second main issue is addressed by an analytical analysis of the strength of a tenonned beam, analogue to the derivation of the strength of a notched beam. After in chapter 7 the experimental program is explained in detail, chapter 8 discusses the test results which are compared with formulas derived in chapter 6. In chapter 9 conclusions are drawn and recommendations are made.

2 COMMON DESIGN AND BUILDING PRACTICE

The design and building practice of wooden mitre gates is for a large part based on tradition. Therefore many gates in practice look very alike qua overall design, dimensions and connections. This chapter first describes the traditional design of wooden mitre gates which is still common today. Secondly traditional versus recently imposed calculations verifying the structure's safety are exampled and compared. Subsequently the main issues concerning the calculation of a mortise and tenon joint are identified and discussed. Finally research to the experience with these gates in practice is presented.

Although notch and tenon strength for hardwoods and the indicative material properties in case of splitting, such as the fracture energy perpendicular to the grain, are a subject in itself the immediate cause for this master's thesis are the problems encountered in the calculation of wooden mitre gates. Common design and building practice of these gates therefore give important guidelines to which this thesis should give account for; it determines the framework for this thesis.

2.1 TRADITIONAL DESIGN OF WOODEN MITRE GATES

In previous century's the design and construction of mitre gates made of wood has become a real craftsmanship, using experience to perfect the structure in time. Ing. B. van Leusen describes a mitre gate made of wood as: "Geperfectioneerde, vrijwel volmaakte constructie" (Van Leusen, 1991). Translated to English: "Perfected, nearly ideally structure". Each part of the gate and its connections are thoroughly designed through the years. In fact, as Van Leusen (1991) describes, most dimensions relative to its thickness are about equal for most wooden mitre gates. These dimensions can also be determined by calculations but still they are mostly based on experience due to the fact that loads like a ship-collision are difficult to calculate.

As was mentioned briefly in the introduction, in contrast to common perception wooden mitre gates are very durable; it is not uncommon for a gate to function well for 40 years in practice. This has lots to do with good design and detailing but very importantly also with the wood species used. Further, maintenance costs are low compared with e.g. steel mitre gates. Next to the usual regular normal inspections, during more intensive inspections seal strips and steelwork possibly can be replaced. The main drawback of wooden mitre gates compared to steel mitre gates is that dimensions are restricted. Wooden gates measuring 9 by 12 meters are not uncommon, but they do form an upper limit of size. (Van Leusen, 1991)

Traditionally wooden mitre gates where made of Oak and in most cases treated with a mixture of wood tar and carbolineum. Oak was applied until about 1950-1955 after which a period followed in which also Greenheart was applied. From 1965-1970 Azobé became the main wood species used for wooden mitre gates. Azobé is still mostly used today because of its very good strength and durability properties. (Hakkers, 2012) The main parts of a mitre gate made of wood are: front and rear post, crossbeams, compression strut, shoes and planking. The common design for a wooden mitre gate is illustrated in Figure 15 in which the main parts and specialist terms are indicated. For insiders within the branch special reference is made to Appendix A where the specialist terms considering wooden mitre gates are translated to and from Dutch.

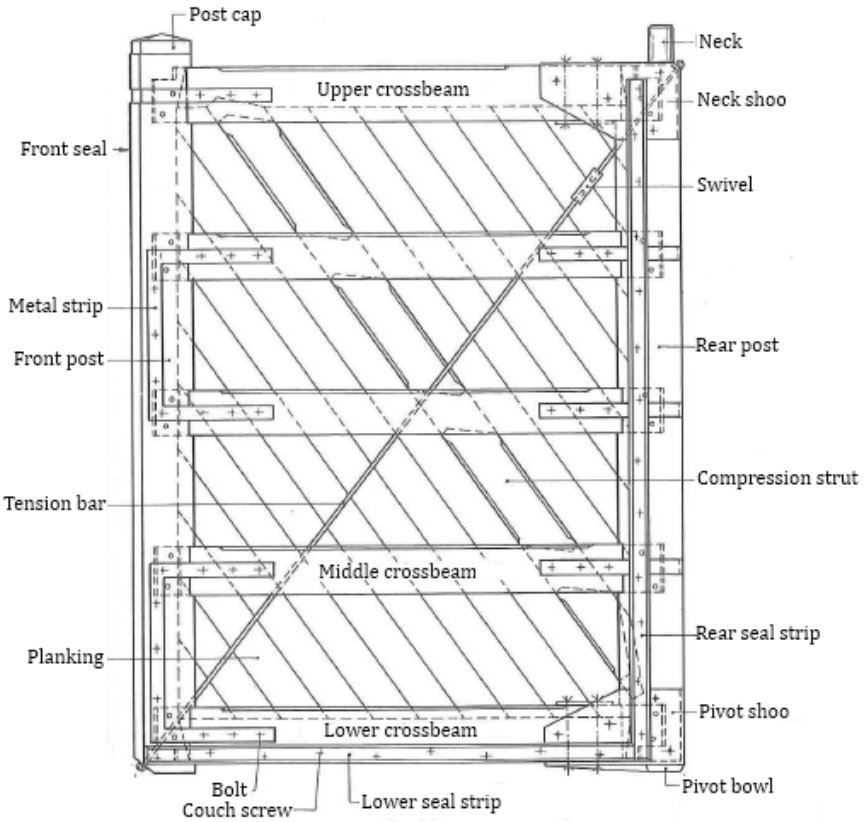

Figure 15: Common design wooden mitre gate with specialist terms (Van Leusen (1991), fig. 52.3)

As in every structure its performance depends largely on the design and construction of the connections. A very important connection in the wooden mitre gate design is the mortise and tenon joint between the crossbeams and the posts. This connection is depicted in Figure 16 and is visible in Figure 15 too. Traditionally its dimensions are based on experience: the tenon depth is one third the depth of the door and its length is two thirds the width of the posts. In the top view it can be seen that the two notches do not have the same length, about 40 mm difference. Traditionally in this way the bearing surface was increased, but it could also be said the 'effective' length of the tenon is decreased.

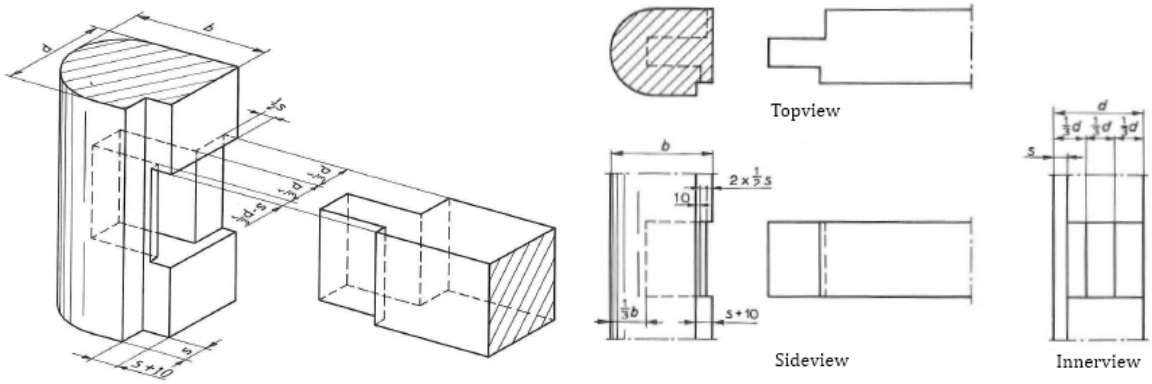

Figure 16: Design mortise and tenon joint (Van Leusen (1991), fig. 63.16 and 63.18)

The doors are still constructed for a large part by hand but using modern tools as is depicted in Figure 17. As Figure 18 depicts the door can be very accurately constructed; dimensions can be very precise and corners very sharp. Actually the tenon depth is always sawn a bit too large; when putting the connection together the tenon is planed so that every tenon fits precisely into the mortise. When constructed the door is slightly tilted upwards on the cantilevering side, 20 to 30 mm difference in diagonals, to counteract sagging through self-

weight and time dependent effects. Therefore the crossbeam is slightly off perpendicular and in height-direction the tenon fits slightly loose, about 2 mm when just constructed. Behind the tenon there is about 20 mm of open space to make sure the crossbeam fits tight to the post as is achieved in Figure 18.

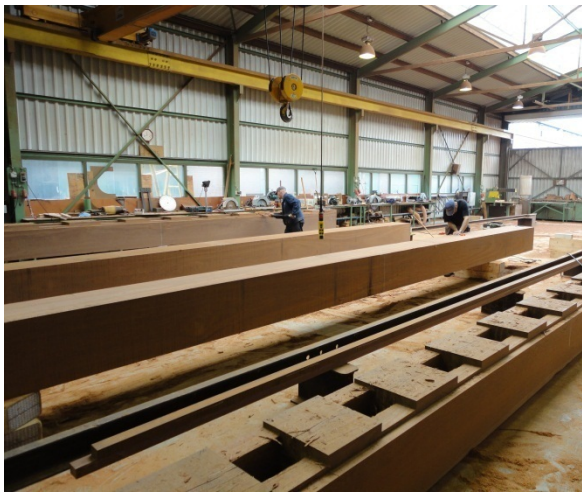

Figure 17: Work done by hand on posts

Figure 18: Tight fitting of the connection

To secure the mortise and tenon joint the tenon is pre-tensioned. As is illustrated in Figure 19, the holes drilled in the post and the tenon are not aligned by about 3 mm for a dowel of about Ø40 mm. At this stage the crossbeam cannot be inserted further as the faces of the post and the crossbeam already touch. When inserting the wooden dowel the joint is thus firmly tightened by pre-tensioning the tenon in length direction. Practice shows that this joint remains tight through the years and does not suffer from relaxation or shrinkage much. The wooden dowels are mostly made of Greenheart as radial shrinkage is very low for this wood species. Besides these pre-tensioning stresses and 'normal' stresses due to the loading, additional stresses are not present. Although the door is constructed in a dry workshop the timber still maintains a high moisture content of 30 – 40 % during construction which is about the same for the timber in application. The time from felling the tree to application is too short for the big wooden elements to dry much. However, it is common that drying cracks appear during construction due to drying of the outer layer of the timber elements. (Hakkers, 2012) and (Van Leusen, 1991).

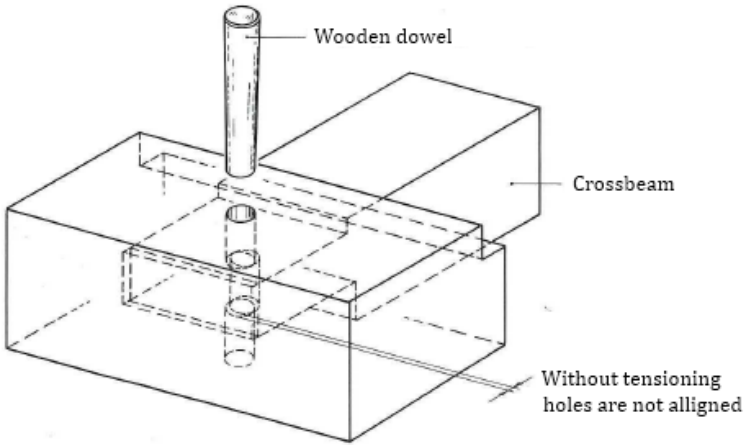

Figure 19: Pre-tensioning mortise and tenon joint (Van Leusen (1991), fig. 63.5)

The compression strut prevents tilting of the door. The angle of the compression strut is designed in such a way that the framed joints in the rear post and upper crossbeam have sufficient space to transmit forces. By connecting the compression strut with the rear post

and the upper crossbeam instead of connecting it with respectively the lower crossbeam and the front post the forces are transmitted to the lock walls through the most direct route. It is preferable to end the shore at the height of the upper pivot to transfer the horizontal component of the force from the compression strut as directly as possible to the upper pivot. The planking is inclined in the same angle as the compression strut. Each plank is preferably one piece and is connected to the following watertight by a half-lap joint glued together.

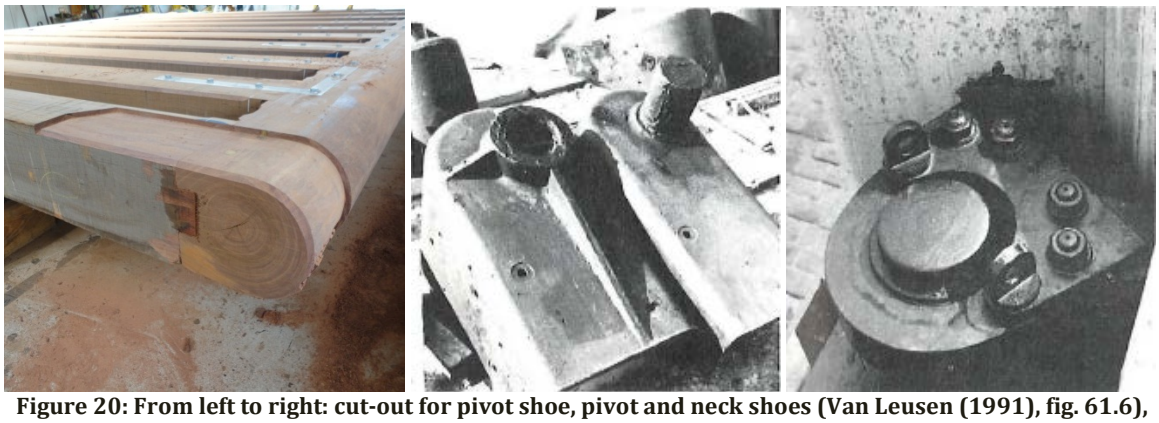

Figure 20: From left to right: cut-out for pivot shoe, pivot and neck shoes (Van Leusen (1991), fig. 61.6), neck and bracket (Van Leusen (1991), fig. 61.8)

The door's pivots are placed at the bottom and top of the rear post as illustrated in Figure 15. Large casted or welded steel shoes are connected with bolts to the rear post and upper or lower crossbeam. The shape of this steel shoe is cut into the post and crossbeam to provide a tight connection. For applications where large water differences will be present the upper pivot is often connected by a bracket which does not fully surround the pivot's neck and the pivot bowl is slightly larger than the pivot. Tolerances can then be somewhat relaxed; when the doors close they can settle under influence of the large loading. The front posts will then fully seal the opening and forces will be transferred entirely to the lock wall via the quoin post instead of partly via the pivots. The lower pivot only carries the dead weight of the door itself and any secondary structures as a gangway. When the door is opened the upper pivot transmits tension forces from the upper crossbeam to the bracket.

The opening is sealed watertight by the front posts (depicted in Figure 21) and seal strips fixed to the lower crossbeam and the rear post. The front posts are pushed firmly together while the seal strips are pressed against the rise in the floor of the lock and against the quoin post at the corner of the door socket (Figure 22). The seal strips are made from relatively soft wood species such as Oak or Douglas to assure good water tightness on the irregular stone surface. Although it is possible to construct the sealing edges very accurately, especially for older gates, leakage may occur; the application allows this to happen though.

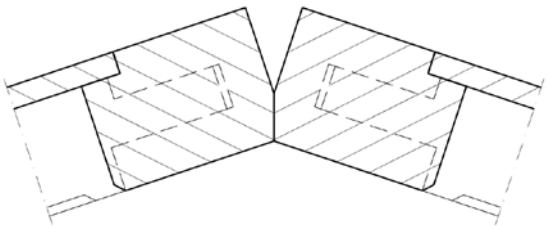

Figure 21: Vertical section of front posts (Adapted from Wijma Kampen B.V. (2012c))

The rise supports the lower crossbeam at the horizontal seal strip. It is made of natural stone or precast concrete blocks or steel and runs over the entire width of the door. The door is supported by the quoin post at the vertical seal strips and at the back of the rear

post. This support is made of natural stone, steel or precast concrete and has a highly worked shape. Usually this shape runs over the entire height of the door. In Figure 22 the quoin post and door are visible during hanging in the door.

Figure 22: Quoin post and door during hanging in the door. (Wijma Kampen B.V. (2012a))

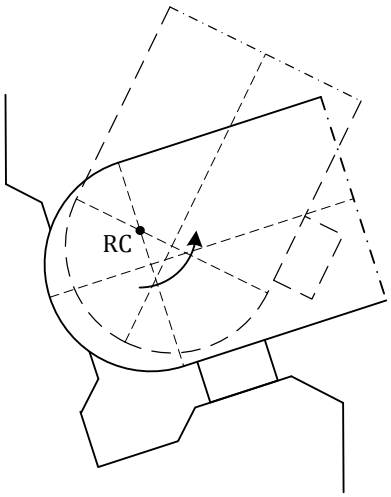

Figure 23: Door rotates clear from concrete wall

Because the seal strip fixed to the rear post and the rear post itself should not scrape against the quoin post the rotation center of the door is not located in the center of the rear post, as can be seen in the middle photograph in Figure 20. In Figure 23 it is illustrated that when the door opens the seal strip and rear post rotate clear from the quoin post when the rotation center is not centered.

Many wooden mitre gates are fitted with a tension bar as is also depicted in Figure 15. It is designed to prevent tilting of the door. By turning the swivel the bar can be tensioned. It is however debatable if such a bar has any function because the shore-action of the compression strut and planking is much greater due to the much larger stiffness of these elements. Although sufficiently thick bars will carry a part of the load, e.g. creep of the connection with the timber may almost certainly reduce this part fast. As tensioning of the bar is dependent on relatively unreliable human intervention it seems safer not to take the tension bar into account. In Figure 15 also metal strips are illustrated, these do not resist forces. They are not capable of doing so but they fix the connections in place.

2.2 Experience from practice with wooden mitre gates

As part of this thesis some research was done to the experiences of regional water authorities and the executive organization of the ministry of transport Rijkswaterstaat with timber lock gates. In the Netherlands the water authorities are among other things responsible for the management of many locks including its gates. All 25 Dutch regional water authorities and Rijkswaterstaat where approached and questioned about the performance of the wooden mitre gates under their management.

It was found that the water authorities which responded manage a total of about 72 locks in which about 270 wooden mitre gates are applied. From these gates it is known that 140 are made from Azobé and 26 gates from Oak. None of the water boards encountered problems with the mortise and tenon joint in all these gates; any loss or damage caused by the mortise and tenon joint was absent.

As will be exampled in the following paragraph, when determining the safety of wooden mitre gates with traditional (relative) dimensions and applying calculation rules from EC5 on the mortise and tenon joint, unity checks larger than 3.0 or 4.0 are not uncommon.

Considering the fact that the regional water authorities report average lifetimes of 30-50 years and that cases of old Oak doors having a lifetime of 60 years are known, there must have been damage or loss caused by failing mortise and tenon joints if the obtained unity checks would be correct.

Visuals inspection find place according protocols (inspection framework 'risicogestuurd inspecteren' from Rijkswaterstaat) for which the exact interpretation differ somewhat per water authority. The protocols aim to control the existing risk and verify that the accepted risk is met. It implies three types of inspections (Banning, 2012):

- Operators and users check the structure daily to prevent immediate danger ('schouw' in Dutch).
- Once or twice a year (depending on the risk) wooden mitre gates are visually inspected to draw up/confirm maintenance routines ('toestandsinspectie' in Dutch), usually according NEN 2767.
- About every 8-15 years the wooden doors are removed and inspected on dry ground. The state of the structure can then be inspected closely and repairs can be performed. During these inspections the seal strips and steel parts can be replaced when needed and possible damage to the wood can be repaired. Also cosmetic repairs of the wood can be carried out.

Reasons for repair or replacement of a gate reported by the water boards are all from the same type: deteriorated wood and/or worn-out steel parts. Namely:

- As the seal strips are made from softer wood species than used for the remainder of the structure, these strips may need to be replaced due to degradation although the structure itself is still in good condition.
- Steel parts like pivots, pivot shoes and sluice valves can be worn out.
- Deterioration of the wood at the water line eventually takes place (Figure 24).
- On top of the crossbeams water and eventually sand and overgrowth gathers. After a period of time the wood will decay. Good drainage and regular cleaning will slow this process considerably though.
- The planking decays at its ends at the posts and upper and lower crossbeams (Figure 25). The end of the planking is susceptible to degradation as the grain is exposed.

It has to be remarked that the first two points can relatively easy be solved when the door is removed for inspection. When the last three points have reached an excessive state it is often the reason to replace the entire door.

Figure 24: Deteriorated wood at the water line of an Oak door. Note that the door is being renovated and some parts are already replaced.

Figure 25: Deteriorated planking of an Oak door (Van Dongen, 2012)

To tackle the problem of the joint failing the unity check according calculations two solutions are applied in practice: firstly the joint is adapted by changing relative dimensions of the mortise and tenon (Figure 26). Then, by employing all calculation possibilities the unity check can be brought to a value below 1.0, as will be illustrated in paragraph 2.3. Secondly the joint can be reinforced with steel brackets or other reinforcing structures (Figure 27). The load is then transferred (according the calculation though) through the steel parts. Unfortunately the problem is thus often circumvented instead of dealt with at its root.

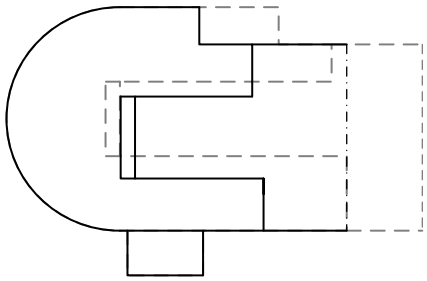

Figure 26: Adapted relative dimensions mortise and tenon joint

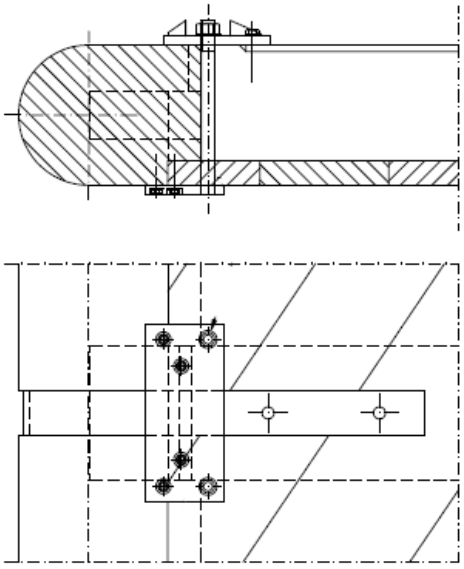

Figure 27: Example of steel reinforcement mortise and tenon joint (Plokkaar, 2012)

From (regular inspections in) practice it is clear the traditional mortise and tenon joint design functions very well. The calculations which result in unity checks several times higher than unity must be incorrect as not a single case of damage or loss is known where the mortise and tenon joint is involved during many decades in which a single gate functions. The need for a proper calculation or strength verification method is therefore obvious.

2.3 TRADITIONAL AND RECENT STRENGTH VERIFICATION

For a lock gate it is very important to know its strength is sufficient and the structure meets safety standards. Especially for gates which have to resist large water level differences and/or are part of the flood defence system. In the past wooden mitre gates were calculated very basically. After hundreds of years of development and application the entire design has proven to be safe. Today every part and connection of the structure has to be checked by calculation to verify its strength and safety. As will be described in the following paragraphs for a mortise and tenon joint in a wooden mitre gate no applicable calculations rules are available. Construction companies therefore run into trouble when building departments demand a complete calculation.

Traditionally most dimensions like the height of the crossbeam or width of the rear post are deduced from the thickness of the door which is determined by experience. During the last decades the crossbeam was checked for bending and the mortise and tenon joint was taken into account sometimes by checking the shear force using the tenon height (thus without any reduction factor to take into account splitting) for loading by water level difference and waves. Because the traditional design takes account of large loads like e.g. a ship-collision the mentioned checks were seldom decisive. Hereby compression in the crossbeam and in the joint due to the pointing shape of the two doors was not taken into account. Further the compression strut and planking were checked for its ultimate limit state where the planks were not taken into account as a strut.

Recently building authorities imposed construction companies to perform more limit state checks. When taking into account compression in the crossbeam, both for combined bending and compression as for compression at the surface of the post, no problems are encountered and unity checks are still below 1.0. However, when applying paragraph 6.5.2 of Eurocode 5 (NEN-EN 1995-1-1, 2005) to consider splitting of the wood at the lower notch of the tenon, the tenon does not fulfil the ultimate limit state. This is very remarkable because from experience from practice, as described in paragraph 2.2, no failures of the mortise and tenon joint are known.

Using the formula for notch strength from Eurocode 5 the maximum shear stress in a notch needs to be checked using a reduced shear strength as is indicated below:

$$\tau_d = \frac{1.5V}{bh_{ef}} \leq k_v f_{v,d}$$

where:

$$k_v = \frac{k_n + [factor\ notch\ \ inclination]}{\sqrt{h}\left(\sqrt{\alpha(1-\alpha)} + 0.8\frac{x}{h}\sqrt{\frac{1}{\alpha} - \alpha^2}\right)},$$

k_n depends on the wood product: LVL, solid timber or glued laminated timber , $\alpha = h_{ef}/h$ and other variables are depicted in Figure 28.

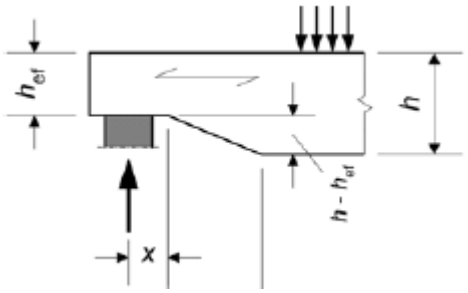

Figure 28: Variables notch strength formula EC5 (NEN-EN 1995-1-1 (2005), Figure 6.11)

When the above formula for notch strength is applied to the mortise and tenon joint in wooden mitre gates in today's practice it is assumed that h_{eff} is equal to the height of the tenon as is described in Ehlbeck and Kromer (1995). The result of this approach is that the ultimate limit state check is not fulfiled in most cases. As mentioned one of the possibilities to satisfy building regulations is to alter relative dimensions of the mortise and tenon joint. In Figure 30 examples of a traditional and adapted design are depicted. Paragraph 2.4.1 examines the background of the notch strength formula, first a simple calculation will illustrate the calculation for two designs.

For the considered designs a distributed load of Q_d = 40 kN/m is assumed. The height of the beam is h = 410 mm and the width is b = 420 mm. The factor k_n is taken as 5 for solid timber. The design shear strength is $f_{v,d} = f_{v,k}\, k_{mod} / \gamma_M$ where k_{mod} = 0.70 (short term loading) and γ_m = 1.3.

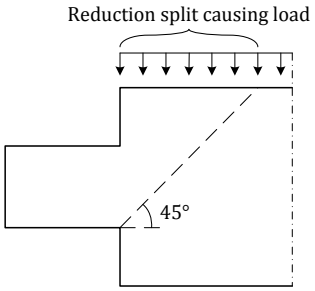

Figure 29: Reduction of the load which causes splitting

Traditional design and calculation

For a beam length of L = 6.25 m the shear force becomes $V_d = ½Q_dL = 125$ kN. Further $h_{eff} = 153$ mm, $\alpha = h_{eff}/h = 0.37$ and x = 250 mm (resultant force left of the middle of the seal strip). Then the reduction factor becomes $k_v = 0.20$.

For strength class D70 the characteristic shear strength is $f_{v,k} = 5$ N/mm² (NEN-EN 338, 2009). Then $f_{v,d} = 2.69$ N/mm².

The occurring shear stress in the tenon is $\tau_d = 2.91$ N/mm². It is remarkable that the design shear strength is already lower than the occurring shear stress without applying the reduction factor.

The unity check becomes: $\tau_d / k_v f_{v,d} = 5.54 >> 1.0$
The unity check becomes very high for the traditional design according a simple calculation.

Adapted design and calculation

The beam length of L = 6.25 m is reduced by 170+120+50 = 340 mm to only take into account the shear force which contributes to splitting. Then the shear force becomes $V_d = ½Q_dL_r = 118$ kN. Further $h_{eff} = 170$ mm, $\alpha = h_{eff}/h = 0.41$ and x = 75 mm (resultant force at the edge of the seal strip). Then the reduction factor becomes $k_v = 0.35$.

Using the results from Van de Kuilen and Blass (2005) the characteristic shear strength is $f_{v,k} = 13.5$ N/mm² . Then $f_{v,d} = 7.27$ N/mm².

The occurring shear stress in the tenon is $\tau_d = 2.48$ N/mm². Then the unity check becomes: $\tau_d / k_v f_{v,d} = 0.98 < 1.0$.
Although the joint passed the strength check it is still remarkable that according the calculation the strength is only just sufficient.

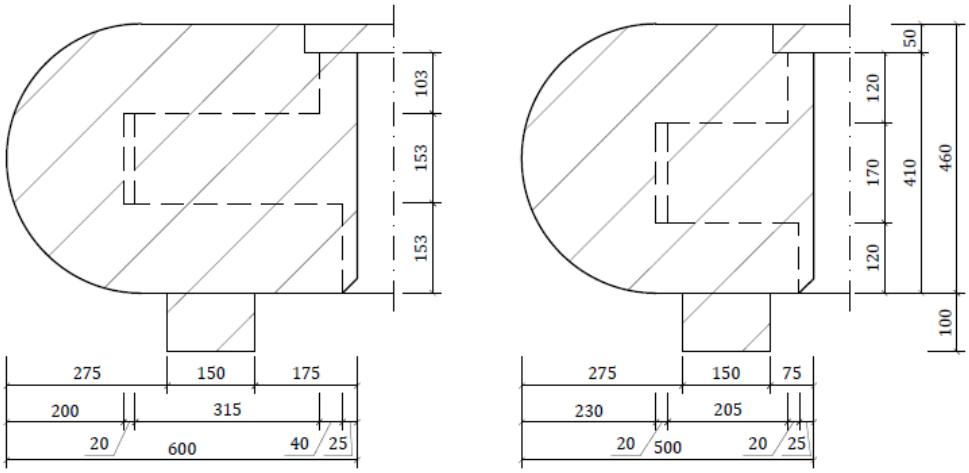

Figure 30: Example of a more traditional (left) and current (right) design mortise and tenon joint (Adapted from Wijma Kampen B.V. (2012c))

2.4 BACKGROUND EC5 EXPRESSION FOR THE STRENGTH REDUCTION OF NOTCHES

It is important to examine the background of the notch strength reduction formula from Eurocode 5 to be able to assess its applicability to hardwood tenonned beams. Gustafsson (1988) derived a theoretical basic expression for the reduced strength of a notched beam by applying linear fracture mechanics. After an extensive testing project to determine the fracture energy perpendicular to the grain of softwoods (Larsen & Gustaffson, 1990) Gustafsson proposed a reduction factor on the shear strength to introduce the splitting failure mechanism. This shear strength check is later introduced in the EC 5.

Starting the derivation Gustafsson (1988) explains that theoretical analysis of crack propagation by developing a maximum stress or strain criterion or by applying Weibull-theory is difficult due to singularity at the crack tip. Gustafsson further explains for normal sized beams and larger the fracture process region is relatively small and therefore when assuming this region concentrated in one point, as is done for linear fracture mechanics, the same results are found as for non-linear fracture mechanics.

2.4.1 DERIVATION THEORETICAL BASIC EXPRESSION FOR NOTCH STRENGTH

According Gustafsson (1988) in the following a theoretical basic expression for the strength of notched beams, as depicted in Figure 31, is derived. Units are indicated between straight brackets [...]. First assumptions are: the material is assumed to be orthotropic and linear elastic. When applying fracture mechanics it is assumed that crack initiation is already present. For this application where rough handling and shrinkage and swelling due moisture differences are to be expected, this assumption is appropriate.

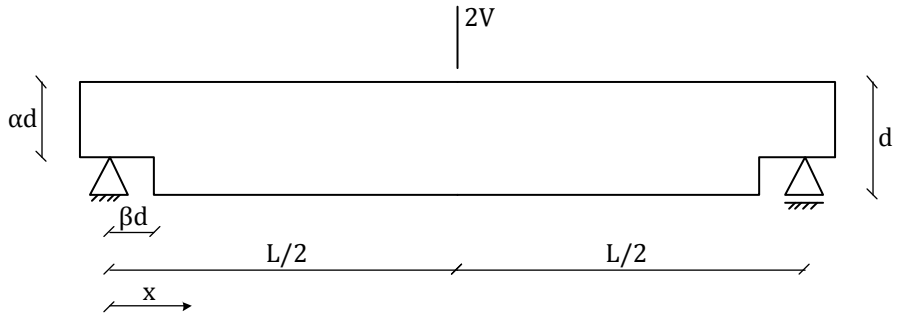

Figure 31: Beam with notched ends

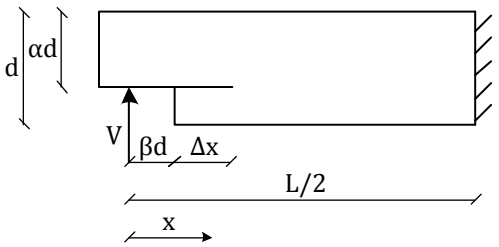

Figure 32: Symmetric half of the notched beam

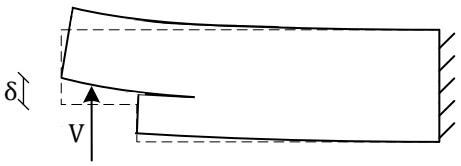

Figure 33: Deflection of a notched beam

From the beam depicted in Figure 31 the symmetric half (Figure 32) is considered. Then, according Figure 33 and Figure 34, the system contains a potential energy [Nm] of:

$$W_p = -\frac{1}{2}V\delta$$

where V [N] is the shear force and δ [m] the deflection at midspan.

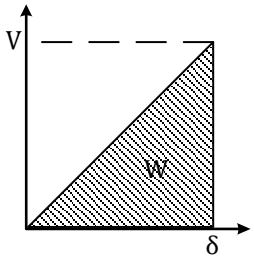

Figure 34: Potential energy for the system

When a crack develops and increases in length with Δx [m] while the shear force V remains constant the potential energy changes with ΔW_p due to the increased deflection $\Delta\delta$:

$$\Delta W_p = -\frac{1}{2}V\Delta\delta = -\frac{1}{2}V^2\Delta\left(\frac{\delta}{V}\right)$$

Next an energy balance can be formed. It is assumed the crack tip is concentrated at one point. Crack development occurs when the loss of potential energy $-\Delta W_p$ due to a shear force V_f equals the energy needed to extend the crack. When G_c [N/m] is noted as the (material dependent) fracture energy per crack area the energy balance then becomes:

$$\frac{1}{2}V_f^2\Delta\left(\frac{\delta}{V}\right) = G_c b\Delta x \qquad [1]$$

where b is de width of the beam and Δx the length of the crack.

The part of the beam below the crack can be considered inactive, therefore an increase of the crack length Δx is equivalent to an increase in length of the notch of $d\Delta\beta$. By inserting this relation into [1], introducing α^2 on both sides of the equation and taking the limit $\Delta\beta \to 0$ it follows that:

$$\left(\frac{V_f}{\alpha}\right)^2 \frac{d\left(\frac{\delta}{V}\right)}{d\beta} = \frac{2G_c bd}{\alpha^2} \quad \rightarrow$$

$$\frac{V_f}{b\alpha d} = \sqrt{\frac{2G_c}{b\alpha^2 d} * \frac{1}{\frac{d\left(\frac{\delta}{V}\right)}{d\beta}}} \qquad [2]$$

The term $\frac{\delta}{V}$ is the compliance of the symmetric half of the beam. To determine the variation of the compliance with β the deflection of the beam needs to be calculated. The beam deflection consists of four terms where the total deflection is equal to the summation of those terms: $\delta_{total} = \delta_l + \delta_v + \delta_r + \delta_b$.

δ_l is the local deformation of the timber at the supports and point of loading. Because δ_l is not dependent on β it does not need to be calculated.

δ_v is the shear deformation of the beam. According linear elastic theory the deflection can be determined by the following equation where the result depends among other variables on β:

$$\delta_v = \frac{1.2V}{G_{xy}}\left[\frac{\beta d}{b\alpha d} + \frac{\frac{l}{2} - \beta d}{bd}\right]$$

where G_{xy} [N/m^2] is the shear modulus.

δ_r is an increase in deflection originating at the transition of the notched part of the beam to the full-size beam. The notch is "clamped" into the full-size beam, but only after some distance from the notch the normal stresses by bending extend over the full height of the beam (Figure 35). Close to the change of cross section the full bending capacity of the full-size beam is therefore not fully activated and some extra deflection develops. It is assumed δ_r varies linearly with both the moment $V\beta d$ and the length of the cantilever βd:

$$\delta_r = V\beta d \cdot c \cdot \beta d = Vc\beta^2 d^2$$

In fact, by this adding the deflection δ_r a fictive moment spring is placed at the discontinuity: multiplying the factor c [(Nm)$^{-1}$] with the moment, causes a rotation, which results in the deflection δ_r when multiplied with the cantilever length. For c the following relation is chosen:

$$c = \frac{12}{b(\alpha d)^2}\sqrt{\frac{(1-\alpha)(1-\alpha^3)}{10G_{xy}E_x}}$$

where E_x [N/m^2] is the modulus of elasticity parallel to the grain.

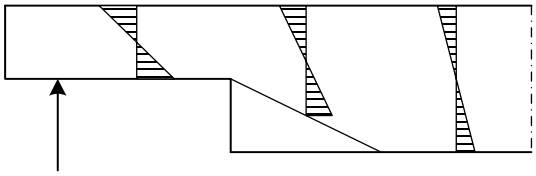

Figure 35: Simplified normal stress distribution notch close to discontinuity

δ_b is the ordinary bending deformation of the beam. According linear elastic theory the following expression can be derived:

$$\delta_b = \frac{V}{E_x \frac{bd^3}{12}}\left[\frac{l^3}{24} + \frac{(\beta d)^3}{3}\left(\frac{1}{\alpha^3} - 1\right)\right]$$

After some rearranging of terms the total beam deflection can be written in the following form:

$$\delta = A(B + \beta d)^3 + C \qquad [3]$$

where C is constant with respect to β,

$$A = \frac{V}{3E_x \frac{bd^3}{12}}\left(\frac{1}{\alpha^3} - 1\right)$$

and

$$B = d\sqrt{\frac{E_x}{10G_{xy}}\frac{\left(\frac{1}{\alpha} - 1\right)}{\left(\frac{1}{\alpha^3} - 1\right)}}$$

Note the expression for the total beam deflection [3] looks similar to the deflection of a cantilevered beam $\frac{PL^3}{3EI}$ where B is the extra deflection caused by shear deformation and additional curvature near the change of cross-section.

As the deflection is now known only the material dependent fracture energy per crack area G_c needs to be defined further. Fracture can occur through different (combined) modes (Figure 36). Two distinctive modes are splitting due to perpendicular tensile stresses called mode 1 and splitting due to shear stresses called mode 2. For a beam for which its notches are on the tension stress side of the beam it is reasonable to assume only mode 1 fracture occurs. Therefore G_c is replaced by the fracture energy in pure tensile spitting perpendicular to the grain $G_{f,y}$ which is also material dependent.

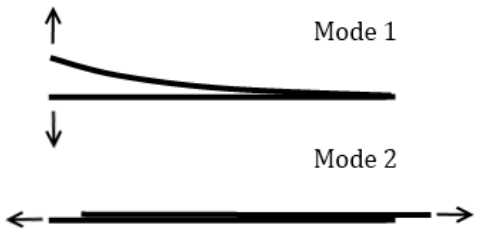

Figure 36: Fracture modes

When equation [3] is differentiated with respect to β the result can be inserted into the energy balance [2]. Replacing the material dependent fracture energy per crack area G_c with fracture energy in pure tensile spitting perpendicular to the grain $G_{f,y}$ then results in the theoretical basic expression for the reduced strength of a notched beam derived by Gustafsson:

$$\frac{V_f}{b\alpha d} = \frac{\sqrt{\frac{G_{f,y}}{d}}}{\sqrt{\frac{0.6(\alpha-\alpha^2)}{G_{xy}}} + \beta\sqrt{\frac{6\left(\frac{1}{\alpha}-\alpha^2\right)}{E_x}}} \qquad [4]$$

where V_f [N] is the shear force, b [m] is the width of the beam, $G_{f,y}$ [N/m] is the fracture energy in pure tensile spitting perpendicular to the grain (mode 1), G_{xy} [N/m²] is the shear modulus and E_x [N/m²] is the modulus of elasticity parallel to the grain. In Figure 31 α [-], β [-] and d [m] are indicated.

Gustafsson (1988) compared the theoretical basic expression with experimental results performed for this research and experimental results from literature on notched beams. Important conclusions are:

- Experimental results show a significant size effect in notch strength for varying beam depth. Weibull theory cannot explain this size effect as the size of the fracture process region is constant and thus the number of possible failure locations do not increase for beams with varying depth. The theoretical analysis of above predicts a size effect proportional to $d^{-0.5}$. Although literature also presents other (comparable) relations which are slightly more accurate, the theoretical relation gives sufficiently accurate results for most engineering applications.

- The derived theoretical basic expression for the reduced strength of notched beams corresponds well with test results.

- The material properties fracture energy perpendicular to the grain, modulus of elasticity along the grain and the shear modulus are decisive for the reduced strength of notched beams.

- No statistical correlation between the tensile strength perpendicular to the grain and the reduced strength of notched beams could be found.

2.4.2 OBTAINING THE FRACTURE ENERGY PERPENDICULAR TO THE GRAIN

To determine the fracture energy in pure tensile spitting perpendicular to the grain $G_{f,y}$ an extensive experimental program was set up executed by several research institutes. Larsen and Gustaffson (1990) report the results. When all results for European softwoods are considered as one population a good relation between the fracture energy in pure tensile spitting perpendicular to the grain and density is found:

$$G_{f,y} = 1.04\rho - 146 \qquad [5]$$

The correlation coefficient for this relation is 0.78, a relatively high value. A graph with the results is depicted in Figure 37. For this relation the unit of $G_{f,y}$ is [N/m] and of ρ is [kg/m^3], the relation applies to mean values.

To be able to obtain characteristic values for the fracture energy equation [5] is adapted. For ρ between 300 en 450 kg/m^3 the relation between fracture energy and density can be replaced by:

$$G_{f,y} = 0.65\rho \qquad [6]$$

For ρ = 375 kg/m^3 both relations [5] and [6] return the same value for the fracture energy.

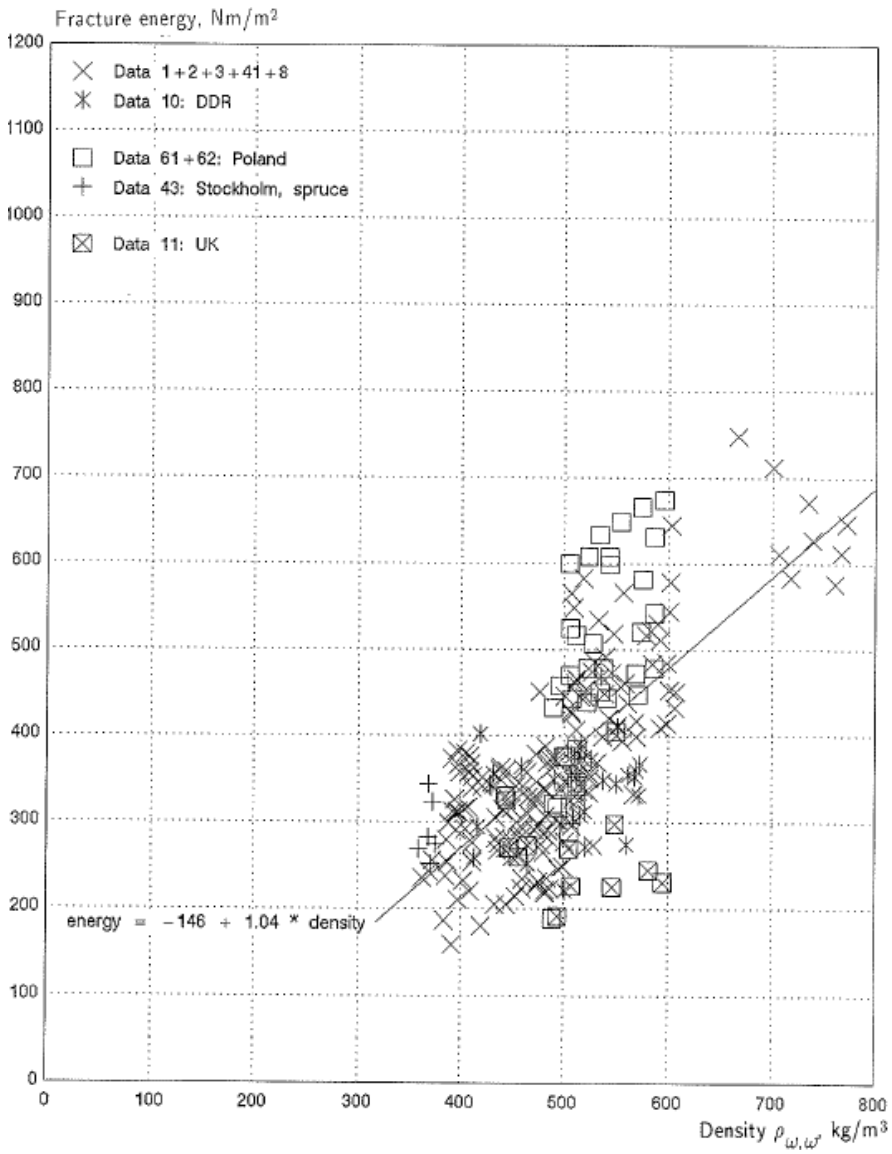

Figure 37: Fracture energy verses density for European softwoods regarded as one population (Source: Larsen and Gustaffson (1990), Fig. 5)

2.4.3 DERIVATION OF A DESIGN FORMULA FOR REDUCED NOTCH STRENGTH

In order to be able to fit the basic theoretical expression [4] to experimental results and obtain a design formula for notch strength Larsen and Gustafsson (1992) first reformulated expression [4] the following way. By introducing a factor 1.5, a factor k [-] and a factor $\frac{f_v}{f_v}$ [N/m² / N/m²] expressions [7] and [8] are derived. Note the shear strength is introduced both in the numerator as in the denominator. Theoretically the factor k is equal to 1.5 (to account for the introduced factor 1.5 on the left side of equation [7]). The shear strength in the denominator is then brought within the square root in the numerator. Finally the reduction factor k_v [-] is introduced which contains the largest part of the theoretical expression.

$$\frac{3}{2}\frac{V_f}{b\alpha d} = k_v f_v \qquad [7]$$

where V_f [N] is the shear force and b [m] is the width of the beam. In Figure 31 α [-], β [-] and d [m] are indicated. k_v is given by:

$$k_v = \frac{k\sqrt{\frac{E_x G_{f,y}}{f_v^2 d}}}{\sqrt{\frac{0.6(\alpha-\alpha^2)E_x}{G_{xy}} + \beta\sqrt{6\left(\frac{1}{\alpha}-\alpha^2\right)}}} \qquad [8]$$

When it is assumed $E_x/G_{xy} = 16$ as is done in Eurocode 5 the denominator of k_v ([8]) can be approximated by:

$$3\left(\sqrt{\alpha-\alpha^2} + 0.8\beta\sqrt{\frac{1}{\alpha}-\alpha^2}\right) \qquad [9]$$

The final approximation of k_v is to move d to the denominator and assuming the numerator constant for different strength classes by introducing the factor K:

$$k_v = \frac{k \cdot K}{\sqrt{d}\left(\sqrt{\alpha-\alpha^2} + 0.8\beta\sqrt{\frac{1}{\alpha}-\alpha^2}\right)} \qquad [10]$$

where

$$K = \frac{1}{3}\sqrt{\frac{E_x G_{f,y}}{f_v^2}} \qquad [11]$$

where k_v [-] is the reduction factor on the shear strength, K $\left[\sqrt{m}\right]$ is a material dependent factor to be determined by tests, $G_{f,y}$ [N/m] is the fracture energy in pure tensile spitting perpendicular to the grain (mode 1), G_{xy} [N/m²] is the shear modulus and E_x [N/m²] is the modulus of elasticity parallel to the grain.

By formulating k_v like equation [10] it is possible to fit this theoretical expression to experimental results of tests on notched beams by adjusting k.

Larsen and Gustafsson (1992) determined K ([11]) using material parameter values from NEN 384 (1991) and by tests. In Table 1 K is determined where it is assumed the ratio's between the material parameters are the same for mean and characteristic values.

Table 1: Determination of K (EN 338, 1991)

Strength class		C14	C22	C27	C30	C35	C40	C70
E_{05}	N/mm²	4700	6700	8000	8000	8700	9200	16700
$f_{v,k}$	N/mm²	1.7	2.4	2.8	3	3.4	3.8	6.2
ρ_k	kg/m³	290	340	370	380	400	420	900
$G_{f,y,k}$	N/mm	0.189	0.221	0.241	0.247	0.260	0.273	0.585
K	$\sqrt{mm}$	5.84	5.34	5.22	4.94	4.66	4.40	5.31

For nine test series $k \cdot K$ was calculated after which for structural timber an average value of $k \cdot K$ = 5.18 was found. This value approximately corresponds with K calculated in Table 1. Therefore, for structural timber a value of $k \cdot K = 5$ is chosen which corresponds with k = 1.

After adding a factor $k_i = \frac{1.1i^{1.5}}{\sqrt{d}}$ to k_v to include tapered beam ends Larsen and Gustafsson (1992) concluded with an expression for the verification of notched beam strength for structural timber which is still part of the Eurocode today:

$$\tau_d = \frac{3}{2}\frac{V_f}{b\alpha d} \leq k_v f_{v,d} \qquad [12]$$

where

$$k_v = \frac{5\left(1 + \frac{1.1i^{1.5}}{\sqrt{d}}\right)}{\sqrt{d}\left(\sqrt{\alpha - \alpha^2} + 0.8\beta\sqrt{\frac{1}{\alpha} - \alpha^2}\right)} \qquad [13]$$

In fact with equation [12] a usual unity check on shear strength is performed where k_v is added to reduce the shear strength to take into account possible splitting at the root of the notch. As the notch is located at the end of the beam, where a shear strength check is usual, a practical strength check is obtained for the engineer. However, the derivation of equation [12] includes adding the shear strength in both the numerator as the denominator. Therefore the failure mechanism itself has nothing to do with this shear strength value.

2.5 Main issues concerning calculation mortise and tenon joint strength

The remarkable case of the joint not fulfiling the ultimate limit state can be addressed to the three main parts of the calculation as exampled in the previous paragraph. These three main parts are the assumed force distribution, material properties and use of the formula for the reduced strength of a notch from EC5.

2.5.1 Force distribution

As is exampled in paragraph 2.3 calculations common in practice assume a very simple force distribution. Bending in the crossbeam caused by water pressure acting normal to the beam axis causes shear forces in the beam. The shear force is transmitted through the tenon to the post at the location of the seal strip. Compression in the crossbeam due to the pointing shape of the two doors is not taken into account. This compression force can however have important consequences for the actual force distribution in the joint regarding amongst other things that the compression force does not have to work centrically in the crossbeam due to the eccentric support at the front post. Different directions of the fibres of the crossbeam and post and the use of a different wood species for the seal strip could also

influence the force distribution. How the load is actually transferred thus remains unknown up to now.

Raadschelders (2012) suggested that by assuming the load is transferred by shear at an enlarged vertical contact surface around the mortise (without further considering the tenon, see Figure 38) higher joint strengths can be obtained. Although the assumed load distribution could be correct the question remains which strength value for rolling shear is appropriate. In the report the shear strength is used which is increased by 15% to take the influence of compression stresses in the connection (interlocking of grains) into account. But it may be more appropriate to use the rolling shear strength which is about four times lower than shear strength according NEN-EN 338.

It is however not known if, or to which extent, the rolling shear strength is increased by compression stresses. Further, perhaps the friction coefficient under compression of timber to timber is indicative or could increase the possible transferable load. Thus there is uncertainty concerning the load transfer and the resulting connection strength.

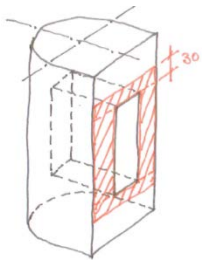

Figure 38: Vertical contact surface around mortise (Source: Raadschelders (2012))

2.5.2 MATERIAL PROPERTIES OF HARDWOODS

Material properties for hardwoods are given by NEN-EN 338 (2009). An extra difficulty in studying the mortise and tenon joint strength is that important material properties for hardwood needed in the calculation are not based on experimental research on hardwoods. This applies to shear strength in bending, tensile strength perpendicular to the grain, rolling shear strength and fracture energy perpendicular to the grain. Further Eurocode 5 (NEN-EN 1995-1-1, 2005) states the rolling shear strength is equal to twice the tensile strength perpendicular to the grain. Referring to the results from Blass and Görlacher (2000) this is correct for European Spruce, but again it remains unknown whether this relation is valid for hardwoods too. Thus not only the (characteristic) values for these material properties are unknown but also their relations.

The first calculation exampled in paragraph 2.3 showed that using the shear strength value from NEN-EN 338 the unity check will easily be larger than 1.0, even without applying the reduction factor from EC5. It is therefore also known that the shear strength of hardwoods given by EN 338 is not based on proper research on large pieces (Van de Kuilen & Leijten, 2002). In the second calculation the shear strength value determined by Van de Kuilen and Blass (2005) is used. It is however questionable if this shear strength value is applicable in this situation because this value is determined for a very different loading situation. Shear strength values show variation for different ways of loading because of different secondary stresses during loading and volume effects.

As will be explained in the following paragraph the relation between both the shear strength and density with the fracture energy perpendicular to the grain is an important part of the notch strength reduction formula. As these relations and the fracture energy perpendicular to the grain itself are unknown for hardwoods it is important to determine or estimate these material properties to be able to assess the applicability of the notch strength reduction formula to tenons.

2.5.3 APPLICABILITY NOTCH STRENGTH FORMULA

As described in paragraph 2.3 the design formula for notched beams is used when calculating the strength of the mortise and tenon joint. Without further information this seems reasonable since the indicative failure mechanism for notches, splitting of the wood underneath the notch, is also indicative for tenons.

Yet Vermeij (2011) indicated in a Bachelor thesis that the notch strength formula given by Eurocode 5 is not valid for hardwood beams with a notch or tenon. Both the ratio between the results for softwood and hardwood beams as the ratio between the results for beams with a tenon and notch where significantly lower according the notch strength formula than the test results indicated. In this research a shear strength value obtained from research by Van de Kuilen and Leijten (2002) and possibility 1 from Figure 39 for α is used.

The background of the Eurocode 5 expression for the strength reduction of notches, expounded in paragraph 2.4, indicates two points of interest when applying the reduction formula from EC5 to hardwood tenons instead of to softwood notches.

DIFFERENCE BETWEEN SOFT- AND HARDWOOD

The reformulation of the theoretical basic expression for notched beam strength from Gustafsson (1988) to the reduction formula from Eurocode 5 (see paragraph 2.4.3) may be the main cause of the notch strength reduction formula not being applicable to a notch in hardwood beams. It is the question whether the relation between material properties for softwoods, expressed in the factor $k \cdot K$, is also valid for hardwoods. The use of the Eurocode 5 expression, as is done for the example in paragraph 2.3, would then be questionable when hardwood is applied.

DIFFERENCE BETWEEN A NOTCH AND TENON

When applying the notch strength reduction formula for tenons it first seems uncertain how to define the variable α for a tenon. The reduction factor k_v highly depends on the ratio α.

For a notch with height d_{eff}, α is simply defined as d_{eff}/d. For a tenon different definitions for α are possible as is depicted in Figure 39. When applying the reduction formula for the strength of a notch to a tenon the traditional and first possible definition of α is division of the tenon height by the beam height. As Figure 39 suggests the assumed geometry does not represent the tenon well, susceptibility to splitting is assumed much greater than present in reality because a much larger part of the beam is separated when splitting occurs. The resulting reduction factor could however be considered safe. This definition of α is in fact prescribed by Ehlbeck and Kromer (1995) in the widely used book Timber Engineering STEP 1. A second possible definition of α includes the right position of the tenon, but it is unsure which influence the upper part of the beam has on the result. Possibly stresses are more spread out in reality and the assumed geometry is too severe. A third possible definition of α includes the effect of the upper part of the beam, but the larger stiffness of the assumed notch with respect to the tenon can have influence on the strength reduction too. Possibly, due to a larger curvature at the root of the notch , reality may be more severe.

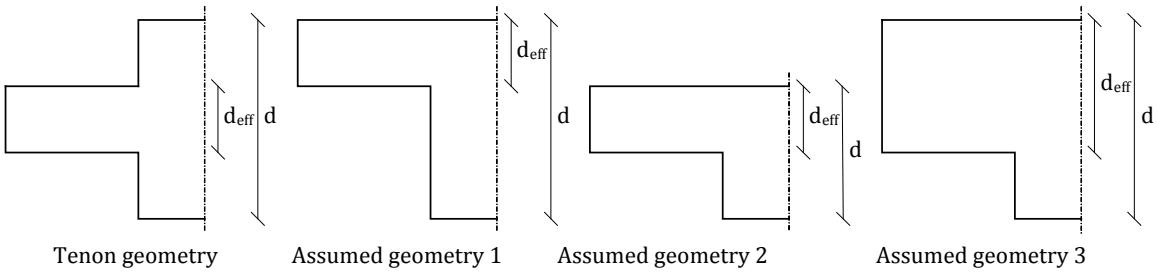

Figure 39: Possible configurations to define ratio α ($\alpha = d_{eff}/d$, if $\alpha_1 = 1/3$ then $\alpha_2 = 1/2$, $\alpha_3 = 2/3$)

However, when a closer look is taken at the derivation of the notch strength reduction formula in paragraph 2.4.1, the only correct definition of α is d_{eff}/d according geometry 1 (Figure 30). To obtain equation [2] in paragraph 2.4.1, α^2 is added on both sides of the equation. Therefore α's definition is not of importance here. Further, α is introduced when determining the deflection of the notched beam. The expressions for both the bending and shear deformation are only correct for a tenon when geometry 1 according Figure 30 is used. An important difference between a notch and tenon lies in the factor 'c' which takes into account that normal stresses need some distance from the tenon to extend the full beam height. The factor 'c' will be different for a notch and tenon as Figure 40 illustrates. Therefore, to determine the reduction of the strength of a tenon due to splitting, in any case the factor c (or equivalent factor) needs to be obtained.

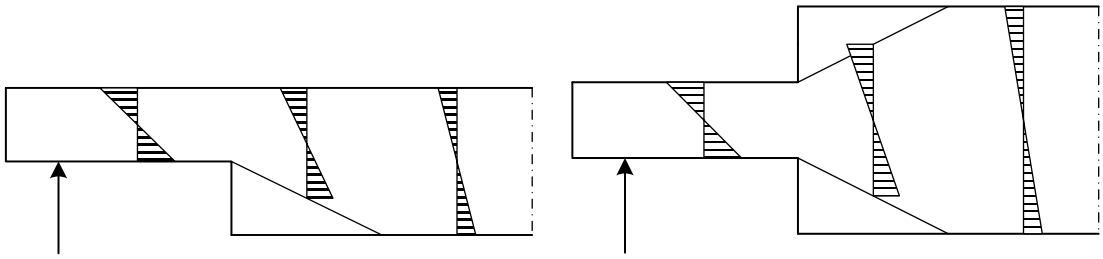

Figure 40: Simplified normal stress distribution for a notch and tenon close to the discontinuity

3 ANALYTICAL ANALYSIS FORCE DISTRIBUTION

Before the mortise and tenon joint is analysed in more detail using finite element modelling (FEM) a first analysis of the force distribution and stresses in the joint is performed by hand to obtain a first insight in the force distribution.

3.1 GLOBAL FORCE DISTRIBUTION

To analyse the internal forces and stresses in the mortise and tenon joint, first the global force distribution needs to be determined. In Figure 41 a wooden mitre gate is depicted including the load and reaction forces, where it has to be reminded that the precise angles of the reaction forces are assumed conveniently. Qualitative and quantitative considerations about the global force distribution are treated respectively.

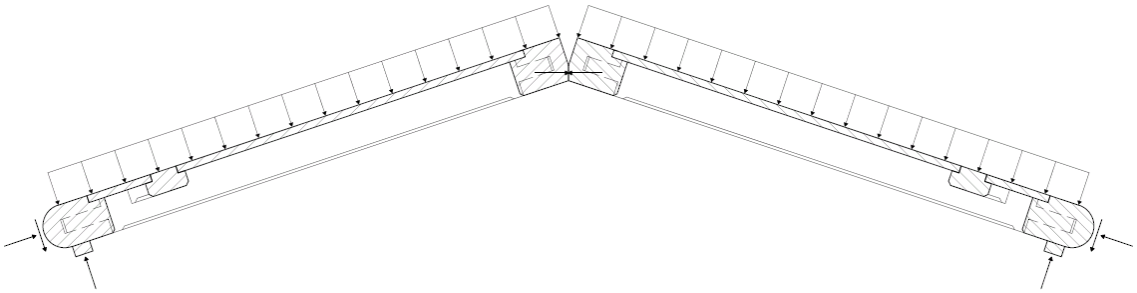

Figure 41: Vertical section of a wooden mitre gate including load and reaction forces (Adapted from Wijma Kampen B.V. (2012c))

3.1.1 QUALITATIVE ANALYSIS

The gate is loaded by the difference of water pressure on both sides of the gate and by waves. The precise value of the distributed load depends on many factors that differ significant for each pair of gates. Extreme water levels and the occurring waves depend on the position of the lock in the system of canals and rivers. Maximum and minimum lockage water levels depend on the characteristics of the canal or river and to the characteristics of ship traffic. Therefore different loads and load combinations can be determined (Figure 42) from which the indicative combination can be different for equivalent locks on different locations. It can for instance occur that the load by water level difference plus wave load during extreme conditions is lower than the load by maximum water level difference during lockage or when the lock is empty during maintenance.

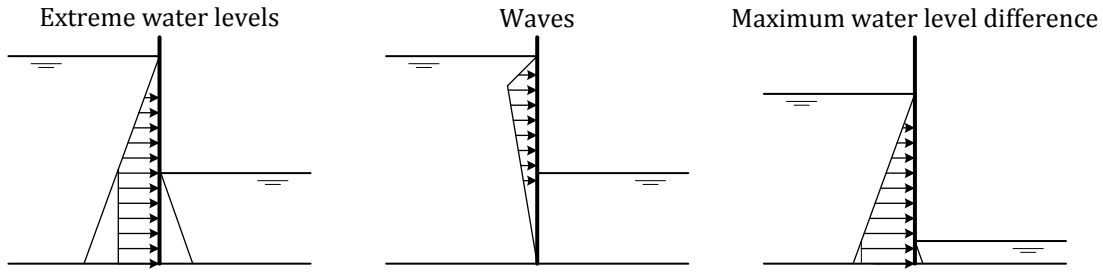

Figure 42: Examples of loads on lock gates

A wooden mitre gate under water level difference loading is depicted in Figure 43 and an illustration of a section of a mitre gate is depicted in Figure 41. The distributed load acts on the surface of the gate which consists of planking. This planking transfers the load to the crossbeams by bending. As the planks are continuous some crossbeams carry more load

than the other. In turn the crossbeams transfer the load by bending to the front and rear posts. The shear force from the crossbeam is transferred to the lock wall via the rear post, seal strip and quoin post. Compression forces from the crossbeam are transferred to the lock wall via the rear post and quoin post at the back of the rear post.

At quoin post it could be possible that frictional forces develop; the crossbeam tries to rotate the rear post as it bends, due to compression at the plane between the rear post and quoin post friction could counteract (a part of) this rotation. The two front posts are in equilibrium with each other. Although is possible to assume that the reaction forces on the front posts work in the width direction of the lock it cannot be assumed without further research at which precise spot on the contact surface this reaction force works.

Figure 43: Wooden mitre gate under water level difference loading

3.1.2 QUANTITATIVE ANALYSIS

Before a first analysis of the internal force distribution in the mortise and tenon joint a simplified force diagram for one of the gates is assumed (Figure 44). The load and reaction forces are assumed to work in the centre line of the mitre gate. The distributed load q is caused by the water level difference on both sides of the gate plus wave load.

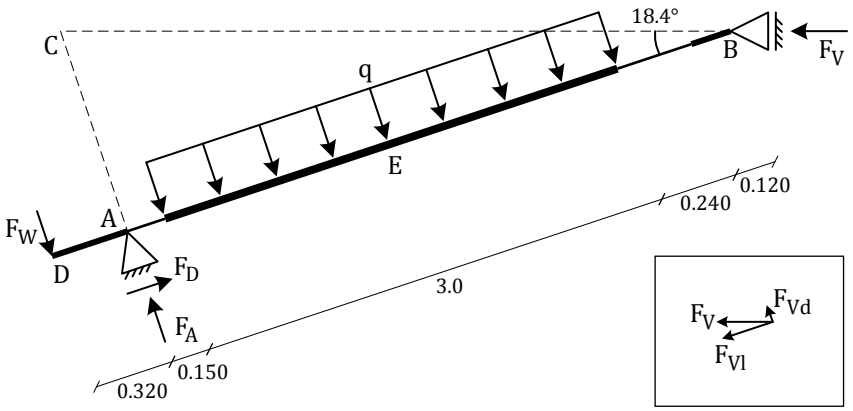

Figure 44: Simplified force diagram (q: distributed load, F_V: reaction force on front post, F_A: reaction force on seal strip, F_D: reaction force on back of rear post, F_W: frictional force on back of rear post, dimensions are given in meters)

In the model the stiffness of the different parts, the full section crossbeam, tenon and posts, are illustrated by varying line thicknesses. Because the simplified model is statically determinate these stiffness differences have no influence on the force distribution. Equilibrium is considered at three points:

Rotational equilibrium at A:
$F_A\, a_{AB} - q\, L\, a_{BE} - F_W\, a_{BD} = 0$
$F_A*(0.150 + 3.0 + 0.240 + 0.120) - q*3.0*(3.0/2 + 0.240 + 0.120) - F_W*(0.320 + 0.150 + 3.0 + 0.240 + 0.120) = 0$

Rotational equilibrium at B:
$-F_V\, a_{AB} \sin(\alpha) + q\, L\, a_{AE} - F_W\, a_{AD} = 0$
$-F_V*(0.150 + 3.0 + 0.240 + 0.120)*\sin(18.4) + q*3.0*(3.0/2 + 0.150) - F_W*0.320 = 0$

Rotational equilibrium at C:
$-F_D\, a_{AB} \tan(\alpha) - q\, L\, a_{AE} - F_W\, a_{AD} = 0$
$-F_D*(0.150 + 3.0 + 0.240 + 0.120)*\tan(18.4) + q*3.0*(3.0/2 + 0.150) - F_W*0.320 = 0$

When the frictional force F_W at the back of the rear post is assumed to be equal to zero, these three equations are sufficient to obtain the reaction forces. When the frictional force at the back of the rear post is assumed to be non-zero a fourth equation is needed. This frictional force depends on the compression force at the contact surface and the friction coefficient μ linearly. The fourth equation thus becomes: $F_W = F_D\, \mu$.

The quoin post at the contact surface between the quoin post and the rear post can either be relatively rough (rough concrete) or smooth (steel). The friction coefficient can therefore vary significantly for different locks as the friction coefficient for wood to concrete or stone is μ = 0.60 and for wet wood to steel is μ = 0.20 (Engineer's Handbook, 2006). The lower value of μ is considered to result in the worst situation for the mortise and tenon joint.

When the above equations are solved for both $F_W = 0$ as for $F_W = F_D\, \mu$ the reaction forces listed in Table 2 are obtained. In appendix A.1 the moment, shear and normal force diagrams for the two possibilities are given. The internal moments for three cross sections are added to Table 2.

Table 2: Reaction forces for simplified model

	$F_W = 0$	$F_W = F_D\, \mu$		
q	32.5	32.5	kN/m	Hakkers (2012)
F_A	51.2	80.1		
F_D	138	130		
F_V	145	137	kN	
F_{Vl}	138	130		
F_{Vd}	45.8	43.4		
F_W	0	26.1		
$M_{midspan}$	48.8	44.7		
M_{tenon}	7.75	-0.25	kNm	
$M_{rear\ post}$	0	-8.35		

The introduction of the frictional force F_W has the following effects on the global force distribution:

- The reaction force at the seal strip F_A increases with F_W and another few percent;
- The difference between $F_A - F_W$ and F_{Vd} increases, thus more shear force is transferred at the rear of the door;
- Due to the more stiff reaction at the rear post the compression force F_D and contact force F_V decrease;
- The maximum bending moment in the crossbeam decreases due to a negative bending moment that develops in the rear post.
- The bending moment in the tenon becomes negative, it is however unsure whether in reality the tenon is actually clamped into the post or that the negative moment is transferred on the faces of the crossbeam.

For the subsequent calculations it is assumed the frictional force F_W does play a role in the load transfer.

3.2 2D ANALYSIS OF INTERNAL FORCES JOINT

Now the reaction forces are known the internal forces and stresses in the mortise and tenon joint can be determined. Material properties and other variables needed for the calculation are given in Table 3 and Table 4.

Table 3: Variables used in the calculation

		According NEN-EN 1995-1-1 (2005)
f_d	$f_k\, k_{mod} / \gamma_M$	Par. 2.4.1
$f_{v,r,d}$	$2\, f_{t,90,d}$	Par. 6.1.7
γ_M	1.3	Table 2.3 for solid timber.
k_{mod}	0.70	Table 3.1 for solid timber, service class 3 and short term action.

Table 4: Material properties according Table 3 and NEN-EN 338 (2009)

	D70 (Azobé)	D30 (Oak)	
$f_{m,d}$	38		
$f_{t,90,d,V0}$	0.32		
$f_{c,90,d}$	7.3	4.3	N/mm²
$f_{v,d}$	2.7		
$f_{v,r,d}$	0.65		

Figure 45 depicts two extreme cases for the internal load transfer. Although the real force distribution is expected to lie between these two extreme cases, both are calculated to obtain some indicative numbers. In the first case friction at the contact planes between the crossbeam and the rear post contributes to the transfer of the shear force from the crossbeam. The negative bending moment in the rear post is equaled by an increase and decrease of the compression forces in the upper and lower part of the post and on the contact planes between the crossbeam and the rear post. In the second case the tenon completely transfers the shear force. Further the negative bending moment is equaled by an internal bending moment in the tenon. The tenon is in fact clamped into the rear post, compression forces at the front upper part and back lower part of the tenon develop. First some calculations valid for both cases are carried out after which additional case-specific calculations are performed.

In the rear post a bending moment is present due to the friction force at the quoin post. At seal strip height a large tensile force in the upper part and a large compression force in the lower part of the rear post is therefore present. For the two cases this bending moment is transferred from the rear post to the crossbeam in a different way.

For both cases it is assumed the compression forces F_d caused by the compression force F_D work symmetrically as indicated. Both planes a and b transfer $F_d = ½F_D = 130/2 = 65$ kN.
The compression stress on the rear post than becomes:
$\sigma_{cD,90,a} = F_d / d_a h = 65*10^3 / 50*300 = 4.33$ N/mm² < $f_{c,90,d}$ (D70)
The compression stress on plane b is non-uniform as the line of action of the compression force is assumed off-centered; assuming $\sigma_{cD,90,b} \leq \sigma_{cD,90,a}$ is considered to be safe.

As the compression force F_D from the crossbeam is transferred to the back of the rear post a tensile force F_h behind the tenon is present. The internal moment does not influence this tensile force. For F_h it follows:
$F_h = F_d \Delta d / \Delta b = 65*75/130 = 37.5$ kN
It is estimated F_h is spread over a width of 40 mm thus for the tensile stress it follows:
$\sigma_{t,90,h} = F_h / h\, b_h = 37.5*10^3 / 40*300 = 3.13$ N/mm²
$f_{t,90,d} = f_{t,90,d,V0}\, (V_0/V)^{0.2} = 0.32 * (0.01/(0.040*0.300*2*0.075))^{0.2} = 0.45$ N/mm² (D70)
$\sigma_{t,90,h} > f_{t,90,d}$ (D70)

The seal strip is compressed by the reaction force F_A. Using 6.1.5 (5) from NEN-EN 1995-1-1 (2005) to determine the effective height, for the compression stress it follows:
$\sigma_{c,90,A} = F_A / b_A h_{ef} = 80.1*10^3 / 125*(300+2*100/3) = 1.75$ N/mm² < $f_{c,90,d}$ (D30)

At the back of the rear post F_D and F_W have to be transferred through a reduced section of the post.
$\sigma_{c,90,D} = F_D / d_D h = 130*10^3 / 180*300 = 2.41$ N/mm² < $f_{c,90,d}$ (D70)
$\tau_{r,W} = 1.5F_W / d_D h = 1.5*26.1*10^3 / 180*300 = 0.73$ N/mm² > $f_{v,r,d}$ (D70)
Although the shear stress already exceeds the rolling shear strength, combination with the compression stress will definitely result in exceedance of the strength.

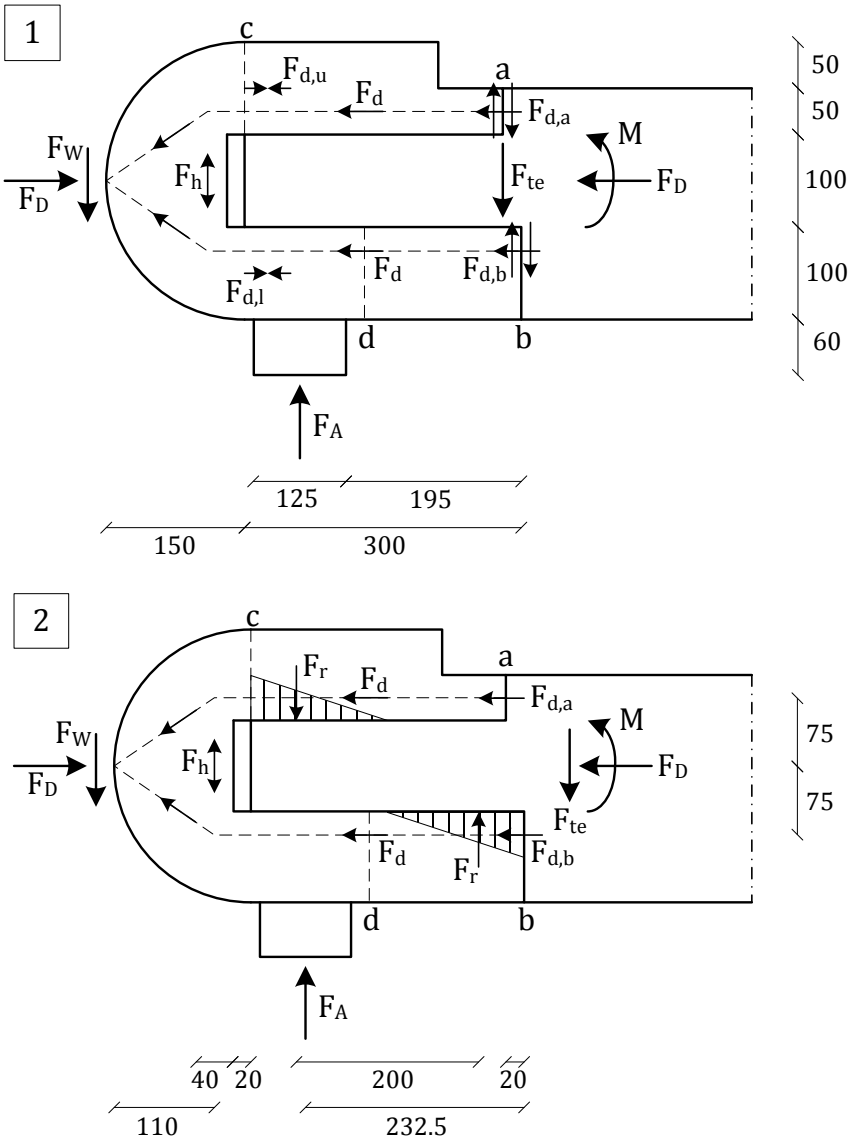

Figure 45: Two extreme cases for the force distribution in the mortise and tenon joint (dimensions given in millimetres)

CASE 1

The following calculations are applicable to case 1.

Friction at the contact plane between the crossbeam and the rear post contributes to the transfer of the shear force from the crossbeam. The negative bending moment in the post and at the end of the crossbeam is equaled by an increase and decrease of the compression forces in the lower and upper part of the post and at the two contact planes.

The friction coefficient for wood to wood (wet) is $\mu = 0.20$ (Engineer's Handbook, 2006).Thus the maximum force which can be transmitted by friction:
$F_{f,max} = F_D\mu = 130*0.20 = 26.1$ kN

The shear force which is transferred through the tenon is:
$F_{te} = F_A - F_W - F_{f,max} = 80.1 - 26.1 - 26.1 = 28$ kN

Applying the notch strength formula from EC5 where $k_n = 5$, d = 250, $\alpha = 100/250 = 0.4$ and x = 232.5:

$$k_v = \frac{k_n}{\sqrt{d}\left(\sqrt{\alpha(1-\alpha)}+0.8\frac{x}{d}\sqrt{\frac{1}{\alpha}-\alpha^2}\right)} = 0.194$$

$\tau_{te} = 1.5F_{te} / d_{eff}h = 1.5*28*10^3 / 100*300 = 1.40$ N/mm² > $k_v f_{v,d} = 0.52$ N/mm² (D70)

An bending moment in the tenon is present:
$M_{te} = F_{te} x = 54*0.2325 = 12.6$ kNm
$k_h = (150/d_{eff})^{0.2} = (150/100)^{0.2} = 1.08 < 1.3$
$f_{m,d,mod} = f_{m,d} k_h = 37.7*1.08 = 40.9$ N/mm²
$\sigma_{m,d} = M_{te} / W_{te} = 12.6*10^6*6 / 300*100^2 = 25.2$ N/mm² < $f_{m,d,mod}$ (D70)
The shear stress τ_{te} is equal to about half the shear strength $f_{v,d}$. Although the combination of the bending and shear stress could result in exceeding the strength, EC5 does not state bending stresses and shear stresses must to be combined.

The negative bending moment at the end of the crossbeam is equalled by two forces ΔF_d at the contact planes a and b:
$\Delta F_d = M_{tenon} / a_d = 0.25 / 0.150 = 1.67$ kN
Then the compression and shear force at plane a and b become:
$F_{d,a} = F_d - \Delta F_d = 65 - 1.67 = 63.3$ kN
$F_{d,b} = F_d + \Delta F_d = 65 + 1.67 = 66.7$ kN

The maximum negative bending moment in the rear post is equalled by two forces ΔF_d in the upper (u) and lower part (l) of the post.
$\Delta F_d = M_{rear\ post} / a_d = 8.35 / 0.150 = 55.7$ kN
Than the compression forces in the upper and lower part of the post become:
$F_{d,u} = F_d - \Delta F_d = 65 - 55.7 = 9.3$ kN
$F_{d,l} = F_d + \Delta F_d = 65 + 55.7 = 121$ kN
The compression and rolling shear stress at plane d becomes:
$\sigma_{c,90,b} = F_{d,l} / d_d h = 121*10^3 / 100*300 = 4.03$ N/mm² < $f_{c,90,d}$ (D70)
$\tau_{r,d} = 1.5\ \mu\ F_{d,b} / d_d h = 1.5*0.20*66.7*10^3 / 100*300 = 0.67$ N/mm² > $f_{v,r,d}$ (D70)
Again the shear stress already exceeds the rolling shear strength, but when combining this stress with the compression stress will definitely result in exceedance of the strength.

CASE 2

The following calculations are applicable to case 2.

The tenon completely transfers the shear force and the negative bending moment is transferred to the crossbeam by the tenon which is clamped into the mortise. Compression forces at the front upper part and back lower part of the tenon are therefore present.

The negative bending moment in the rear post is equalled by two forces F_r on the upper and lower side of the tenon:
$F_r = M_{rear\ post} / a_r = 8.35 / 0.2325 = 35.9$ kN
$\sigma_{c,90,rmax} = F_r / ½ b_r h = 35.9*10^3 / ½*150*300 = 1.59$ N/mm² < $f_{c,90,d}$ (D70)
As F_r is introduced as a shear force in the lower part of the rear post a rolling shear stress check at plane d is appropriate:
$\tau_{r,d} = 1.5*F_r / d_d h = 1.5*35.7*10^3 / 100*300 = 1.79$ N/mm² > $f_{v,r,d}$ (D70)
This shear stress will also be present in the upper part of the rear post as the force F_r is also present there.

The shear force which is transferred through the tenon is:
$F_{te} = F_A - F_W = 54$ kN
For case 1 it was determined that $k_v = 0.194$.
$\tau_{te} = 1.5F_{te} / d_{eff}h = 1.5*54*10^3 / 100*300 = 2.70$ N/mm^2 > $k_v f_{v,d} = 0.52$ N/mm^2 (D70)

An bending moment in the tenon is present:
$M_{te} = F_{te} x - M_{rear\ post} = 54*0.2325 - 8.35 = 4.25$ kNm
$k_h = (150/d_{eff})^{0.2} = (150/100)^{0.2} = 1.08 < 1.3$
$f_{m,d,mod} = f_{m,d} k_h = 37.7*1.08 = 40.9$ N/mm^2
$\sigma_{m,d} = M_{te} / W_{te} = 4.25*10^6*6 / 300*100^2 = 8.5$ N/mm^2 < $f_{m,d,mod}$ (D70)
The shear stress τ_{te} is equal to the shear strength $f_{v,d}$. Would this stress be combined with the bending stress $\sigma_{m,d}$ the unity check will become larger than 1.0.

CONCLUSIONS ON INTERNAL STRESSES

The above calculations show that for many sections stresses are lower than the respective strength values. However, at some locations stress values exceed the respective strength values. These locations are indicated in Figure 46.

For both cases the tensile strength perpendicular to the grain at the end of the mortise and the rolling shear strength at de back of the rear post are exceeded. Although the schematic representation is chosen conveniently this region is a point of interest for further research by FEM.
As could be expected for case 2 the tenon does not fulfil the shear stress check using the notch strength reduction formula from EC5. However, even for case 1 with a reduced shear force, the shear strength is still not sufficient.
For case 1 the rolling shear strength in the lower part of the rear post is exceeded only just with a unity check of 0.67/0.65 = 1.03 while for case 2 the introduction of F_r results in a largely exceeded unity check of 1.79/0.65 = 2.75. As F_r is also introduced in the upper part of the rear post the strength is exceeded there too for case 2.

It can be concluded the tenon strength of hardwoods remains important to research as the different force distributions do not lead to the verification of its strength. Further, both the tensile strength perpendicular to the grain as the rolling shear strength are indicative material parameters.

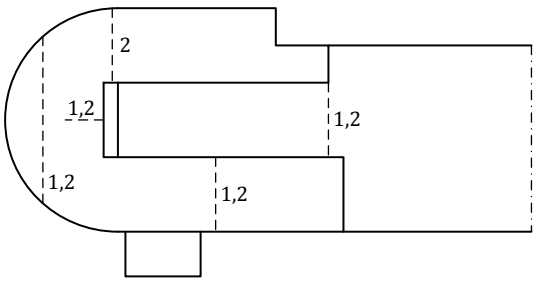

Figure 46: Locations where stresses exceed strength for the indicated cases

3.3 ANALYSIS 3D-GEOMETRY JOINT

In reality the mortise and tenon joint has a 3D geometry. The previous paragraph assumed no applied forces are transferred in the out-of-plane direction. When it is reminded that the fibre direction in the rear post runs along the out-of-plane direction, and therefore force transfer in this direction is relatively stiff, it is obvious that applied forces on the rear post can also be transferred in the third direction. In the following paragraph the analysis of the force transfer is extended with three dimensional considerations.

3.3.1 QUALITATIVE ANALYSIS

Figure 47 illustrates an exploded view of the mortise and tenon joint. In previous paragraphs only the x-y plane was considered at the mid-plane of the crossbeam. Note the fibre direction of the rear post runs along the z-axis and the fibre direction of the crossbeam runs along the x-axis. Taking into account the fibre directions of the parts deformations can be estimated, as is done in Figure 47.

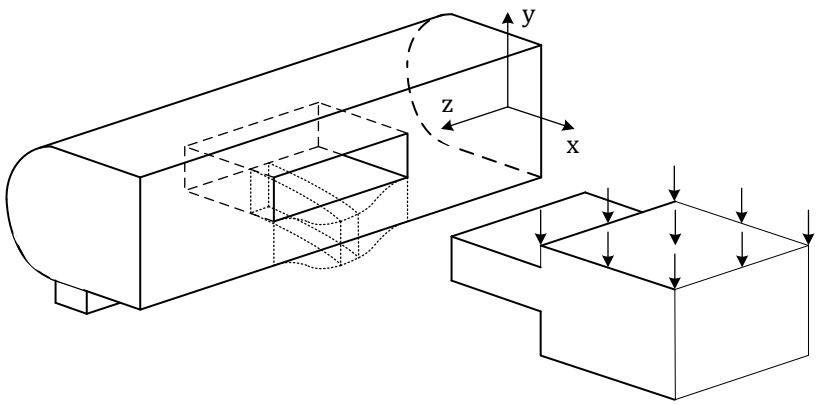

Figure 47: Exploded 3D view of a simplified mortise and tenon joint including magnified deformations. Note the fibre direction of the rear post runs along the z-axis and the fibre direction of the crossbeam runs along the x-axis.

As the deformation of the mortise in the rear post indicate, applied forces from the crossbeam can be transferred in two directions. Firstly, the load can be transferred in the x-direction until the line of action meets the line of action of the support at the seal strip. In the x-direction the stiffness of the rear post is relatively low and therefore, when the analysis is restricted to the x-y plane, most of the load is transferred through the tenon until the support's line of action is reached.

Secondly, the load can be transferred in the relatively stiff z-direction after which the forces need to be transferred to the seal strip support within the full section of the rear post next to the mortise. An important condition for the load to be transferred along this route is that the rear post needs to resist rotation to make it possible for the applied force, when it is first transferred in the z-direction to the full-section rear post, to shift along the x-axis to the seal strip support. In fact, a negative moment needs to develop in the rear post if the line of action of the load would move in the positive x-direction. As a large compression force is present in the crossbeam and friction at the back of the rear post can develop, the rear post could be considered to be clamped in for a certain amount. Note that next to the mortise the full section of the rear post is very stiff. Figure 48 illustrates the mentioned phenomenon.

Note that when the shear force would be transferred at the contact surface between the crossbeam and the rear post, according the suggestion of Raadschelders (2012), a relatively large negative moment in the rear post should occur.

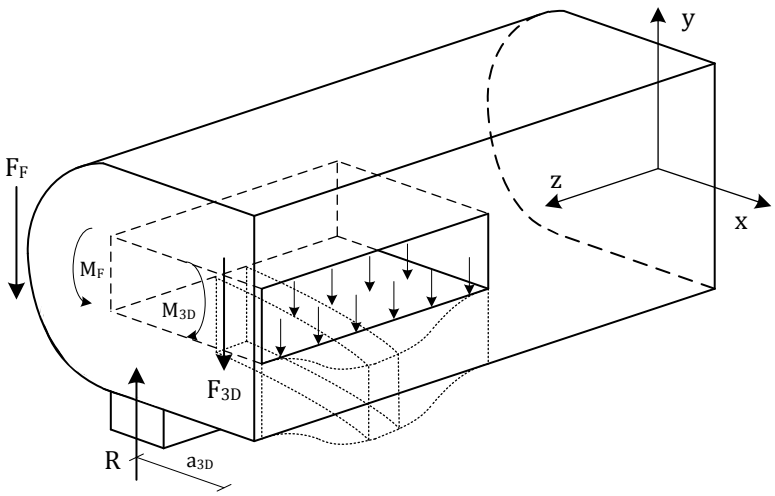

Figure 48: A negative moment in the rear post must develop when (a part of) the shear force from the crossbeam is not transferred from the tenon to the rear post at the line of action of the seal strip support

Considering the front view of the mortise and assuming the applied load is transferred for at least a significant part in the z-direction, it is likely a non-uniform stress distribution like illustrated in Figure 49 develops. When the left part of the rear post around the mortise is considered separately, it can be seen an 'internal' notch is present in the rear post.

When an extreme case of uniform distributed load in the mortise is assumed, for which the notch cantilever is largest, and the entire load is assumed to be transferred in the z-direction, half of the shear force V is transferred through the internal notch with a notch cantilever of βd = ¼d. However, the entire shear force V is transferred through the tenon in the crossbeam with a tenon cantilever probably larger than βd = ¼d. Whether crack growth at this spot is decisive with respect to crack growth in the crossbeam depends on the difference between the strength of notched beams with respect to tenonned beams. Although it is estimated crack growth in the crossbeam is decisive as notches are not expected to be more than twice as weak than tenons, a definite conclusion can only be made later on.

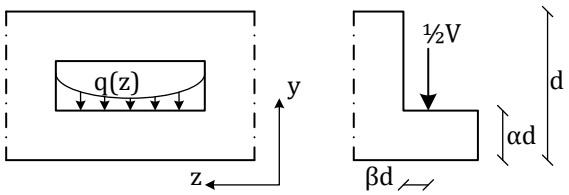

Figure 49: Front view of a mortise in the rear post where on the right the left part of the rear post around the mortise is considered separately.

3.3.2 Modelling 3D behaviour within a 2D FE-model

Because analysis of the force distribution will be investigated using Finite Element Modelling, but 2D analysis is preferred, the 3D geometry needs to be taken into account applying appropriate modelling. The 3D force transfer in the mortise and tenon joint is taken into account by the 2D model by addition of an elastic support with stiffness k to the rear post as is depicted in Figure 50.

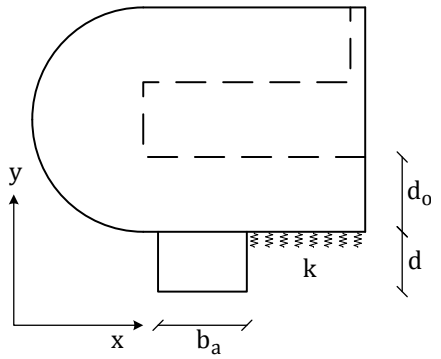

Figure 50: Additional spring support below rear post to account for 3D force transfer

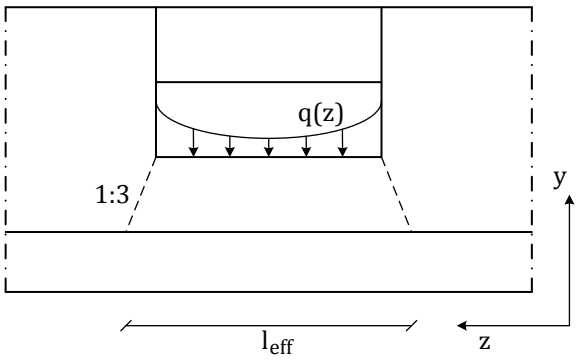

Figure 51: Additional bearing length seal strip

The value of the stiffness parameter k is determined by two components: compression of the seal strip along an additional bearing length and bending of the lower part of the rear post below the mortise.

COMPRESSION OF THE SEAL STRIP

When (a part of) the load is transferred along the z-axis, it will be brought to the support via a part of the seal strip next to the mortise. Analogue to NEN-EN 1995-1-1 (2005) 6.1.5 (4) it is assumed the load is spread along the line 1:3. Then the additional length of the seal strip along which the load concerned is transferred is $h_{a,add} = 2 \cdot ⅓\ d_o$. The stiffness of this part of the seal strip under compression can be determined according the model illustrated in Figure 52. According linear elastic theory this stiffness becomes:

$$k_a = \frac{EA}{L}$$

where $E = E_{90}$ [N/m²] is the modulus of elasticity perpendicular to the grain, $A = b_a h_{a,add}$ [m²] is the surface of the seal strip through which the force is transferred and $L = d_a$ [m] is the thickness of the seal strip.

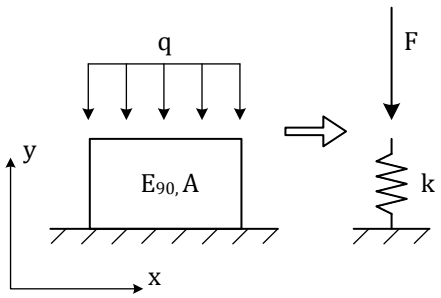

Figure 52: Spring model seal strip

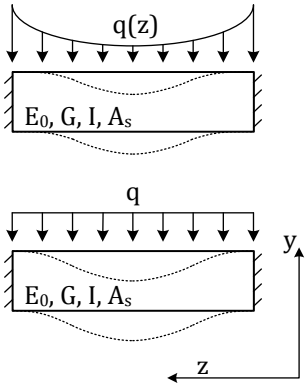

Figure 53: Model fictive beam rear post

BENDING OF THE LOWER PART OF THE REAR POST

The bending deformation of the lower part of the rear post below the mortise can be described by a Timoshenko beam as the fictive beam is relatively stocky. This part of the rear post can be schematised by a fictive beam clamped at both sides (Figure 53). It is chosen to model the load uniformly distributed. The two coupled differential equations which define a Timoshenko beam are derived in Appendix B.

The fictive beam, as depicted in Figure 53, can be modelled by this set of couples differential equations:

$$EI\frac{d^2\varphi}{\mathrm{dx}^2} + GA_s\left(\frac{dv}{dx} - \varphi(\mathrm{x})\right) = 0$$

$$GA_s\left(\frac{d^2v}{dx^2} - \frac{d\varphi}{\mathrm{dx}}\right) = -q$$

where $v(z)$ [m] is the deflection along the z-axis, $\varphi(z)$ [-] is the rotation along the z-axis, $E = E_0$ [N/m²] is the modulus of elasticity along the grain, G [N/m²] is the shear modulus, $I = \frac{bd^3}{12}$ [m⁴] is the second moment of area of the fictive beam and $A_s = bd$ [m²] is the cross-sectional area fictive beam

When the set of coupled differential equations is solved using the boundary conditions:

$$v(0) = 0, \varphi(0) = 0, v(L) = 0 \text{ and } \varphi(\mathrm{L}) = 0$$

for the deflection it follows:

$$v(z) = \frac{1}{24}\frac{qz^4}{EI} - \frac{1}{12}\frac{qLz^3}{EI} + \frac{1}{24}\frac{q(-12EI + L^2GA_s)z^2}{EI\,GA_s} + \frac{1}{2}\frac{qLx}{GA_s}$$

The mean deflection can be determined by dividing the integrated deflection depended on z by the length of the beam:

$$v_{mean} = \frac{1}{L}\cdot\int_0^L v(z)dz$$

Then the mean bending stiffness parameter can be determined by dividing the load by the mean deflection:

$$k_b = \frac{qL}{v_{mean}} = \frac{qL^2}{-\frac{1}{80}\frac{qL^5}{EI} + \frac{1}{72}\frac{q(-12EI + L^2GA_s)L^3}{EI\,GA_s} + \frac{1}{4}\frac{qL^3}{GA_s}}$$

STIFFNESS PARAMETER K

As the models of compression of the seal strip and bending of the lower part of the rear post are coupled as series system a stiffness parameter k_s can be determined by:

$$k_s = \frac{1}{\frac{1}{k_a} + \frac{1}{k_b}}$$

The stiffness parameter k_s results in a value as if one spring is applied. Therefore to determine the stiffness parameter k, k_s needs to be divided by the surface at which the elastic support is applied:

$$k = \frac{k_s}{A_{elastic\ support}}$$

Chapter 4 will include a quantitative analysis of the stiffness parameters above.

NOTES ON THE ASSUMPTIONS MADE

During the derivation of the stiffness parameter k several assumption are made. It is tried to make conservative assumptions which result in a more accurate model than is the case for pure 2D analysis, but is still on the conservative side as the 3D force transfer in reality is most probably too complicated for a simple analytical model.

Firstly it is assumed a frictional force is present at the back of the rear post. Due to this force rotation of the rear post is prevented and a shift of the line of action of the shear force in the tenon is possible. Due to the large compression force, and in most cases a good fit of the rear post into the quoin post, the assumption is judged appropriate.

When (a part of) the load is transferred to the sides of the mortise it is difficult to predict to which part of the seal strip the load is transferred. As the load first needs to travel to the back of the rear post it is likely the additional bearing length is larger than is assumed according the line 1:3. As a smaller additional bearing length leads to a smaller stiffness k and therefore the shift of the line of action of the shear force in the tenon is less, the assumption is judged conservative.

To calculate the mean stiffness of the fictive beam below the mortise a uniformly distributed load within mortise is assumed. With respect to a non-uniformly distributed load a smaller mean stiffness is found. As explained in the previous paragraph, the results is thus conservative.

4 CHARACTERISTICS FINITE ELEMENT MODEL

In order to determine the actual force distribution in a wooden mitre gate, especially within the mortise and tenon joint, finite element modelling (FEM) is applied. This chapter the finite element model is presented and the applied approach, made assumptions and used parameters are treated.

Abaqus is used for all activities related to finite element calculations. Three stages have to be run through, namely:

- Pre-processing/modelling: Abaqus CAE is used to create the model which includes among other things the geometry, material properties and the mesh.
- Processing/finite element analysis: Abacus Standard is used to solve the numerical problem. Its output is stored in an output file and contains displacements, stresses, etc.
- Post-processing: Abaqus Viewer is used to display the results in various ways to evaluate the results. Results can also be exported to a text-file after which it can be further analysed using Excel and Matlab.

The finite element (FE) model build for this research is characterized by:

- Linear elastic material within 2 dimensions;
- Characteristics of the mitre gate's parts: solid, homogeneous and deformable, where the plane strain assumption is applied;
- The boundary parts are characterised as analytical rigid wires;
- The lower part of the rear post is supported by an elastic support to take account for 3D load transfer;
- Orthotropic material behaviour is assumed where the different fibre directions of the mitre gate's parts are taken into account;
- Calculation steps are of the general static type:
  - Equations are solved directly;
  - The Full Newton solution technique is used;
- Interaction properties at contact surfaces are characterised by
  - interaction by surface-to-surface contact;
  - normal behaviour by "hard" contact, where separation is allowed;
  - friction is defined by isotropic Coulomb friction;
- Definition of the mesh:
  - Parts are meshed separately;
  - The element type used is a 4 node bilinear plane strain quadrilateral. Reduced integration and enhanced hourglass control are applied.

More explanation about the above points is written in the following paragraphs.

4.1 DESIGN OF THE MITRE GATE'S MODEL

The dimensions of the mitre gate including the mortise and tenon joints are determined fully according the traditional (relative) dimensions from literature. One parameter, the depth of the beam, needs to be chosen after which all other dimensions follow.

Assumed parameters	Character	Value	
Total depth mitre gate	d	300	mm
Length crossbeam between posts	l	3000	mm
Depth planking	s	50	mm
Angle gate when closed	γ	30	degrees

Derived parameters	Relation	Value	
Width rear post	1.5d	450	mm
Width front post	1.2d	360	mm
Length rear tenon	⅔ width rear post	300	mm
Length front tenon	⅔ width front post	240	mm
Length rear mortise	tenon length + 20 mm	320	mm
Length front mortise	tenon length + 20 mm	260	mm
Depth lower notch crossbeam	⅓ d	100	mm
Depth tenon	⅓ d	100	mm
Depth upper notch crossbeam	⅓ d – s	50	mm
Upper/lower notch length difference		20	mm
Depth bevelled edge front post	⅓ d	100	mm
Size seal strip	d x b	75 x 125	mm^2

An applied load which would be 'normal' for a gate with these dimensions is q = 32.5 kN/m.

An overview of the model and its separate parts are depicted in Figure 54 and Figure 55.

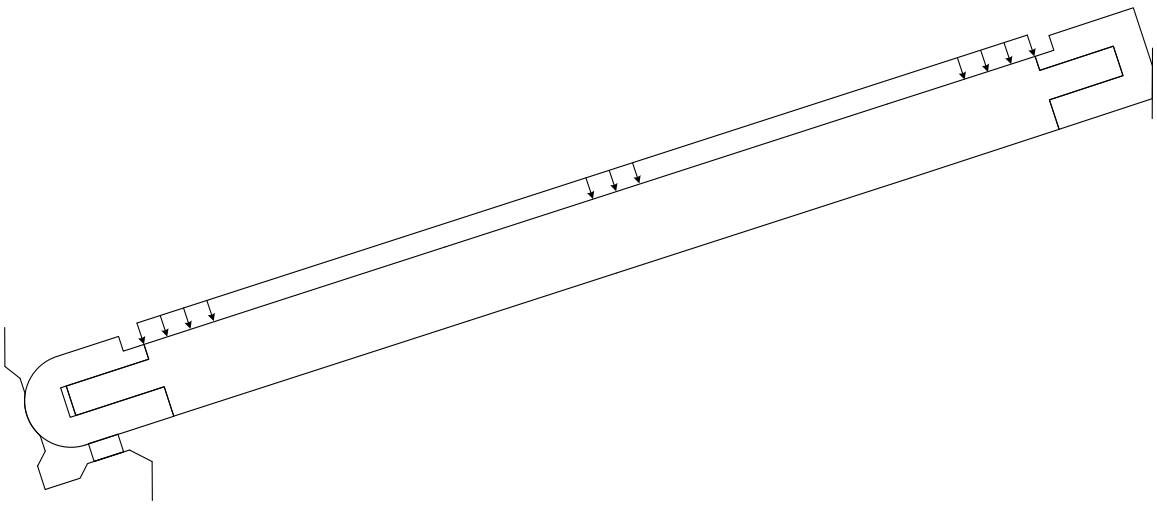

Figure 54: Overview model

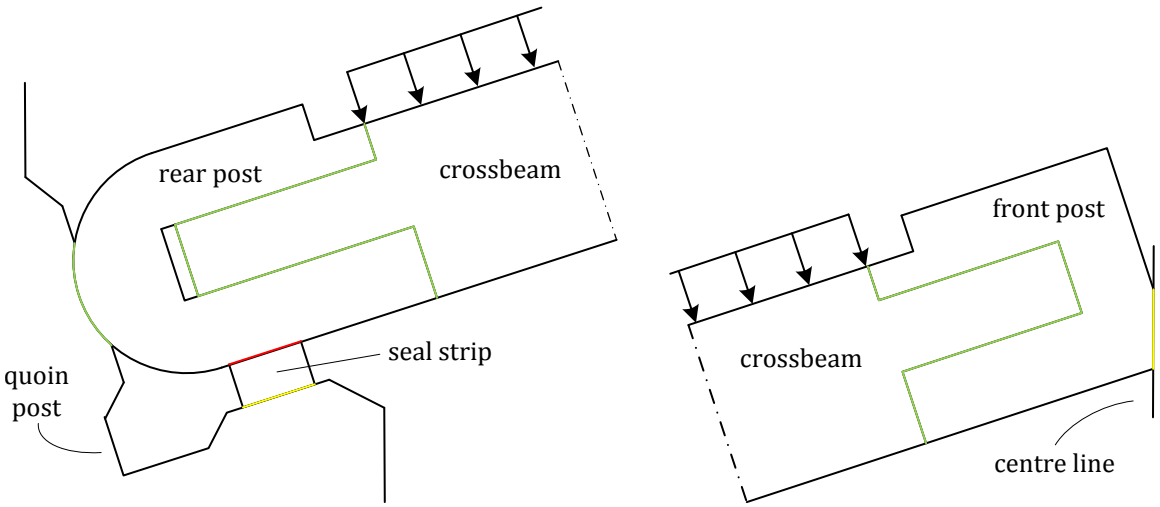

Figure 55: Overview parts front and rear side of the gate with interaction properties indicated (green: hard contact & friction, yellow: hard contact, red: fixed)

4.2 CHARACTERISTICS CALCULATION PROCEDURE

The calculation procedure applied in finite element modelling can have many different characteristics. The applied method for this model is presented here.

The main characteristic of the used method is the use of linear elastic materials within 2 dimensions. On one hand this makes modelling more easy and straightforward. On the other hand accurate results can still be obtained as the joint is rather thick, failure behaviour is not considered and peak stresses near discontinuities are not used for the analysis.

The model is characterized by six main parts: quoin post, rear post, seal strip, crossbeam, front post and the centre line. These parts touch at contact surfaces where appropriate interaction properties are defined (paragraph 4.4). In reality in 3D the joint is rather thick and therefore, when modelling in 2D, plane strain is an appropriate assumption. The rear post, seal strip, crossbeam and front post are modelled as homogeneous deformable parts. These parts separately are one solid piece. The quoin post and centre line are modelled as rigid analytical wires, which are in fact simple continuous lines that do not deform.

The calculation procedure is split up into several, so called, steps. It is of great importance to model the steps in the right sequence and usually 'in between' steps are necessary to make it possible for the calculation to succeed.

For the calculation steps a relatively straightforward procedure is chosen: within every step iterations are used following the Full Newton solution technique until equilibrium is reached. Friction results in discontinuous and thus non-linear equations and therefore the Full Newton solution technique is applied.

Using the following steps a result is obtained for the model:

1. Initial step

In the initial step boundary conditions are applied. The quoin post and centre line are fixed for all degrees of freedom. Further the front and rear post are fixed temporarily.

2. Second step

During the second step the crossbeam and seal strip are pressed against the front and rear post using a pressure load at the contact surfaces. In this way the connection is 'pre-compressed' and the calculation is more likely to succeed during the subsequent steps.

3. Third step

At the start of the third step the boundary conditions on the front and rear post are released. Then the entire mitre gate is shifted against the quoin post and centre line as if the load by water level difference is already applied. The contact surfaces concerned are thus also pre-compressed. Meanwhile the pressure load at the contact surfaces between the front and rear post and the crossbeam and seal strip is maintained.

4. Fourth step

During the fourth step the pressure load within the connection is removed and the load by water level difference is applied. Due to the pre-compression applied in the previous steps and the linear decrease of the pressure load and linear increase of the global load a result is obtained without much difficulty.

4.3 MATERIAL DEFINITION

For the FE model orthotropic material behaviour is assumed where the different orientation of the fibres of the crossbeam and posts/seal strip have been taken into account. The material properties used are listed in Table 5.

To obtain the rolling shear stiffness it is assumed that the ratio between the longitudinal and rolling shear stiffness G_v/G_{roll} is equal for different wood species; as is assumed by Sandhaas (2012). Thus analogously for Spruce (C24) $G_{mean}/G_{roll,mean} = 690/50 = 13.8$. Then for Azobé (D70) $G_{roll,mean} = G_{mean}/13.8 = 1250/13.8 = 91$ MPa and for Oak (D30) $G_{roll,mean} = G_{mean}/13.8 = 690/13.8 = 50$ MPa.

Due to the microstructure of tropical hardwoods, with its relatively large rays, material parameters depend on the considered direction, longitudinal, radial or tangential. The radial rays make that material parameters differ between radial and tangential directions. As it is not possible to take the ray orientation into account on the construction site, NEN-EN 338 does not differentiate between the modulus of elasticity in radial direction E_R and in tangential direction E_T, but prescribes one value E_{90}. As the rays obviously influence the Poisson ratio's for the different planes a choice needs to be made which value should be used within the FE model. Forest Products Laboratory (2010) reports Poisson ratio's for several wood species, obtained by tests on small clear specimens. It can be seen $\nu_{LR} \neq \nu_{LT} \neq \nu_{RL} \neq \nu_{TL}$ and $\nu_{RT} \neq \nu_{TR}$.[1]

The assumed values appropriate for Azobé are (Forest Products Laboratory, 2010):

ν_{LR}	ν_{RL}	ν_{LT}	ν_{TL}	ν_{RT}	ν_{TR}
0.35	0.060	0.60	0.030	0.60	0.35

The variation of Poisson ratio values results in a problem when modelling the material behaviour. Firstly, orthotropic material behaviour assumes $\nu_{12}/E_1 = \nu_{21}/E_2$, $\nu_{13}/E_1 = \nu_{31}/E_3$, $\nu_{23}/E_2 = \nu_{32}/E_3$. Secondly, for the crossbeam $\nu_{12} = \nu_{LR}$ or ν_{LT} or ν_{RL} or ν_{TL} and for the posts and seal strip $\nu_{12} = \nu_{RT}$ or ν_{TR}. It is assumed the Poisson ratio's do not influence the results too much and therefore the values and definitions according Table 5 and Table 6 are assumed.

[1] L: longitudinal direction, R: radial direction, T: tangential direction

Table 5: Definition material properties

	Azobé		Oak		
$E_{0,mean}$	20000	MPa	11000	MPa	NEN-EN 338 (2009)
$E_{90,mean}$	1330		730		
G_{mean}	1250		690		
$G_{roll,mean}$	91		50		Sandhaas (2012)
ν_{LR}	0.35	-			Assumed using Forest Products Laboratory (2010)
ν_{RT}	0.60		0.60	-	

As the structure is modelled in 2D in the x-y or 1-2 plane according a Cartesian coordinate system (Figure 56) material parameters considering the z or 3 direction are not active within the model. The material parameters from Table 5 are therefore entered according the definitions in Table 6.

Table 6: Material parameters definition 1-2 plane

Crossbeam	Posts and seal strip
$E_1 = E_0$	$E_1 = E_{90}$
$E_2 = E_{90}$	$E_2 = E_{90}$
$\nu_{12} = \nu_{LR}$	$\nu_{12} = \nu_{RT}$
$G_{12} = G$	$G_{12} = G_{roll}$

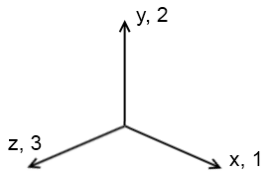

Figure 56: Cartesian coordinate system

4.4 INTERACTION BETWEEN SURFACES

Interaction of the separate parts with each other takes place on surfaces for which interaction properties and surface 'pairs' are defined and which make contact. Dependent on the loading and rotation of the parts only some areas of the contact surfaces transfer forces. Six contact planes can be distinguished and are listed in Table 7, more explanation on the characteristics is given below.

Table 7: Contact surfaces and their properties

Master surface	Slave surface	Hard contact	Friction	Friction coefficient
Quoin post	Rear post	Yes	Yes	0.20
Quoin post	Seal strip	Yes	No	-
Rear post	Seal strip	Yes	Yes	1000
Tenon	Rear post	Yes	Yes	0.20
Tenon	Front post	Yes	Yes	0.20
Centre line	Front post	Yes	No	-

For every surface pair a master and slave surface must be defined. For the master surface a surface is created between the master nodes which cannot be penetrated by the slave nodes. For the standard 'node-to-surface' discretisation method the slave surface only makes contact with the master surface at discrete points at the slave nodes and the master surface can therefore penetrate the slave surface, as depicted in Figure 57. Therefore the largest, most stiff or the surface with the courser mesh should be chosen as the master surface then.

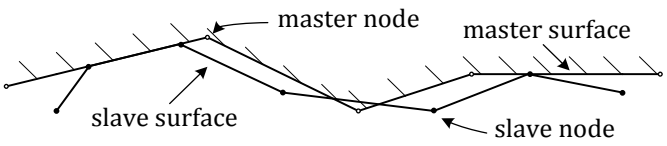

Figure 57: Master and slave surfaces. Note the master surface penetrates the slave surface.

The interaction of surfaces for the model build for this research is characterised by the discretisation method 'surface-to-surface' contact. Instead that the nodes on the slave surface make contact at discrete points with the master surface, both surfaces are considered. Therefore it is much less common that (large) parts of the master surface penetrate the slave surface. Especially near corners more accurate stress and pressure results are obtained using surface-to-surface contact.

Interaction at the contact surfaces are characterized by two interaction properties: 'hard contact' and isotropic Coulomb friction. To obtain a fixed connection between the rear post and seal strip a very large friction coefficient is applied.

Hard contact implies pressure stresses develops when the gap between surfaces is closed, when a gap is present no stresses develop as depicted in Figure 58. Separation after contact is allowed.

Friction is modelled according Coulomb friction and works isotropic over the surfaces. Coulomb friction is illustrated in Figure 59. In order to reduce numerical problems a small amount of elastic slip is allowed, indicated by the dashed line in Figure 59. The maximum allowable elastic slip is automatically chosen to be much smaller than the characteristic length of the elements used. It is assumed the maximum possible frictional force is not reached and therefore no shear stress limit is given.

The friction coefficients used are: (Engineer's Handbook, 2006)
Stone - wood: $\mu = 0.20$
Wood - wood (wet): $\mu = 0.20$
Fixed connection: $\mu = 1000$

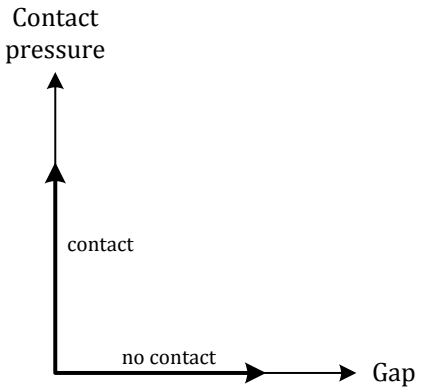

Figure 58: Definition 'hard contact'

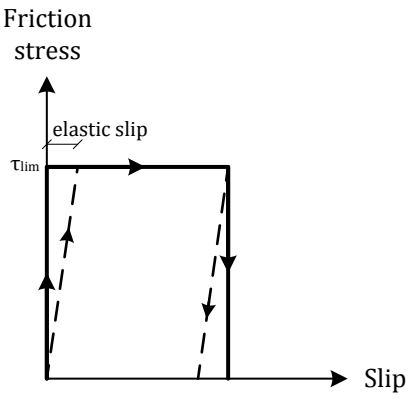

Figure 59: Definition Coulomb friction

To take into account the relative motion of two surfaces the approach 'small-sliding' is assumed. This approach assumes very little sliding occurs between the surfaces. The nodes which are in contact are identified once and are then fixed throughout the analysis. As linear elastic calculation is applied and no large deformations are to be expected the approach seems valid in this case.

4.5 MESH DESIGN

The design of a mesh can have large influence on the results en therefore care is taken with the design. When designing the mesh two main choices need to be made: which element type is used and how is the mesh shaped?

The element type used is a 4 node bilinear plane strain quadrilateral. Reduced integration and enhanced hourglass control are applied. The following considerations form the base for the choice for this element:

- For contact analysis' first order quadrilateral elements are recommended to obtain the best results;
- To prevent shear locking reduced integration is applied;
- When using reduced integration hourglass modes can appear. Therefore enhanced hourglass control is applied.

The element is characterised by its four nodes. For full integration, where the stiffness matrix is integrated exactly, 2 by 2 integration points are necessary. Because reduced integration is applied only one integration point is used, located in the middle of the element. Subsequently, to prevent hourglass modes, where a deformation mode not contributes to energy, enhanced hourglass control is applied.

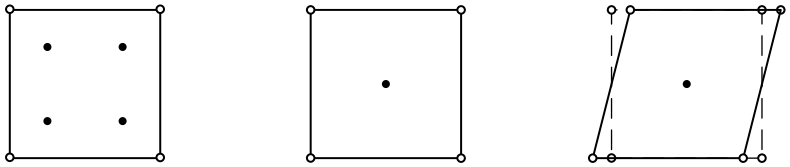

Figure 60: A 4 node bilinear plane strain quadrilateral with fltr; 2 by 2 integration points, reduced integration, an hourglass mode appearing.

The mesh used is depicted in Figure 61 to Figure 63. A fine mesh is chosen near the joint to obtain accurate results where a complex force distribution is present. A coarse mesh in the middle of the beam will reduce the model's size and is sufficient to determine bending and compression stresses at that location.

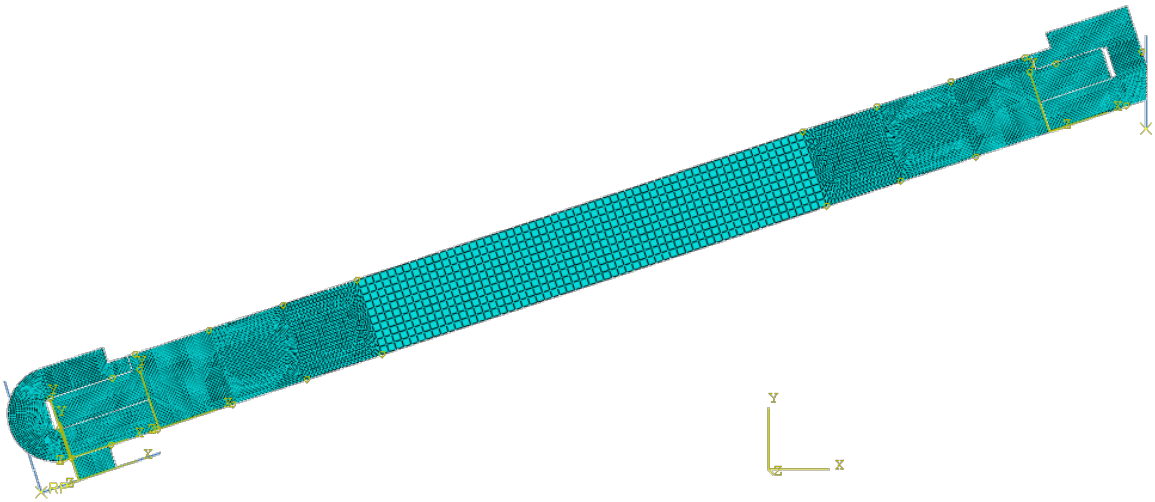

Figure 61: Overview model's mesh

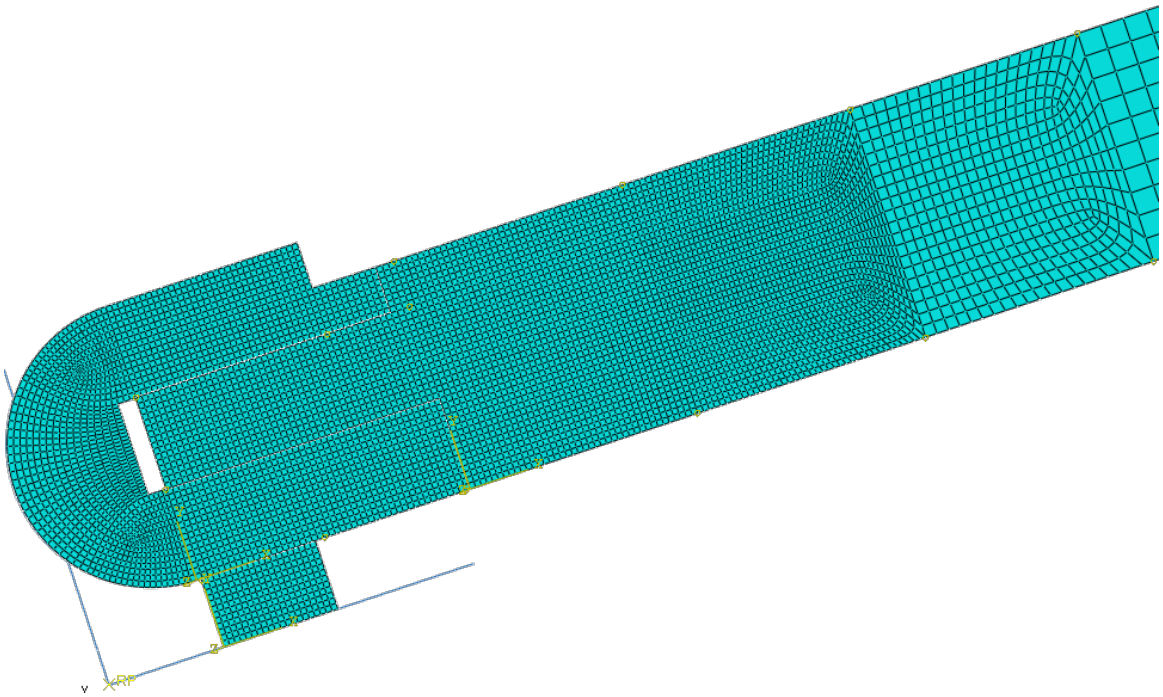

Figure 62: Overview mesh rear side of the gate (Note the different parts are difficult to distinguish but are modelled according Figure 55)

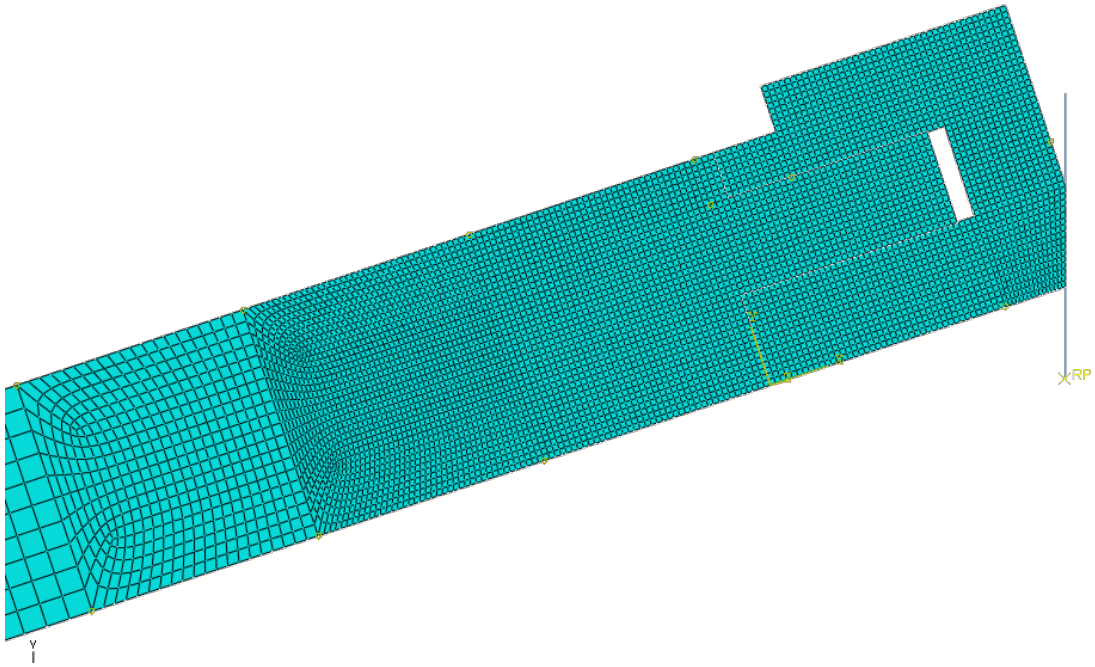

Figure 63: Overview mesh front side of the gate (Note the different parts are difficult to distinguish but are modelled according Figure 55)

4.6 ELASTIC SUPPORT STIFFNESS PARAMETER

The derivation of the stiffness parameter for the elastic support below the rear post is performed in paragraph 3.3.2. Below the value is determined which is used for the FE model, Figure 64 depicts the location where the elastic support is applied.

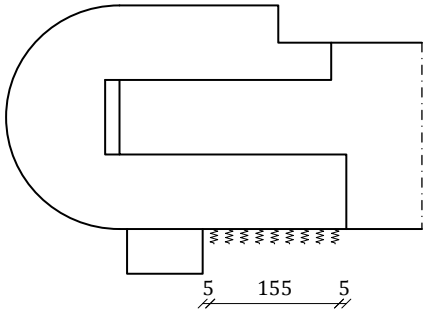

Figure 64: Location application elastic support (measures in mm)

The stiffness of the seal strip along the additional bearing length becomes:

$$k_a = \frac{E_{90} b_a h_{a,add}}{d_a} = 8.03 \cdot 10^7 \; N/m$$

where E_{90} is the modulus of elasticity perpendicular to the grain, $b_a h_{a,add}$ is the surface of the seal strip through which the force is transferred and d_a is the thickness of the seal strip.

The stiffness of the fictive beam below the mortise becomes:

$$k_b = \frac{qL^2}{-\frac{1}{80}\frac{qL^5}{EI} + \frac{1}{72}\frac{q(-12EI + L^2 GA_s)L^3}{EI\, GA_s} + \frac{1}{4}\frac{qL^3}{GA_s}} = 1.3483 \cdot 10^9 \; N/m$$

where $E = E_0$ is the modulus of elasticity along the grain, G is the shear modulus, $I = \frac{bd^3}{12}$ is the second moment of area fictive beam, $A_s = bd$ is the cross-sectional area fictive beam and L is the length of the fictive beam.

The total stiffness can then be calculated:

$$k_s = \frac{1}{\frac{1}{k_a} + \frac{1}{k_b}} = 7.5786 \cdot 10^7 \; N/m$$

The surface at which the elastic support works is equal to:

$$A_{elastic\ support} = 0.155 \cdot 0.300 = 0.0465 \; m^2$$

The stiffness parameter value entered in the model is:

$$k = \frac{k_s}{A_{elastic\ support}} = 1.6298 \cdot 10^9 \; N/m/m^2$$

5 FORCE DISTRIBUTION ACCORDING FINITE ELEMENT MODEL

In this chapter the results obtained by the finite element model, as described in the previous chapter, will be analysed and discussed.

The output data can be analysed in two ways. Firstly contour plots can be created by the post-processor within Abaqus. The contour plots give an impression of the magnitudes and spread of stresses. Secondly, at several sections the sectional forces are determined using Excel and stresses along the section are depicted in graphs using Matlab. Peak stresses at discontinuities such as at the pit under the tenon are not used for further analysis as the way of modelling is not appropriate to determine these stresses.

5.1 AMPLIFICATION OF THE FORCE DISTRIBUTION

For the analysis of the output of the finite element model three stages are distinguished:

1. Contour plots are analysed with which a global impression of the appearing stresses and the path the forces follow can be obtained.
2. For a number of sections the sectional forces are determined which indicate where the forces are transferred to.
3. For the same sections where sectional forces where determined for all stress components are depicted in graphs.

The sections mentioned under analysis stage 2 and 3 are illustrated in Figure 65.

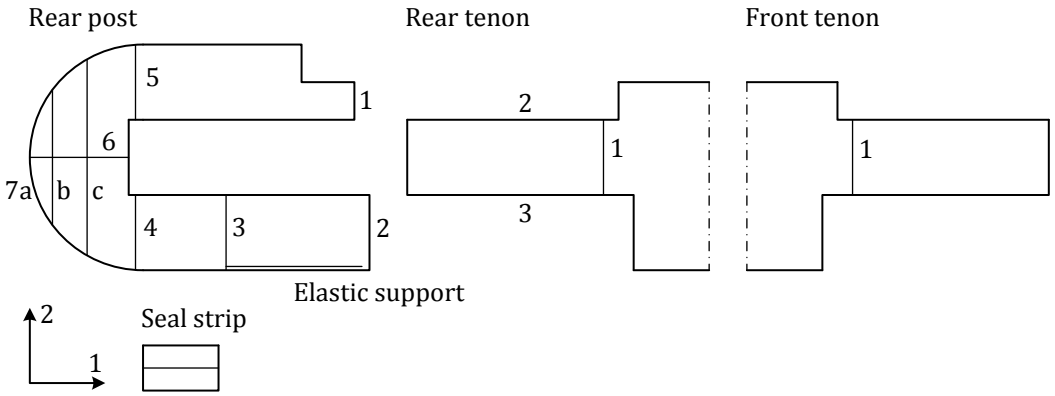

Figure 65: Analysed sections FE model

5.1.1 GLOBAL ANALYSIS USING CONTOUR PLOTS

Contour plots can be created by the post-processor within Abaqus. The contour plots for the model of the mortise and tenon joint are depicted in Figure 67 to Figure 69. Appendix C depicts the contour plots too, both with and without magnified deformations and in a larger size.

Within the 1-2 plane three stress components are present which are all included in the analysis; normal stress in the x direction S11, normal stress in the y direction S22 and the shear stress in the x-y plane S12. For the crossbeam these stress components correspond to receptively the normal stress along the grain, normal stress perpendicular to the grain and the shear stress. For the posts and seal strip these stress components correspond to twice the normal stress perpendicular to the grain and the rolling shear stress.

The orientation of the 1-2 coordinate system is depicted in Figure 66. Axis 1 runs parallel and axis 2 runs perpendicular to the normal axis of the crossbeam.

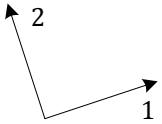

Figure 66: Coordinate system 1-2

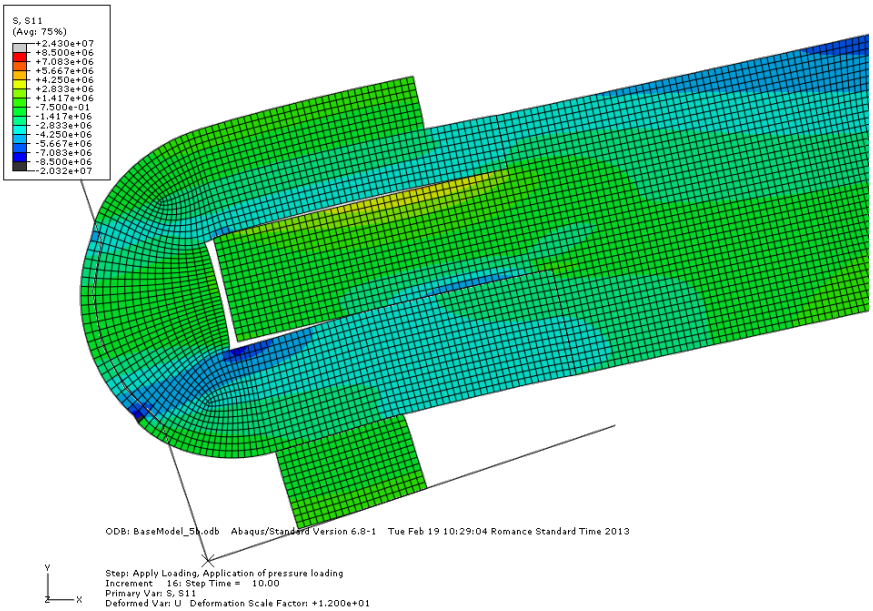

Figure 67: Contour plot of the stresses S11 for the mortise and tenon joint at the rear post (Unit is Pa = $N/mm^2 \cdot 10^6$, deformations scaled 10:1)

Figure 67 depicts a contour plot of the stresses S11 at the rear post. These are the normal stresses parallel to the 1-axis. For the crossbeam this stress component corresponds to the normal stress along the grain. For the rear post and seal strip these stress components correspond to the normal stress perpendicular to the grain.

From Figure 67 the following observations can be made:

- Both compression stresses parallel and perpendicular to the grain in the different parts seem to remain below critical values.
- The compression force from the crossbeam is transferred through the upper and lower parts of the rear post to the back of the rear post according about the ratio of sectional surfaces. The two forces are transferred in almost a straight line to the quoin post behind the upper and lower part of the rear post.
- That the compression stresses in the upper and lower part of the rear post are equal to each other can be understood by considering the strains are equal, caused by the relatively stiff crossbeam which deforms the rear post equally.
- A negative bending moment is present in the tenon. The tenon is in fact clamped into the mortise.

Figure 68 depicts a contour plot of the stresses S22 at the rear post. These are the normal stresses parallel to the 2-axis. For the crossbeam this stress component corresponds to the normal stress perpendicular to the grain. For the rear post and seal strip these stress components correspond to the normal stresses perpendicular to the grain.

From Figure 68 the following observations can be made:

- Behind the mortise high tension stresses have developed as the clamped tenon presses upwards on the rear post.
- Due to the large compression force being transferred on a concave surface, at the back of the rear post large compression stresses perpendicular to the grain develop. The compressive stresses are slightly higher than design strength, but taking the confined stress state into account, strength is estimated to be large enough.
- The upper end of the tenon is pressed against the mortise on a small surface. Therefore also relative high stresses develop here.
- A large part of the load is transferred via the elastic support and a smaller part via the seal strip as the spread of normal stress for the first mentioned part is much larger. It is remarkable that the values of the stress at both parts seem to be comparable.
- At the pit of the tenon relatively small tension stresses are visible.

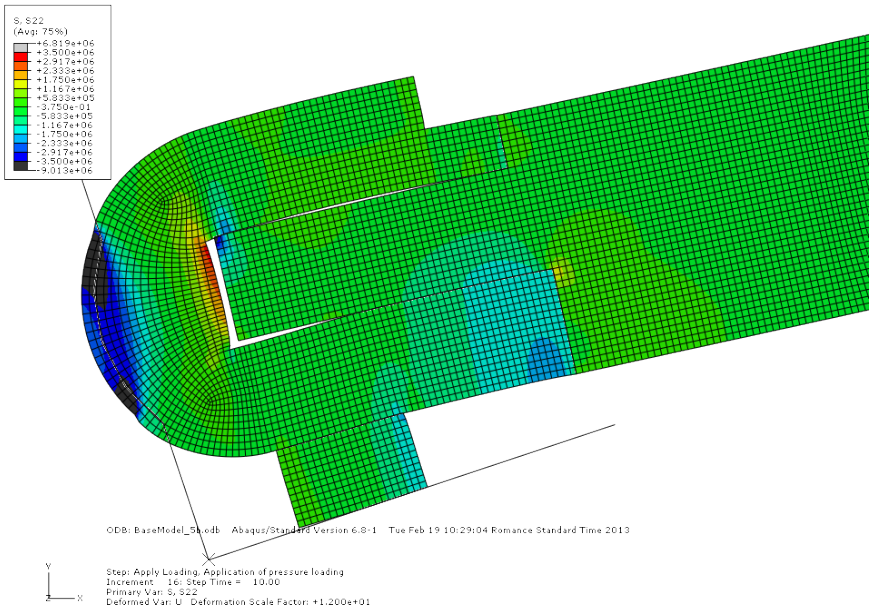

Figure 68: Contour plot of the stresses S22 for mortise and tenon joint at the rear post (Unit is Pa = $N/mm^2 \cdot 10^6$, deformations scaled 10:1)

Figure 69 depicts a contour plot of the stresses S12 at the rear post. These are the shear stresses in the 1-2 plane. For the crossbeam this stress component corresponds to the normal shear stress. For the rear post and seal strip these stress components correspond to the rolling shear stress.

From Figure 69 the following observations can be made:

- At the pit of the tenon relatively large shear stresses develop. Shear stresses actually have to occur, as the lower part of the beam is forced to bend along with the upper part of the beam.
- In the tenon it is clearly visible the shear force changes sign. The line of action of the reaction force on the tenon lies at the point where the shear force is equal to zero. The sign of the shear force also indicates a negative moment acts in the tenon.
- Due to the transfer of compression forces on a concave shape, at the lower back side of the rear post high shear stresses develop.
- As the tenon presses onto the top part of the rear post, shear stresses also develop in the upper part of the rear post.

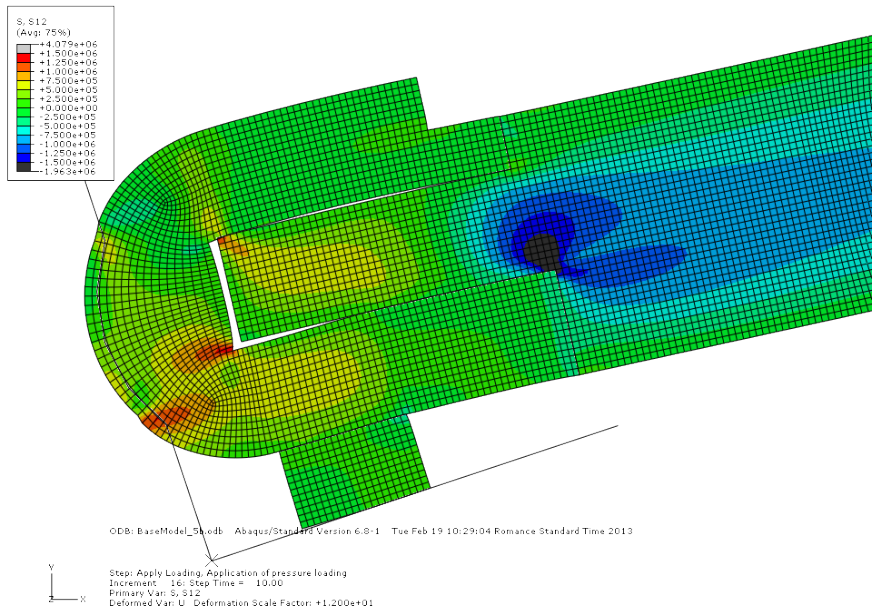

Figure 69: Contour plot of the stresses S12 for mortise and tenon joint at the rear post (Unit is Pa = N/mm² · 10⁶, deformations scaled 10:1)

5.1.2 ANALYSIS OF SECTIONAL FORCES

To further analyse the transfer of forces through the joint, at the sections depicted in Figure 65 the sectional forces are determined. Within Abaqus an output file is generated with the stresses S11, S22 and S12 for the given sections. Excel is then used to obtain sectional forces and lines of action. The results for the mortise and tenon joint are depicted in Figure 70. Results for some additional sections are listed in Table 8. In the following first some observations will be made after which some equilibrium checks are performed. The sectional forces subscribe global conclusions made on the contour plots in the previous paragraph.

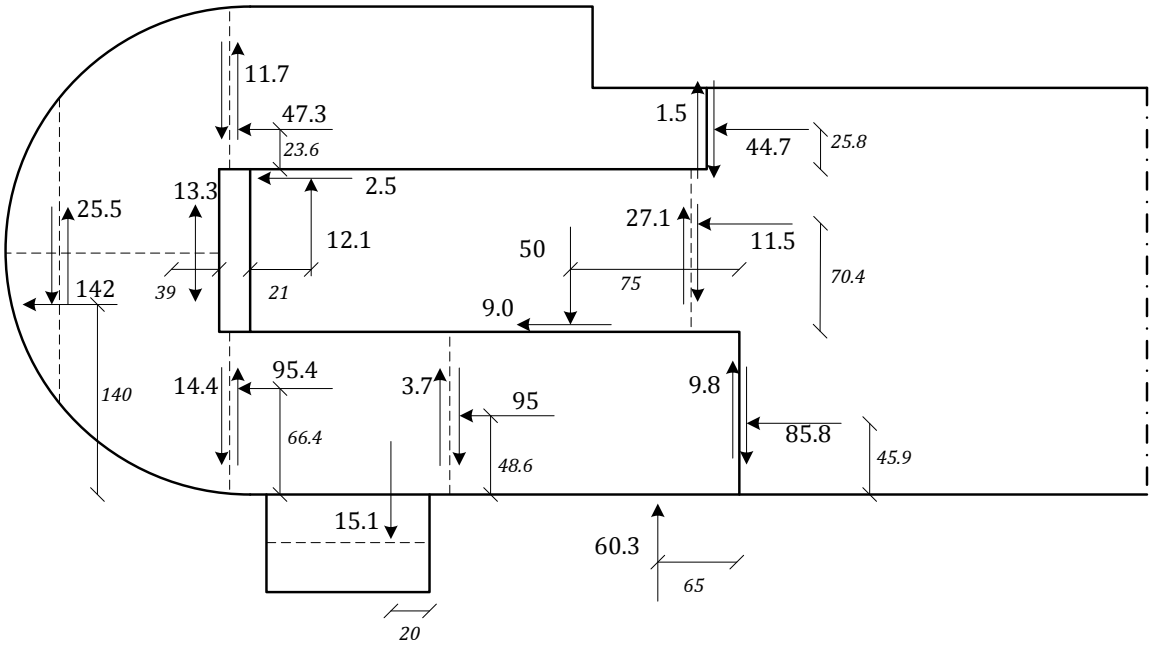

Figure 70: Sectional forces rear mortise and tenon joint (Forces indicated in kN, measures indicated in mm in a smaller font size)

Table 8: Sectional forces at additional sections

Location	Force	Value	Unity
Rear end crossbeam	Normal force	143	kN
	Shear force	50	kN
Mid-section crossbeam	Bending moment	54.5	kNm
	Normal force	143	kN
Front end crossbeam	Normal force	143	kN
	Shear force	47.5	kN
Front tenon	Shear force	38.7	kN

The compression force from the crossbeam is transferred through the upper and lower parts of the rear post to the back of the rear post according about the ratio of sectional surfaces. The ratio of sectional surfaces (lower / upper part rear post) is 100 mm / 50 mm and the compression force's ratio is 95 kN / 45 kN which corresponds well. It is also striking the compression force at section 5 of the rear post only changed height about 2 millimetres with respect to section 1 and is thus transferred along an almost straight line. In contrast to the assumption made in paragraph 3.2 the compression forces in the upper and lower part of the rear post do not bend off to the middle of the back of the rear post. The tension force behind the mortise is thus not caused by these compression forces. A part of the compression force from the crossbeam is transferred through the tenon and is transferred to the lower part of the rear post by friction.

The tension force behind the mortise is caused by the upward acting force the tenon exerts. It is however to be expected this tension force reduces when force transfer within 3D geometry is considered as the upward acting force can be transferred to a greater area.

Only a small part, about 20%, of the shear force is transferred via friction at the contact surfaces between the crossbeam and the rear post. The largest part, about 80%, is transferred via the tenon. Apparently transfer via the tenon reacts most stiff. Another explanation is that the further the line of action is removed from the seal strip, the greater the negative moment in the rear post must be to counteract the shift of the shear force. As a test for another model the friction coefficient was raised to 0.7 instead of 0.2. Even then the ratio's did not change significantly.

A large part of the shear force from the crossbeam is transferred through the elastic support and thus to the sides of the mortise after which eventually through the additional bearing length of the seal strip the load is transferred to the quoin post. A smaller part of the shear force is transferred to the quoin post directly via the seal strip. For this to happen the rear post needs to be fixed, as depicted in Figure 48, the frictional force at the back of the rear post is actually present according the FE-model. Paragraph 3.3.1 explains the resistance to rotation of the rear post elaborately.

For the checks of the equilibrium the following abbreviations are used: RP: rear post, SS: seal strip, RT: rear tenon, C: crossbeam, FT: front tenon, ES: elastic support and CL: Centre line. Further R: external reaction force, F: internal reaction force, V: shear force and N: normal force. The forces are numbered according to the section considered (Figure 65) and their direction within the 1-2 coordinate system (Figure 66). Example: the vertical force on section 4 of the rear post is named $F_{RP4,2}$.

Global equilibrium rear mortise and tenon joint
For the following calculations it is referred to Figure 70.

Horizontal equilibrium:

$$R_{RP7,1} = 142\ kN \approx 143\ kN = N_C$$

Vertical equilibrium:

$$R_{RP7,2} + V_C = 25.5 + 50 = 75.5\ kN \approx 75.4\ kN = 15.1 + 60.3 = R_{SS} + R_{ES}$$

The maximum frictional force at the back of the rear post is 0.2·142 = 28.4 kN which is higher than the force present.

Rear tenon
For the following calculations it is referred to Figure 71.

Horizontal equilibrium for the combination of the two parts:

$$N_C = 143\ kN \approx 142\ kN = 44.7 + 2.5 + 9 + 85.8 = F_{RP1,1} + F_{RT2,1} + F_{RT3,1} + F_{RP2,1}$$

Horizontal equilibrium of the middle area:

$$F_{RT2,1} = 2.5\ kN = 2.5\ kN = 11.5 - 9 = F_{RT1,1} + F_{RT3,1}$$

Horizontal equilibrium of the right part:

$$N_C = 143\ kN \approx 142\ kN = 44.7 + 11.5 + 85.8 = F_{RP1,1} + F_{RT1,1} + F_{RP2,1}$$

Vertical equilibrium for the combination of the two parts:

$$V_C = 50\ kN \approx 48.5\ kN = 1.5 + 50 - 12.8 + 9.8 = F_{RP1,2} + F_{RT3,2} - F_{RT2,2} + F_{RP2,2}$$

Vertical equilibrium of the middle area:

$$F_{RT3,2} - F_{RT2,2} = 50 - 12.8 = 37.2\ kN \approx 38.7\ kN = 50 - 1.5 - 9.8 = V_C - F_{RP1,2} - F_{RP2,2}$$

Vertical equilibrium for the combination of the two parts referring to Figure 70:

$$F_{RT3,2} - F_{RT2,2} = 50 - 12.8 = 37.2\ kN \approx 34.5\ kN = 27.1 + 7.4 = F_{RT1,2} + F_{RT3,2,right}$$

The force $F_{RT3,2,right}$ is transferred at section RT3 between the pit of the tenon and section RT1.

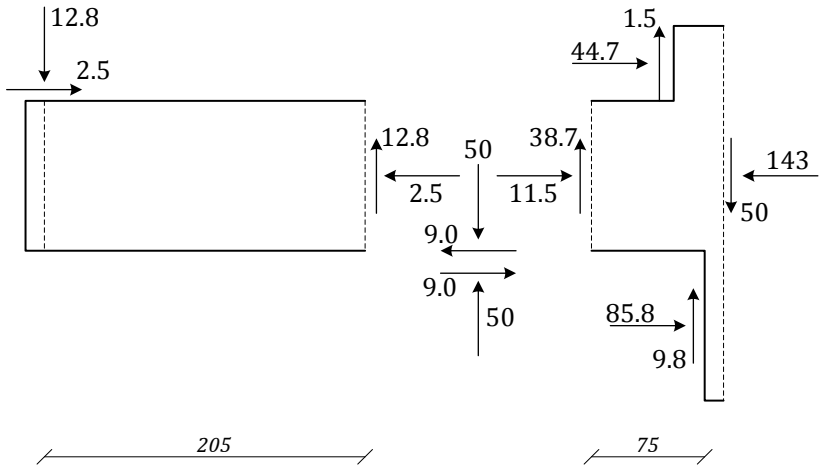

Figure 71: Force diagram rear tenon

Back rear post
For the following calculations it is referred to Figure 70.

Horizontal equilibrium:

$$R_{RP7,1} = 142\ kN \approx 143\ kN = 47.3 + 95.4 = F_{RP5,1} + F_{RP4,1}$$

Vertical equilibrium:

$$R_{RP7,2} = 25.5\ kN \approx 26.1\ kN = 11.7 + 14.4 = F_{RP5,2} + F_{RP4,2}$$

Lower right part rear post
For the following calculations it is referred to Figure 70.

Horizontal equilibrium:

$$F_{RP3,1} = 95\ kN \approx 94.8\ kN = 9 + 85.8 = F_{RT3,1} + F_{RP2,1}$$

Vertical equilibrium:

$$R_{ES} = 60.3\ kN \approx 63.5\ kN = 3.7 + 50 + 9.8 = F_{RP3,2} + F_{RT3,2} + F_{RP2,2}$$

Upper part rear post
For the following calculations it is referred to Figure 70.

Horizontal equilibrium:

$$F_{RP5,1} = 47.3\ kN \approx 47.2\ kN = 2.5 + 44.7 = F_{RT2,1} + F_{RP1,1}$$

Vertical equilibrium:

$$F_{RP5,2} = 11.5\ kN \approx 10.6\ kN = 12.1 - 1.5 = F_{RT2,2} + F_{RP1,2}$$

5.1.3 ANALYSIS OF STRESSES

For all sections indicated in Figure 65 the normal stresses (perpendicular to the grain) and (rolling) shear stresses are determined. For the most interesting sections the graphs are shown at convenient size and are explained in this paragraph. All graphs are shown at large size in Appendix C. The horizontal axis for each graph indicates the section's length from left to right or from down to up for the respective sections. Tension stresses are positive and compressive stresses are negative.

For design strength values of the timber it is referred to Table 4.

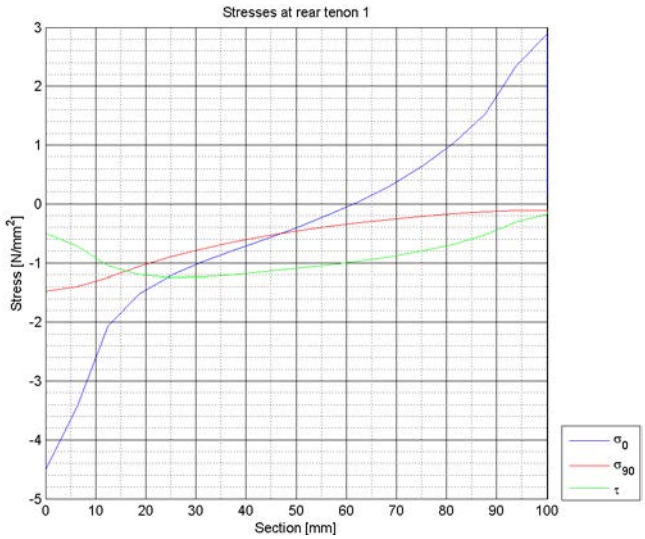

Figure 72: Stresses at section rear tenon 1

Figure 72 depicts the stresses on the section rear tenon 1. A common shape for the normal and shear stresses can be distinguished for a bending moment. A negative moment is present as tension stresses act on the upper part and compression stresses act on the lower part of the tenon. As at the location of the section already vertical load is transferred to the rear post compression stresses perpendicular to the grain are present too. All values of stresses are well below design values.

Figure 73 depicts the stresses on the section rear tenon 2. Only at the very end of the tenon (beginning of the axis in the figure) large compressive stresses perpendicular to the grain

and shear stresses are present. As the tenon is clamped into the mortise at the upper end contact is made here. It can also be seen a negative moment is present for about the whole length of the tenon as the normal stress parallel to the grain is positive. All values of stresses are well below design values.

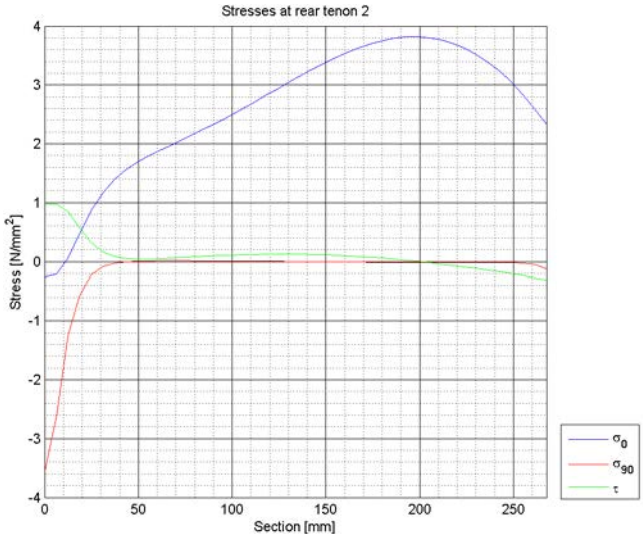

Figure 73: Stresses at section rear tenon 2

Figure 74 depicts the stresses on the section rear tenon 3. From the distribution of compressive stress perpendicular to the grain is can be seen the vertical load from the tenon is transferred quite close to the pit of the tenon. Again it is visible a negative moment is present for about the whole length of the tenon as the normal stress parallel to the grain is negative. Due to the discontinuity at the pit of the tenon the shear stress becomes considerably high. Ignoring the singularity effect of the shear stress again all values of stresses are below design values.

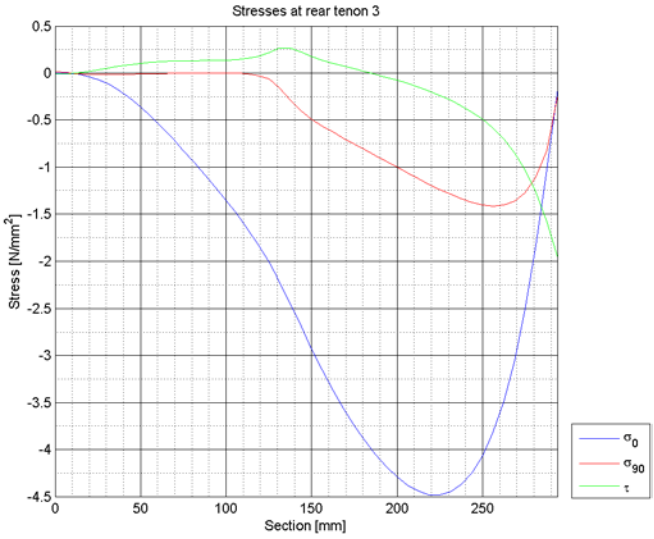

Figure 74: Stresses at section rear tenon 3

Figure 75 depicts stresses along the elastic support. As the elastic support is a "trick" to include the 3D effect in the 2D analysis the stresses are not actually present. These stresses are of interest to check if the result is valid. Along the entire support compressive stresses in the 2-direction are present which are relatively high over a significant length. That the rear post rotates around the seal strip is well noticeable on the increase of stress further from the seal strip. The normal stress in the 1-direction increases as compressive force is transferred from the tenon to the lower part of the rear post by friction.

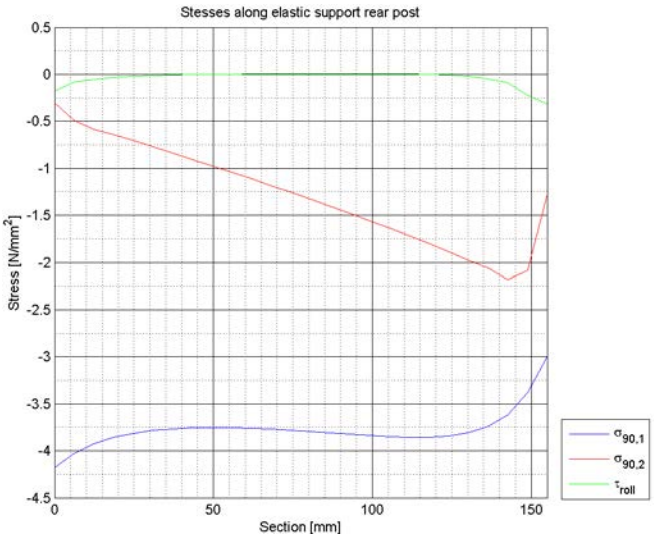

Figure 75: Stresses at section elastic support

Figure 76 depicts stresses along the elastic support. Most of interest is the normal stress perpendicular to the grain in the 2-direction. Due to the transfer of compression forces on a concave support compressive stresses develop close to the support. Near the mortise high tension stresses develop due to the upward pressing tenon in the mortise. As mentioned, it is to be expected these tension stresses reduce when force transfer within 3D geometry is considered as the upward acting force can then be transferred to a greater area.

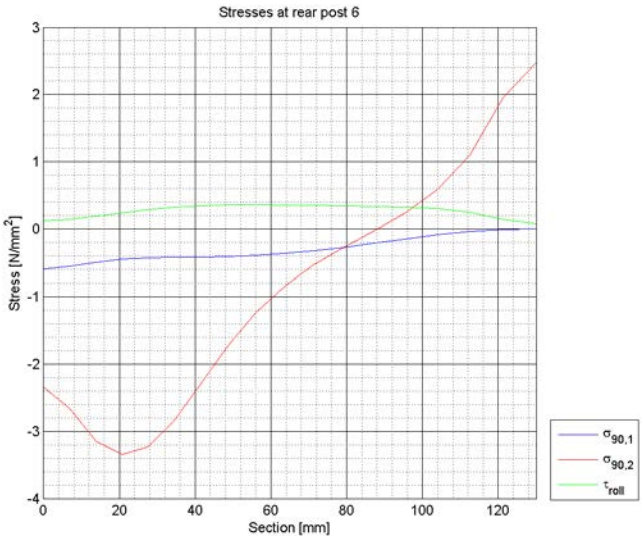

Figure 76: Stresses at section rear post 6

Figure 77 depicts stresses along rear post 7c. Very well noticeable is the transfer of the compression force via the upper and lower part of the rear post. The compression force through the lower part of the rear post is twice as large as through the upper part which can also be noticed by the larger and wider stress distribution at the lower part. Compressive stresses perpendicular to the grain are well below design values. The rolling shear stress at the lower part of the rear post adopts too high values. These peaks are restricted to a small length of 30 mm though.

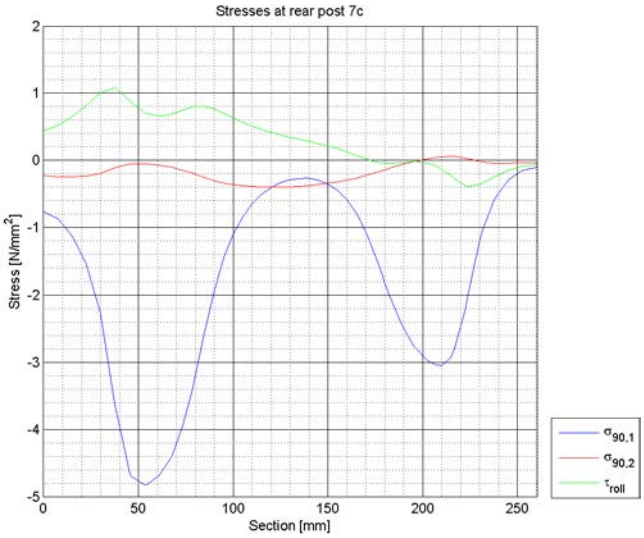

Figure 77: Stresses at section rear post 7

In general from the graphs it can be seen stresses do not exceed design strength values. Ignoring singular effects near discontinuities, only the rolling shear strength at the lower back side of the rear post and the tension strength perpendicular to the grain behind the mortise are exceeded. The areas where these stresses are exceeded are however that small, that due to size-effects it is estimated no failure will occur.

5.2 CONCLUSIONS ON FORCE DISTRIBUTION

For a wooden mitre gate designed according traditional dimensions the following conclusions can be drawn from the statements made in the previous paragraphs.

Conclusions relating to the force transfer:

- A large part of the shear force from the crossbeam, about 80%, is transferred through the tenon. About 20% is transferred via friction at the square contact surfaces between the crossbeam and the rear post.

- A potentially high friction coefficient between the crossbeam and rear post due to interlocking grains does not increase the percentage of shear force transferred via friction.

- A 3D effect is present in the joint whereby a part of the load is transferred to the sides of the mortise after which the load is transferred to the seal strip through the full section of the rear post.

- Due to the 3D effect the line of action of the reaction force on the tenon lies closer to the pit of the tenon than the line of action of the reaction force at the seal strip support does. At approximately one third of the tenon length the shear force is transferred from the tenon to the rear post according the 2D model.

- The reaction force from the tenon introduces a negative moment in the rear post as its line of action does not coincide with the line of action of the reaction force at the seal strip support. The tenon is clamped into the mortise and at the back of the rear post a frictional force at the concave support counteracts the negative moment.

- At the pit of the tenon relatively small tension stresses and relatively large shear stresses develop.

- The compression force from the crossbeam is transferred through the upper and lower parts of the rear post to the support at the back of the rear post according the ratio of sectional surfaces of the upper and lower part. The two forces are transferred in almost a straight line to the quoin post behind the upper and lower part of the rear post.

- Ignoring singular effects near discontinuities within the finite element model's results, appearing stresses throughout the joint satisfy design strength values.

- The following critical areas are identified:
  - behind the mortise high tension stresses have developed as the clamped tenon presses upwards on the rear post.
  - at the lower back side of the rear post high shear stresses develop due to the transfer of compression forces on a concave shape.

  Due to expected 3D effects, the small size of the critical locations and the limited extend in which design strength values are exceeded the critical areas are determined to satisfy strength requirements.

6 ANALYSIS HARDWOOD TENON

In paragraph 2.4.1 the theoretical background of the expression for the reduced strength of notched beams is amplified on. In this chapter a similar theoretical analysis for a tenonned beam is performed. First a theoretical basic expression for tenonned beams is derived after which some aspects of this expression are researched further and several methods to model tenon strength are identified. These expression can then be compared with experimental results in chapter 8.

6.1 ADAPTED THEORETICAL BASIC EXPRESSION FOR TENON STRENGTH

The derivation of a theoretical basic expression for the strength of tenonned beams (TET) is for a large part equal to the derivation of the theoretical basic expression for notched beams (TEN) from paragraph 2.4.1. This derivation starts after the energy balance for a notched beam, equation [2] from paragraph 2.4.1, is formed. This energy balance is obtained in precisely the same way for a beam with a tenon on its ends when Figure 32 is replaced by Figure 78. The average shear stress at which the change of potential energy for the system is equal to the fracture energy per crack area is given by equation [14].

$$\frac{V_f}{b\alpha d} = \sqrt{\frac{2G_c}{b\alpha^2 d} \cdot \frac{1}{\frac{d\left(\frac{\delta}{V}\right)}{d\beta}}} \qquad [14]$$

where V_f [N] is the shear force at which a crack will develop, b [m] is the width of the beam, d [mm] is the full height of the beam, δ [mm] is the deflection at the line of action of the reaction force and G_c [N/m] is the fracture energy per crack area. The ratios α and β are defined in Figure 78. For a tenon the variable γ needs to be defined which indicates the height at which the tenon is located.

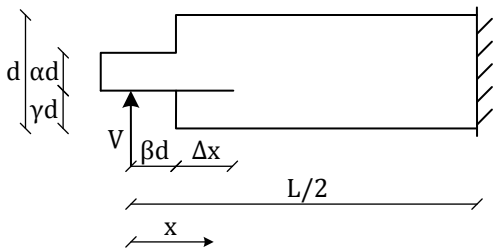

Figure 78: Symmetric half of a tenonned beam

The deflection of a tenonned beam at the line of action of the reaction force is different with respect to a notched beam. Therefore to determine the variation of the compliance δ/V with β the deflection of the beam needs to be calculated again, taking the tenon into account instead of a notch.

The beam's deflection consists of four terms where the total deflection is equal to the summation of those terms: $\delta_{total} = \delta_l + \delta_v + \delta_r + \delta_b$.

δ_l is the local deformation of the timber at the supports and point of loading. Because δ_l is not dependent on β, it does not need to be calculated.

δ_v is the shear deformation of the beam. According linear elastic theory the deflection can be determined by the following equation where the result depends among other variables on β:

$$\delta_v = \frac{1.2V}{G_{xy}}\left[\frac{\beta d}{b\alpha d} + \frac{\frac{l}{2} - \beta d}{bd}\right]$$

where G_{xy} [N/m^2] is the shear modulus.

δ_b is the ordinary bending deformation of the beam. According linear elastic theory the following expression can be derived:

$$\delta_b = \frac{V}{E_x \frac{bd^3}{12}}\left[\frac{l^3}{24} + \frac{(\beta d)^3}{3}\left(\frac{1}{\alpha^3} - 1\right)\right]$$

where E_x [N/m^2] is the modulus of elasticity parallel to the grain.

The terms δ_l, δ_v and δ_b are not changed with respect to the notch considered in paragraph 2.4.1 when the definitions for a tenon from Figure 78 are used. However, an important note is that when the crack is growing the formula's for δ_v and δ_b, as mentioned above, are not valid anymore. The remaining beam's height above the crack is larger along the length Δx in Figure 78 than the tenon's height alone. However, for a tenon cantilever length of βd the equations do apply at the moment the crack starts to grow.

The increase of deflection originating at the discontinuity at the end of the notch or tenon is referred to as δ_r. For both a notch and a tenon, which are "clamped" into the full-size beam, only after some distance from the discontinuity the normal stresses by bending extend over the full height of the beam (Figure 40). Close to the change of cross section the full bending capacity of the full-size beam is not fully activated and some extra deflection develops than when common linear elastic theory is used.

As is depicted in Figure 40 the different geometries of a notched beam and a tenonned beam will result in a different normal stress distribution and therefore different values of δ_r. The figure depicts designs for which b, d and α have equal values according the definitions of Figure 32 and Figure 78.

It is assumed δ_r varies linearly with both the moment $V \cdot \beta d$ and the length of the cantilever βd:

$$\delta_r = V\beta d \cdot c \cdot \beta d = Vc\beta^2 d^2$$

In fact, by this adding the deflection δ_r a fictive moment spring is placed at the discontinuity: multiplying the factor c [(Nm)$^{-1}$] with the moment, causes a rotation, which results in the deflection δ_r when multiplied with the cantilever length. Obviously for a tenonned beam a different expression for c needs to be chosen than was chosen for a notch in paragraph 2.4.1.

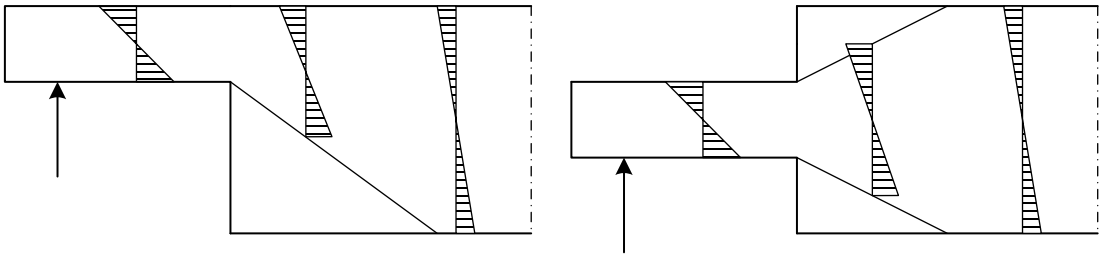

Figure 79: Simplified normal stress distribution for a notch and a tenon close to the discontinuity

The factor c thus introduces the influence of tenon geometry on stresses and strains near the transition from tenon to beam. The factor c depends on α, γ, the modulus of elasticity and the shear modulus. For a tenon no analytical expression could be obtained and the background of the chosen expression for c for notched beams could not be retrieved. In paragraph 6.3 the phenomenon is investigated further using approximations.

When c is left in the equation the compliance becomes:

$$\frac{\delta}{V} = \frac{\delta_l + \delta_v + \delta_r + \delta_b}{V} = \frac{1.2}{G_{xy}}\left(\frac{\beta d}{b\alpha d} + \frac{\frac{l}{2} - \beta d}{bd}\right) + c\beta^2 d^2 + \frac{12}{E_x b d^3}\left(\frac{l^3}{24} + \frac{(\beta d)^3}{3}\left(\frac{1}{\alpha^3} - 1\right)\right)$$

Taking the derivative of the compliance with β, simply filling the result into equation [14] and replacing the material dependent fracture energy per crack area G_c with fracture energy in pure tensile spitting perpendicular to the grain $G_{f,y}$ the result is a theoretical basic expression applicable to tenonned beams (TET):

$$\frac{V_f}{\mathrm{b\alpha d}} = \sqrt{2}\sqrt{\frac{G_{f,y}}{b\alpha^2 d\left(\frac{1.2\left(\frac{1}{b\alpha} - \frac{1}{b}\right)}{G} + 2c\beta d^2 + \frac{12\beta^2\left(\frac{1}{\alpha^3} - 1\right)}{Eb}\right)}} \qquad [15]$$

where V_f [N] is the shear force, b [m] is the width of the beam, $G_{f,y}$ [N/m] is the fracture energy in pure tensile spitting perpendicular to the grain, G_{xy} [N/m²] is the shear modulus and E_x [N/m²] is the modulus of elasticity parallel to the grain. In Figure 78 α [-], β [-] and d [m] are indicated.

The only difference with TEN is that c is left into the expression and the expression is not reformulated by moving variables. Indicative material properties for the strength of a tenonned beam are the fracture energy, modulus of elasticity and the shear modulus.

6.2 Fracture energy for hardwood

The fracture energy for softwoods was researched extensively by Larsen and Gustaffson (1990). A similar research project has not (yet) been performed for hardwood. In fact, very little, to nothing, is known about the fracture energy of hardwoods.

Figure 80 again depicts the results Larsen and Gustaffson found for the fracture energy of softwoods. It can be seen the largest densities lie between 700 and 800 kg/m³. These values are large enough to assume with some certainty the indicated regression line accounts for densities around a 1000 kg/m³ too. Further the cloud of test results seem to suggest for higher densities the fracture energy increases more than linearly. However, two important notes need to be made in this respect. Firstly, when a closer look is taken on the distribution of the results per individual test series, it is noticeable the scatter of the results is very large. The suggested regression line then seems to hold no more. Secondly, the tests are all performed on softwoods while hardwood is considered for this research. As the microstructure of softwoods and (especially tropical) hardwoods differ in important aspects like cell wall thickness and rays it is likely to expect differences in fracture energy value.

In the following the fracture energy for hardwood is determined in two ways:

1. The regression line from Larsen and Gustaffson (1990) is used. It is thus assumed this relation holds for tropical hardwood with densities around a 1000 kg/m^3.
2. From the test results from Vermeij (2011) on notched Azobé beams, for which TEN is quite reliable, the fracture energy can be calculated.

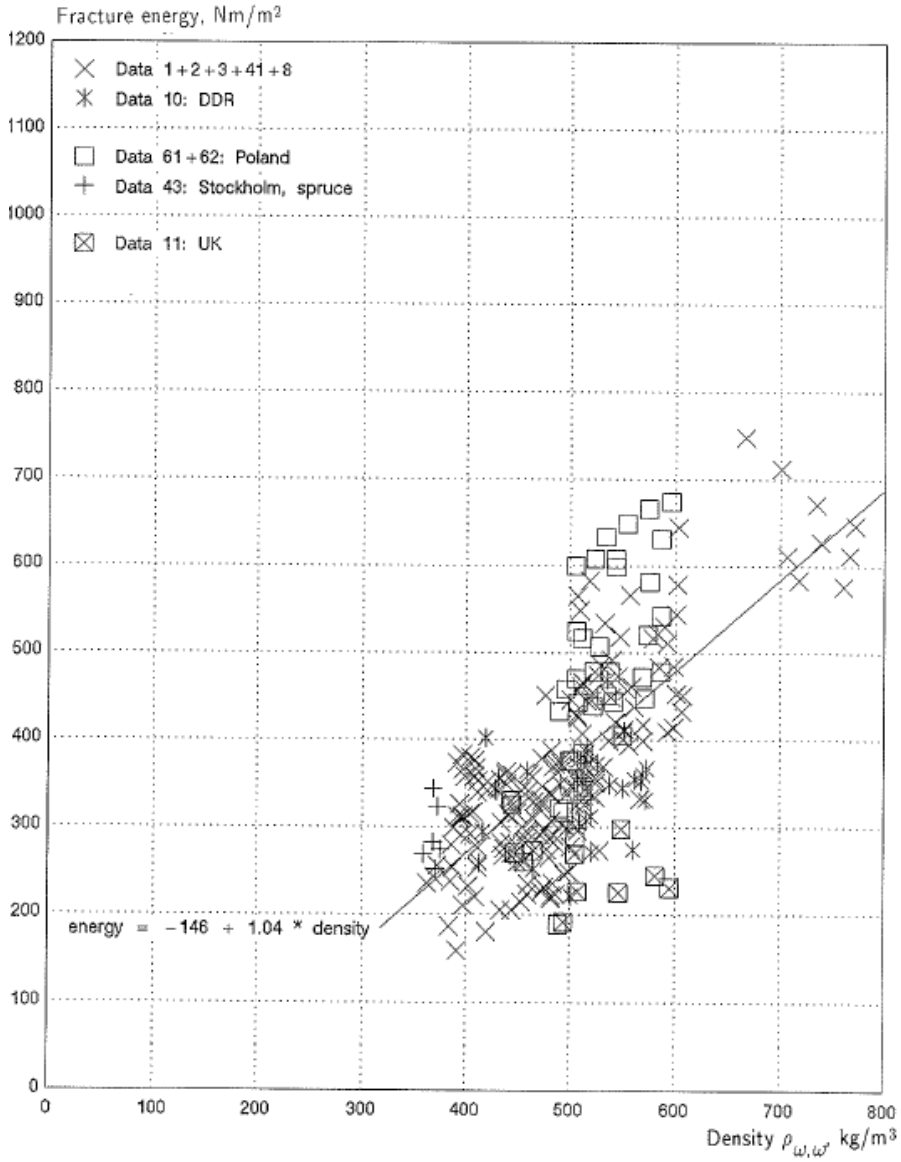

Figure 80: Fracture energy verses density for European softwoods regarded as one population (Source: Larsen and Gustaffson (1990), Fig. 5)

6.3 STRESSES AND DISPLACEMENT NEAR DISCONTINUITY TENON

To approximate the development of stresses and displacement near the discontinuity in a tenonned beam different options are possible:

1. Complete theoretical description

Analogue to the derivation of TEN a analytically determined factor c could be derived for a tenonned beam. This is preferred as the obtained theoretical expression TET then is complete and theoretically correct. However, the derivation of the factor c for a notched beam is not explained by Gustafsson (1988) and it has not been managed within this research to explain the factor c for a notched beam or to derive a factor c for a tenonned beam.

2. Common linear elastic theory

It could be decided to ignore the phenomenon of development of stresses near the discontinuity of the tenon. Then common linear elastic theory is used to obtain TET and a certain factor could be introduced to account for the phenomenon which will be determined by tests on tenonned beams.

3. Investigation of the development of stresses

Using FEM the development of stresses near the discontinuity could be investigated. When this development is found the reduction of stiffness can be calculated.

4. Investigation of the development of deflection

Using FEM the development of deflection of the tenonned beam can be determined. This development can then be compared with the deflection calculated according linear elastic theory.

Method 2 is performed in chapter 8. Method 3 and 4 will be explained further below.

INVESTIGATION OF THE DEVELOPMENT OF STRESSES

To investigate the development of stresses a FE-model was constructed according the FEM properties explained in paragraph 4.2 to 4.4. The model is designed according the test pieces used by Vermeij (2011) which is depicted in Figure 81 and explained further in paragraph 7.1.

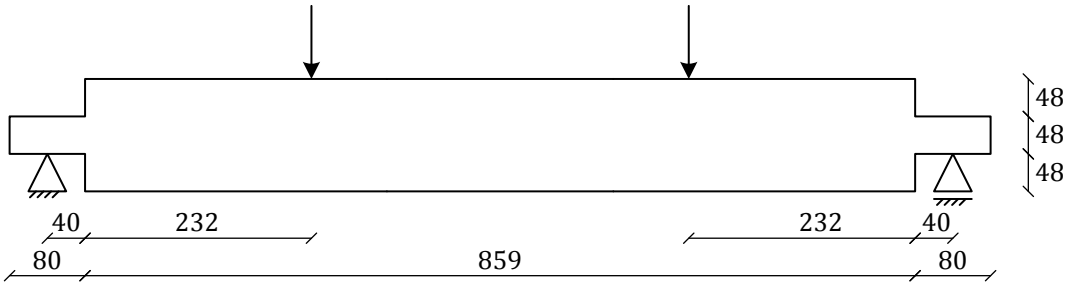

Figure 81: Model for the investigation of the development of stresses after the discontinuity at the tenon (dimensions in mm)

At intervals of 6 and further on 14 mm a section is created where the normal stress normal to the beam's axis is determined. Figure 82 depicts three of those sections at 3, 57 and 145 mm from the tenon. It can be clearly seen the stresses spread out further away from the tenon. In the most left graph it is clear that the bending stresses are only present between 48 and 96 mm of the section which is the tenon height. In the most right graph a common bending stress diagram is obtained. As the bending moment increases until the first point load is reached, the surface below the diagrams do not need to be equal to each other.

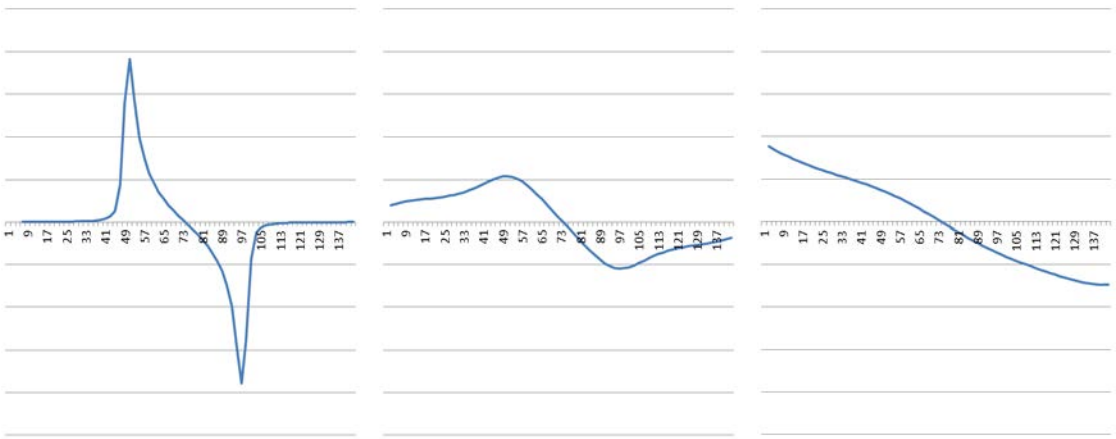

Figure 82: Normal stresses at sections at 3, 57 and 145 mm from the tenon

In order to obtain a fictive height of the beam at all sections the following calculations are performed, Figure 83 visualizes the variables. First the stress at every FE-element is multiplied with the surface of the element for half the section. Summation then gives the equivalent force at the lower half of the section:

$$dF_i = \sigma_i A_i$$
$$F = \sum dF_i$$

The equivalent forces per element are then multiplied with the distance of the element with the lower side of the beam. These values are summed up and divided by the equivalent force by which the distance of the line of action of the equivalent from the lower side of the beam is obtained.

$$dM_i = dF_i a_i$$
$$a_z = \frac{\sum dM_i}{F}$$

Assuming a common linear bending stress diagram the fictive height of the beam for each section can be calculated by:

$$h_f = \frac{6}{4}(h - 2a_z)$$

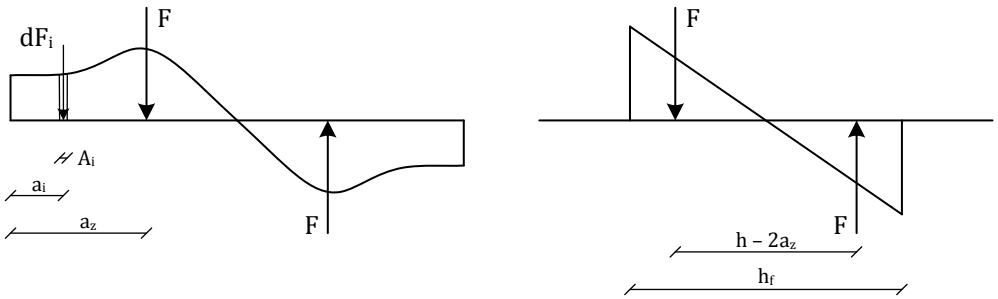

Figure 83: Calculation of the fictive height per section

When the fictive height for every section is put into a graph, Figure 84 is obtained. The fictive height of the beam increases linearly, closer to the range of influence of the point load the result start to deviate from the linear relation. A regression line is added to obtain the function of the line.

The fictive height of the beam needs to begin at 48 mm, the tenon's height, and end at 144 mm, the beam's height. Using the regression line the length is obtained after which the full height of the beam is utilized:

$$\frac{(144 - 48)}{4.8484} = 198\ mm$$

Using the results from above a fictive additional length of the tenon can be calculated. Keeping the surface of the beam geometry constant the additional tenon length becomes:

$$x_{add} = \frac{\frac{1}{2}(144 - 48) \cdot 198}{2 \cdot 48} = 99\ mm$$

By adding x_{add} to x the influence of the factor c is approximated within TET.

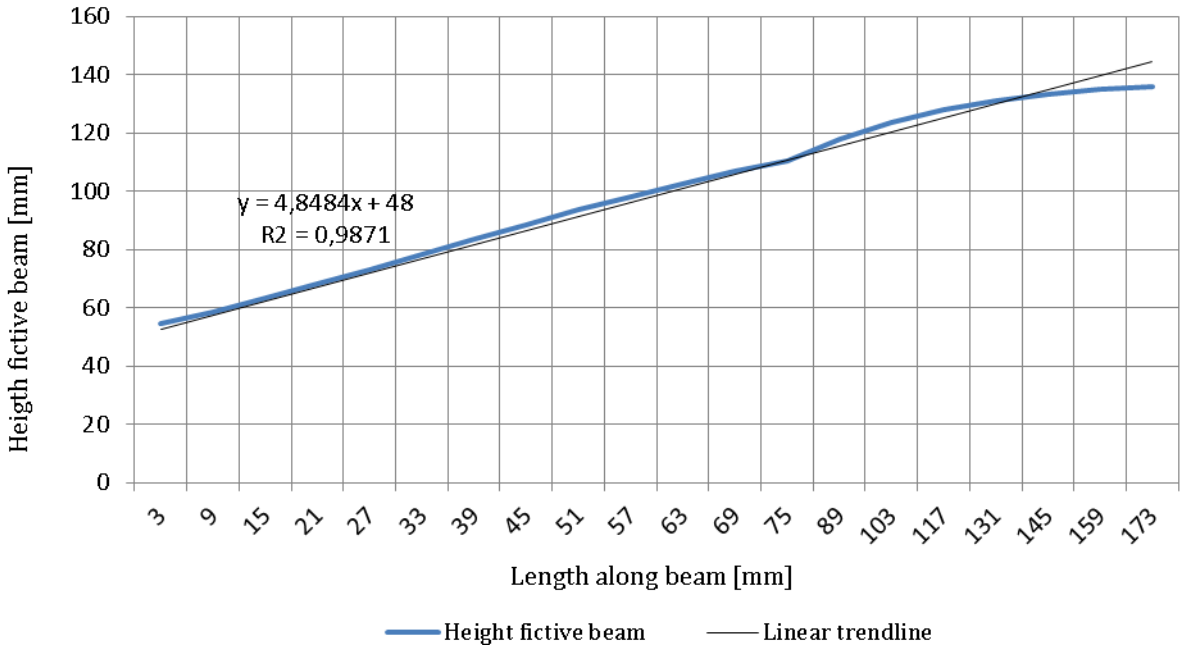

Figure 84: Height fictive beam vs. length along the beam (starting from the discontinuity)

INVESTIGATION OF THE DEVELOPMENT OF DEFLECTION

Using the same model as for the investigation of the development of stresses, the deflection along the beam is researched. The deflection according the FE-model is compared to the deflection obtained by solving the differential equation for a Timoshenko beam. The latter results does not take the stress distribution near the discontinuity into account.

The differential equation for a Timoshenko beam is derived in Appendix B. To solve the differential equation the symmetric half of the beam is cut in three parts, as depicted in Figure 85. The boundary conditions used are:

$$v_1(0) = 0 \text{ and } \mathrm{EI}\frac{\mathrm{d}\varphi_1}{\mathrm{dx}}(0) = 0$$

$$v_1(L_1) = v_2(L_1),\ \varphi_1(\mathrm{L}_1) = \varphi_2(\mathrm{L}_1),\ \mathrm{EI}\frac{\mathrm{d}\varphi_1}{\mathrm{dx}}(L_1) = \mathrm{EI}\frac{\mathrm{d}\varphi_2}{\mathrm{dx}}(L_1) \text{ and}$$
$$GA_s\left(\frac{\mathrm{dv}_1}{\mathrm{dx}}(L_1) - \varphi_1(\mathrm{L}_1)\right) = GA_s\left(\frac{\mathrm{dv}_2}{\mathrm{dx}}(L_1) - \varphi_2(\mathrm{L}_1)\right)$$

$$v_2(L_2) = v_3(L_2),\ \varphi_2(\mathrm{L}_2) = \varphi_3(\mathrm{L}_2),\ \mathrm{EI}\frac{\mathrm{d}\varphi_2}{\mathrm{dx}}(L_2) = \mathrm{EI}\frac{\mathrm{d}\varphi_3}{\mathrm{dx}}(L_2) \text{ and}$$
$$-GA_s\left(\frac{\mathrm{dv}_2}{\mathrm{dx}}(L_2) - \varphi_2(\mathrm{L}_2)\right) + GA_s\left(\frac{\mathrm{dv}_3}{\mathrm{dx}}(L_2) - \varphi_3(\mathrm{L}_2)\right) - F = 0$$

$$\varphi_3(L_{mid}) = 0 \text{ and } GA_s\left(\frac{\mathrm{dv}_3}{\mathrm{dx}}(L_{mid}) - \varphi_3(\mathrm{L}_{\mathrm{mid}})\right)$$

where $v(z)$ [m] is the deflection along the z-axis, $\varphi(z)$ [-] is the rotation along the z-axis, $E = E_0$ [N/m²] is the modulus of elasticity along the grain, G [N/m²] is the shear modulus, $I = \frac{bd^3}{12}$ [m⁴] is the second moment of area of the fictive beam and $A_s = bd$ [m²] is the cross-sectional area fictive beam

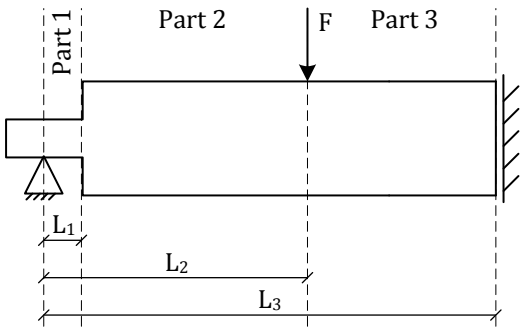

Figure 85: Symmetric half of the beam

Solving the differential equation using the boundary conditions from above, three expressions for the deflection are obtained for the three parts of the beam. These expressions are depicted in Figure 86 where the deflection according the FE-model and the difference between the two are also depicted.

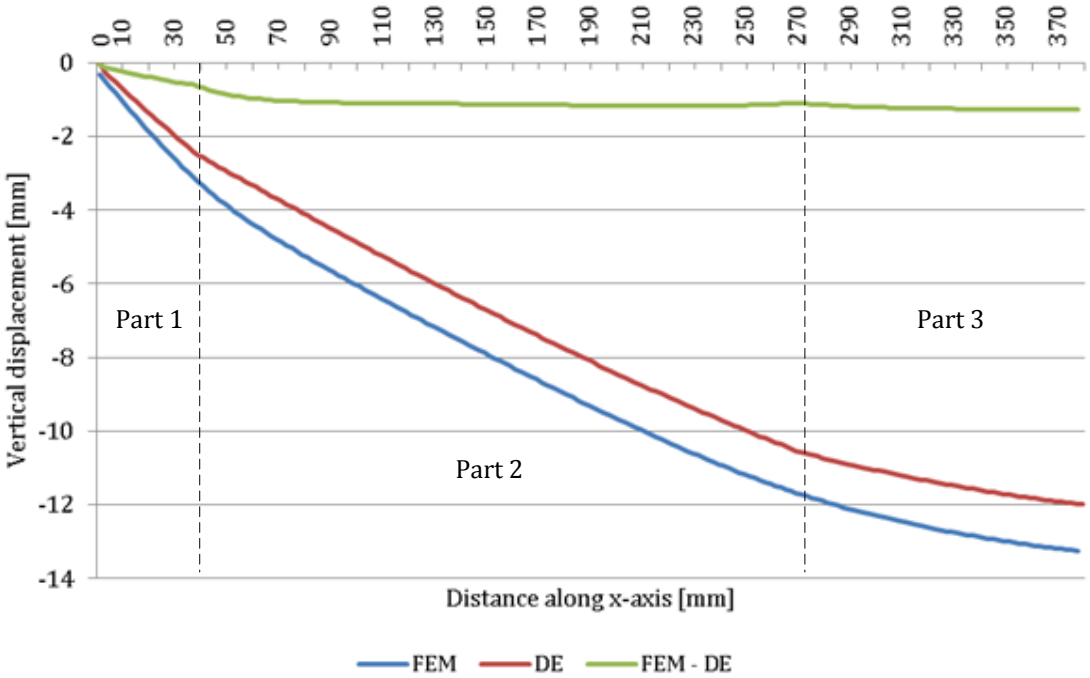

Figure 86: Comparison of the vertical displacement according FE-model and differential equation

From Figure 86 the following observations can be made: along the tenon the difference between the two equations increases approximately linearly. From the discontinuity the difference increases after which a constant but small difference increase remains present. The difference increase remains constant after about 120 mm. This increase is however that small, the two deflection curves can be considered parallel from then on.

The slope of the line "FEM – DE" is depicted in Figure 87. The additional length of the tenon, obtained in the investigation of the development of stresses, can be added to the actual tenon length after which a total fictive length of the tenon follows of $x_f = 40 + 99 = 139$ mm. The value of the slope at this length is equal to the boundary which the slope of the line "FEM – DE" approaches. The two investigations to the fictive tenon length, which takes the influence of the transition from tenon to beam into account, result in a comparable result.

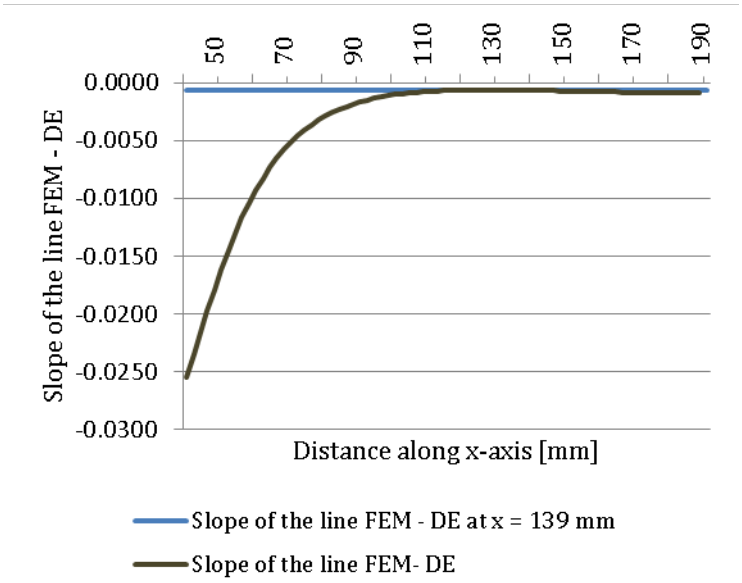

Figure 87: Slope of the line "FEM - DE"

6.4 MODEL FORMULA'S TO BE COMPARED WITH TEST RESULTS

To be compared with test results following formulas are listed:

The first and most obvious formula which will be compared with test results is the expression stated by paragraph 6.5.2 from Eurocode 5 (NEN-EN 1995-1-1, 2005) for the calculation of the strength of notched beams. To be able to compare the obtained values the formula is rewritten in the following form:

$$\frac{V}{b\alpha d} = \frac{\frac{2}{3} \cdot 5 \cdot f_{v,k}}{\sqrt{d}\left(\sqrt{\alpha(1-\alpha)} + 0.8\frac{x}{d}\sqrt{\frac{1}{\alpha} - \alpha^2}\right)}$$

where $k_n = 5$ for solid timber is considered. Note that the obtained shear stress value is a characteristic value and in the derivation of this formula material parameter (ratios) for softwoods are assumed.

The second formula is the theoretical basic expression for notched beams (TEN), derived in paragraph 2.4.1:

$$\frac{V}{b\alpha d} = \frac{\sqrt{\frac{G_c}{d}}}{\sqrt{\frac{0.6\,(\alpha - \alpha^2)}{G}} + \beta\sqrt{6\frac{\left(\frac{1}{\alpha} - \alpha^2\right)}{E}}}$$

This formula is not fitted on test results as is done for the Eurocode 5 expression. Therefore it can be researched whether notched Azobé beams are described well by this equation and which value for the fracture energy would be appropriate for the wood species Azobé as the expression is derived for the geometry of a notch and material parameters are not yet incorporated.

The following theoretical basic expression for tenonned beams (TET) is derived in paragraph 6.1 to be applicable for tenon geometries:

$$\frac{V_f}{\text{b}\alpha\text{d}} = \sqrt{2}\sqrt{\frac{G_{f,y}}{b\alpha^2 d\left(\frac{1.2\left(\frac{1}{b\alpha}-\frac{1}{b}\right)}{G} + 2c\beta d^2 + \frac{12\beta^2\left(\frac{1}{\alpha^3}-1\right)}{Eb}\right)}}$$

As for the theoretical basic expression derived for a notch geometry, no material parameters are yet incorporated in this formula. Though the factor c can be defined in different ways. For the comparison with test results c is set to zero after which TET is compared using both the actual tenon length and the fictively extended tenon length.

For the fracture energy different models are used. For both wood species the relation determined by Larsen and Gustaffson (1990) is used:

$$G_{f,y} = -146 + 1.04\rho$$

For Spruce the approximation by Larsen and Gustafsson (1992) is used too:

$$G_{f,y} = 0.65\rho$$

For Azobé a relation is determined by using the "Solve" function within Excel. The function tries to minimize the sum of the squares of the difference between the modelled value and the value according the test. The functions tries to optimize the variables A to E within the following linear relation:

$$G_{f,y} = A \cdot \rho + B \cdot \omega + C \cdot E_0 + D \cdot G + E$$

where $G_{f,y}$ [N/m] is the fracture energy in pure tensile spitting perpendicular to the grain, ρ [kg/m^3] is the density, ω [%] is the moisture content, E_0 is the modulus of elasticity parallel to the grain, G is the shear modulus and A to E are variables to be determined by Excel's solve function.

7 EXPERIMENTAL PROGRAM

In order to compare en possibly verify the theoretical analysis' from previous chapters test results from Vermeij (2011) were analysed and additional tests were performed. Analogously to chapter 20 from NEN-EN 408 (2010) in the following chapter first Vermeij's experimental program is discussed after which the additional experimental program performed within this Masters' Thesis is amplified on.

7.1 EXPERIMENTAL PROGRAM VERMEIJ (2011)

Within the framework of a Bachelor's Thesis, Vermeij (2011) researched if the calculation rules given by paragraph 6.5.2 from NEN-EN 1995-1-1 (2005) are applicable to hardwood tenonned beams. To answer this question Vermeij carried out tests on notched and tenonned beams, with and without an inclined lower notch. Within this research the crude results from this BSc Thesis were analysed and compared with the theoretical models formulated above. The test results from beams with an inclined lower notch where not analysed within the framework of this research.

The wood species' tested were Spruce, originating from Scandinavia, and Azobé, originating from Cameroon. Sufficient time before and in between tests the timber was stored in a climate chamber where constant humidity and air temperature is maintained. The timber was not graded but according non-destructive tests on the modulus of elasticity it was found that the Spruce test pieces belong to grade C30 and the Azobé test pieces belong to D70. Especially for Azobé it is important to know whether the grains do not deviate too much from the beam's axis. Therefore, when it appears from the journal of the test series the grains of a certain piece deviates significantly the result is excluded from the analysis.

The geometry of the test pieces is depicted in Figure 88. Unfortunately the exact sizes per test piece were not reported. The intended sizes, also given in the figure, are therefore used for the analysis. VNS and ANS indicate respectively a Spruce and Azobé beam, both with a sharp notch. VPS and APS indicate respectively a Spruce and Azobé beam, both with a tenon without inclination.

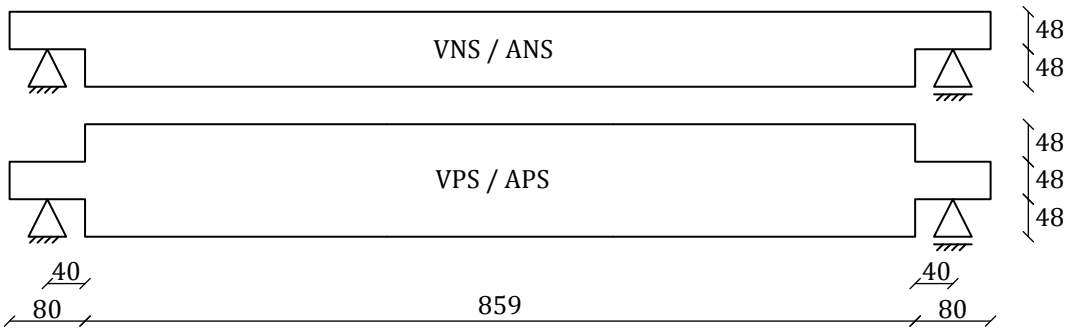

Figure 88: Geometry test pieces without notch inclination, sizes are given in millimeters, width is 30 mm (Vermeij, 2011)

As depicted in Figure 89 a non-symmetric 4-point-bending test set-up was applied to make the beam fail at the desired side of the beam after which a second test could be performed to test the other notch/tenon. Most test pieces were indeed tested at both sides of the beam, a few though were damaged too much or could not be repaired properly enough to perform a second test. From the tests only the failure load is reported by Vermeij. More specific information per test piece is given in Appendix D1

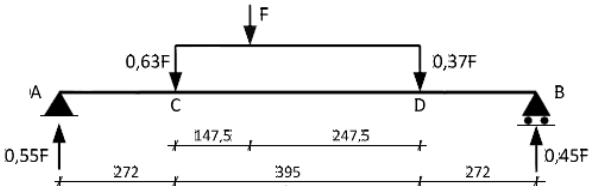

Figure 89: Test set-up experimental program Vermeij (2011)

A few notes in relation to the use of these test results need to be made:

- As mentioned only the failure load per test piece is known. It is not known which (sequence of) failure mechanism(s) led to failure.
- For the beams from which the test pieces are sawn size, weight, moisture content and modulus of elasticity is determined. This data is however not know per test piece. Experience with the additional experiments performed within this research shows that sizes, weight and modulus of elasticity vary between test pieces. The analysis of these test results and comparison with the theoretical models could therefore be less accurate than would have been possible.
- The previous note already mentioned sizes per test piece are not determined. Further, the specific dimensions of the test set-up per test are not determined as well. It is e.g. imaginable per test the notch/tenon cantilever length varied as well.
- The angle of the grain with the beam's axis per test piece are not determined. It is also difficult to determine this angle from the limited number of picture's available. Therefore only test pieces with excessive deviation of the grain's angle can be identified and excluded.

7.2 ADDITIONAL EXPERIMENTS

After analysis of the test results from Vermeij (2011) it was decided to perform additional experiments. The notes mentioned in the previous paragraph are judged to be of enough importance to perform additional tests as the origin of scatter in the results of Vermeij could not be identified. A small test series is carried out according the following goals:

- Gain insight into the (sequence of) failure mechanism(s).
- Obtain a (small but) complete dataset where data on size, weight, moisture content and modulus of elasticity is known per test piece.
- Accurate measurement of the test set-up per test.
- Determination of (an indication of) the angle of the grain of the test pieces and angle of the crack when failure occurs.
- Testing different geometries making a broader comparison with the theoretical models possible.

7.2.1 TEST PIECES' WOOD SPECIES AND HISTORY

The wood species used for the additional tests is Azobé originating from Cameroon. The botanical name of the wood is *Lophira alata*. Besides Azobé the wood is also referred to as Ekki or Bongossi. Wijma Kampen B.V. provided the wood with FSC certificate from one of their concessions. The wood belongs to the same bathes as the wood used by Vermeij (2011).

Before testing the timber was stored for a significant amount of time in a climate chamber where a constant humidity of 85% and temperature of 20 degrees Celsius is maintained. The beams from which the test pieces are sawn are remainders of bending tests in the past. Therefore bending strength values are also available. The timber is classified to strength grade D70. Before, during and after testing the angle of the grain is closely examined.

7.2.2 NON-DESTRUCTIVE TESTS METHODS

Before destructive testing was performed the following material parameters were determined non-destructively: the dimensions and weight of the timber and dynamic modulus of elasticity at various stages of preparation and the moisture content. In the following the methods are explained.

At various stages of the preparation process of the test pieces dimensions of the timber are determined. For this purpose a flexible steel rule is used with an accuracy of 1 mm. With precise measurement dimensions can be estimated fairly good at 0.1 mm. Weight is measured with an accuracy of 0.01 kg using a regular scales.

To determine the modulus of elasticity before destructive testing is performed electronic devises can be utilized. The Timber Grader MTG is an electronic devise which can measure the dynamic modulus of elasticity.

Figure 90: Timber Grader MTG in use

The Timber Grader MTG works by introducing a vibration in the test piece which travels through the test piece back and forth while measuring accelerations at the surface of the timber by a receiver. The devise can simply be hold with its receiver onto the end of the test piece while on one of the ends a vibration is introduced with a hammer, as is depicted in Figure 90. From the measured spectrum of frequencies the eigenfrequency can be determined.

Using the eigenfrequency the dynamic modulus of elasticity can be determined using the following formulas:

$$c = 2fL \cdot 10^{-3}$$
$$E_{dyn} = \rho c^2 \cdot 10^{-6}$$

where:
c : wave speed [m/s]
f : first eigen frequency [s^{-1}]
L : length test piece [mm]
E_{dyn} : dynamic modulus of elasticity [N/mm^2]
ρ : specific weight [kg/m^3]

The moisture content of the test pieces is determined according NEN-EN 13183-1 (2002). From the test piece a test slice is sawn[2], for which the requirements are illustrated in Figure 91, after which the weight of the test slices is determined immediately. The test slices are then dried in an oven at 103 ± 2 °C until the weight difference between two successive weighings is less than 0.1%. The accuracy of the scales used is 0.01 g.

[2] Note that according paragraph 7.2.3 the requirements illustrated in Figure 91 are not fully met.

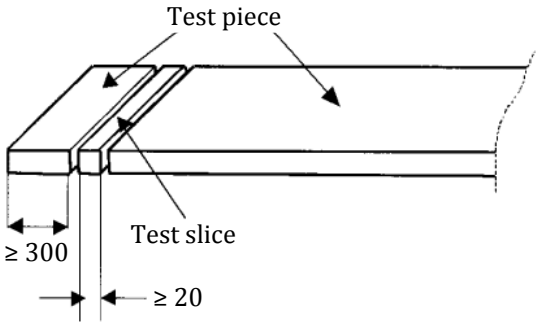

Figure 91: Requirements on position test slice (NEN-EN 13183-1, 2002)

The moisture content is calculated as follows:

$$\omega = \frac{m_1 - m_0}{m_0} * 100\%$$

where
m_1 : mass of the test slice before drying [g];
m_0 : mass of the oven dry test slice [g];
ω : moisture content [%], rounded off to the nearest 0.1 percentage point.

7.2.3 CHARACTERISTICS PREPARATION OF THE TEST PIECES

The preparation of the test pieces is described in the following paragraph. The design of the test pieces is depicted in Figure 92. On both sides of a test piece a tenon is present. The first tenon is designed as if the wooden mitre gate is very thick, therefore the thickness of the planking can be ignored and the height of the test piece is about equal to the thickness of the gate. Then the length of the tenon is equal to the height of the test piece and the upper notch - tenon - lower notch ratio is ⅓ - ⅓ - ⅓. The second tenon is designed according the design also considered analytically and using FEM. The height of the test piece is ⅝ the thickness of the gate. Then the length of the tenon is equal to 1⅕ the height of the test piece and the upper notch - tenon - lower notch ratio is ⅕ - ⅖ - ⅖.

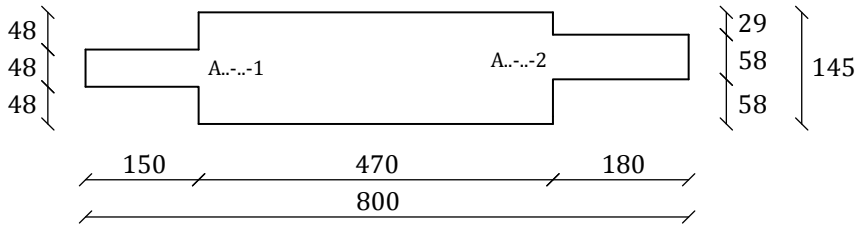

Figure 92: Geometry test pieces, indicated sizes (mm) are approximate. Note the encoding of the two distinct tenon geometries.

First six parent beams where selected from the available stock on the TU Delft. Wood species, size and minimal bow distortion where the selection criteria. From these six beams dimensions, weight and dynamic modulus of elasticity were then measured.

The test pieces are sawn from the original beam as is depicted in Figure 93 for beam A1. The beams where first sawn into two pieces in the length direction and sawn in the specified length. Then the side surfaces were planed in order to make the grain and crack development during failure clearly visible. For every test piece again dimensions and dynamic modulus of elasticity were measured. Unfortunately their weight was not measured.

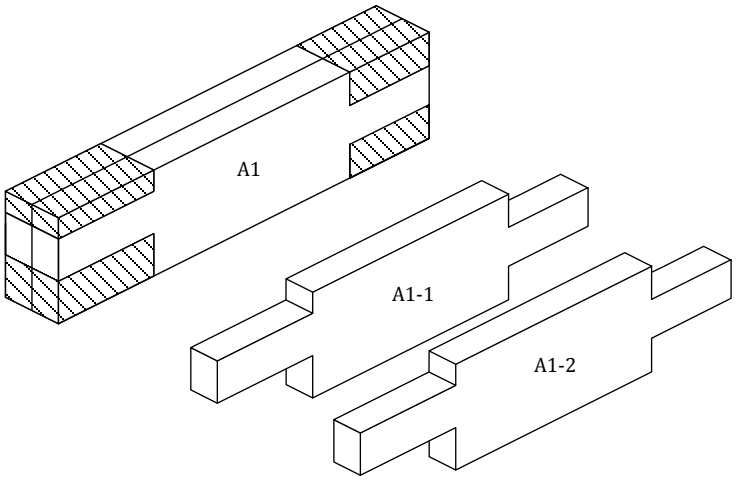

Figure 93: Beam A1 from which the test pieces A1-1 and A1-2 are sawn

Finally the hatched parts illustrated in Figure 93 were removed. To determine the moisture content from one of the hatched parts for all test pieces a small block was sawn off as is described in paragraph 7.2.2 and is depicted in Figure 94. Note the test slices do not satisfy the requirements from NEN-EN 13183-1 (2002) fully.

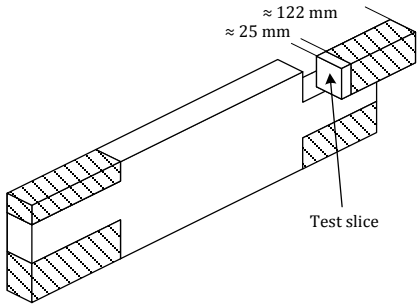

Figure 94: Specification location and size test slice

The test pieces and test results are encoded the following way: the parent beams are encoded from A1 (Azobé nr. 1) to A6. The test pieces sawn from e.g. beam A3 are then encoded A3-1 and A3-2. As all test pieces will be loaded on both sides test results are encoded according the tenon geometry too. Test results for e.g. test pieces A3-1 and A3-2 are thus encoded A3-1-1, A3-1-2, A3-2-1 and A3-2-2. Therefore 12 test pieces are sawn with which 24 tests can be performed.

7.2.4 TEST METHOD

After the test pieces are prepared and all non-destructive tests are performed destructive tests can be performed. The destructive tests are characterised by each test piece being tested on both sides and four test set-ups where two different tenon geometries and tenon cantilever lengths are combined. Figure 95 depicts the test set-up in the lab.

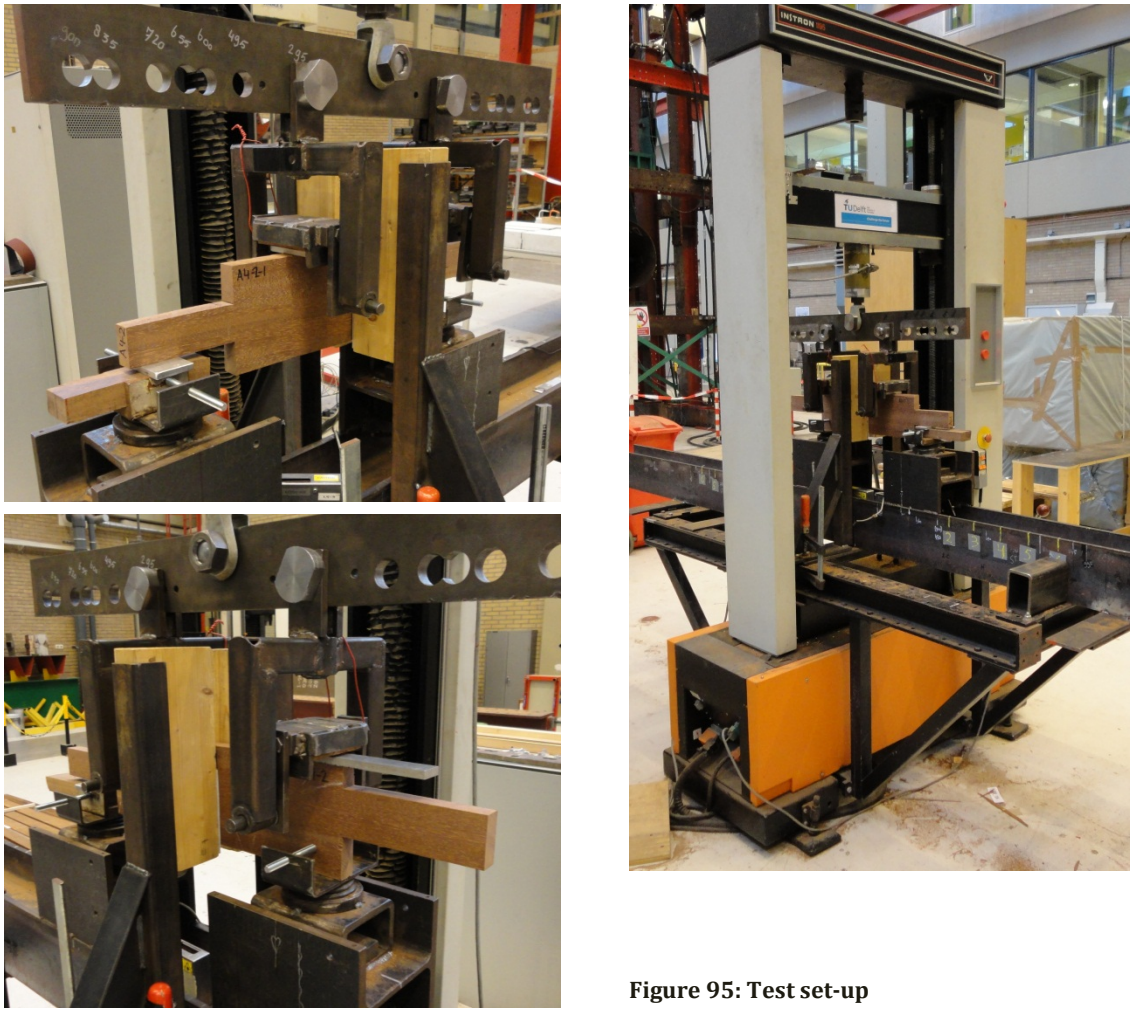

Figure 95: Test set-up

During destructive testing the following data is gathered:

- Load values with corresponding crack length and the failure load;
- The (sequence of) failure mechanism(s);
- Angle of the crack with the beam axis.

Each test piece needs to be tested twice as both tenons are tested. Therefore the test set-up principle depicted in Figure 96 is applied by which the two tenons of every test piece can be tested separately without possibly damaging the wrong tenon. Due to limitations of the available test bench at the Stevin Laboratory at the TU Delft only a four point bending test could be performed. One of the two applied forces is introduced directly above one of the supports. Due to the size of the test bench compared to the size of the test pieces it was decided to perform a three point bending test as depicted. Checks on maximum bending stresses and compression stresses perpendicular to the fibre are reported in Appendix D2.

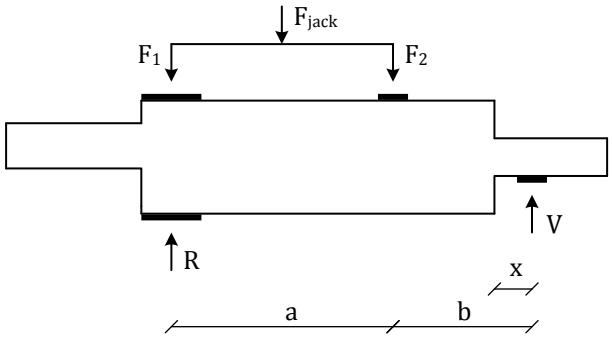

Figure 96: Test set-up principle

As already briefly mentioned the destructive tests are characterised by four test set-ups where two different tenon geometries and tenon cantilever lengths are combined. Both tenon geometries are tested with two different tenon cantilever lengths. Test pieces are divided according their encoding. Test pieces encoded with the second number being a 1 are tested with a short tenon cantilever length. Test pieces encoded with the second number being a 2 are tested with a long tenon cantilever length. Furthermore tests encoded with the last two numbers being 1-1 are related to tenon geometry 1 with a short tenon cantilever length, 2-1 are related to tenon geometry 1 with a long tenon cantilever length, 1-2 are related to tenon geometry 2 with a short tenon cantilever length, 2-2 are related to tenon geometry 2 with a long tenon cantilever length. Table 9 clarifies the division of tests visually.

Table 9: Four test set-ups

		Tenon cantilever length	
		Short	Long
Tenon geometry	1	A..-1-1	A..-2-1
	2	A..-1-2	A..-2-2

It is chosen to apply a short tenon cantilever length of ⅓ the tenon length and a long tenon cantilever length of ¾ the tenon length. In Figure 97 the mechanical schemes for the four combinations of tenon geometry and tenon cantilever length are depicted where the designed measures are reported in Table 10. The actual measures during testing deviate from the design though, therefore these measures are determined for each test. The forces F_2 and V are transferred over a length of 50 mm and the whole width of the test piece. The forces F_1 and R are tried to spread as much as possible.

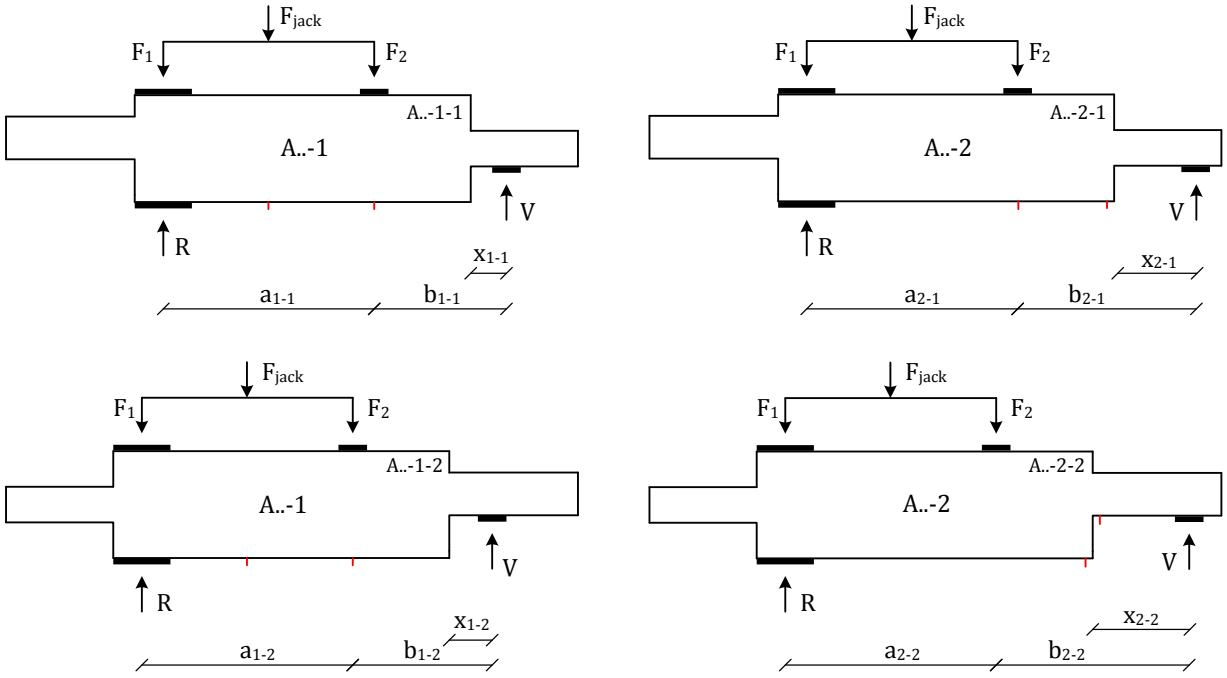

Figure 97: Mechanical schemes for the four combinations of tenon geometry and tenon cantilever length. Note the encoding principle for the four distinct test set-ups and the locations of the deflection measuring lasers in red.

The deflection is measured as close to the tenon as possible, as is indicated in Figure 97 in red. The laser set-up applied for the tests A..-2-2 is considered most appropriate, but due to space limitations other arrangements where necessary. The obtained values of the deflection are not used to determine e.g. the global modulus of elasticity, but are only used to obtain an indication of the load – deflection diagram which in that way contributes to identifying the failure mechanism. The loading speed was 0.2 mm per minute by which a failure time of 5 to 10 minutes was realised. The first three tests a slower loading speed was used as the failure time was uncertain yet.

Table 10: Characterizing measures mechanical schemes

	A..-1-1	A..-2-1	A..-1-2	A..-2-2
Tenon geometry	1	1	2	2
x [mm]	50	112.5	60	135
b [mm]	185	247.5	195	270
a [mm]	295	295	295	295

More specific information regarding the test pieces and each test it is referred to Appendix D3 to D6 for e.g. the test journal.

8 TENON STRENGTH ACCORDING TESTS

In this chapter the test results, performed according chapter 7, are analysed and compared with the formula's reported in *paragraph 6.4*.

Although this research is aimed at Azobé beams with a tenon still the results on notched and tenonned Spruce beams and notched Azobé beams are wise to analyse. Results on notched Spruce beams are shortly analysed to confirm theory and Eurocode 5. As the material parameters of Spruce are relatively well known the effect of the tenon geometry on the results can be analysed separately using the results on tenonned Spruce beams. Analogue, as the effect of geometry on the results is well described for notched beams the results on notched Azobé beams can be used to research the fracture energy of Azobé. The two aspects come together in the analysis of the results on tenonned Azobé beams.

It should be realised the test series is of small size. The results should therefore be used as indicative and definite conclusions should be drawn after more tests have been performed. Further, TET need further developing as the influence of tenon geometry on stresses and strains at the transition of tenon to beam is not yet fully researched. It is however of value to analyse the results of TET to determine its use.

For the test results and approximating formula's three values are determined: average, coefficient of variation (COV) and the 5th percentile value. The COV is defined as the standard deviation divided by the average. The 5th percentile value is determined according paragraph 5.3.1 of NEN-EN 384 (2010).

Appendix D reports all data, the test journal and photographs of both the undamaged and failed test pieces.

8.1 TEST RESULTS FOR NOTCHED SPRUCE BEAMS

The rough test data for notched Spruce beams originates from Vermeij (2011) and is analysed again for this research. For these beams it is expected the Eurocode 5 expression and TEN give well corresponding results. In Figure 98 and Table 11 the results are reported.

From Figure 98 it can be observed all three formulations give good results. In Table 11 a rather high COV is reported though. It is striking TEN using the regression line for fracture energy corresponds worse than when the simplified expression to determine the fracture energy is used. TEN therefore seems too optimistic. The 5th percentile values of the tests, and the Eurocode 5 expression correspond very well with a ratio of Eurocode 5 / tests of 1.10. The ratios TEN without and with modelled $G_{f,y}$ / test results for average values are respectively 1.28 and 1.04.

Table 11: Average shear stress at failure for notched Spruce beams [N/mm^2]

	Average	COV	5th percentile
Tests	1.66	0.29	1.25
TEN	2.13	0.16	
TEN, modelled G_{fy}	1.72	0.16	
Eurocode 5 expression			1.37

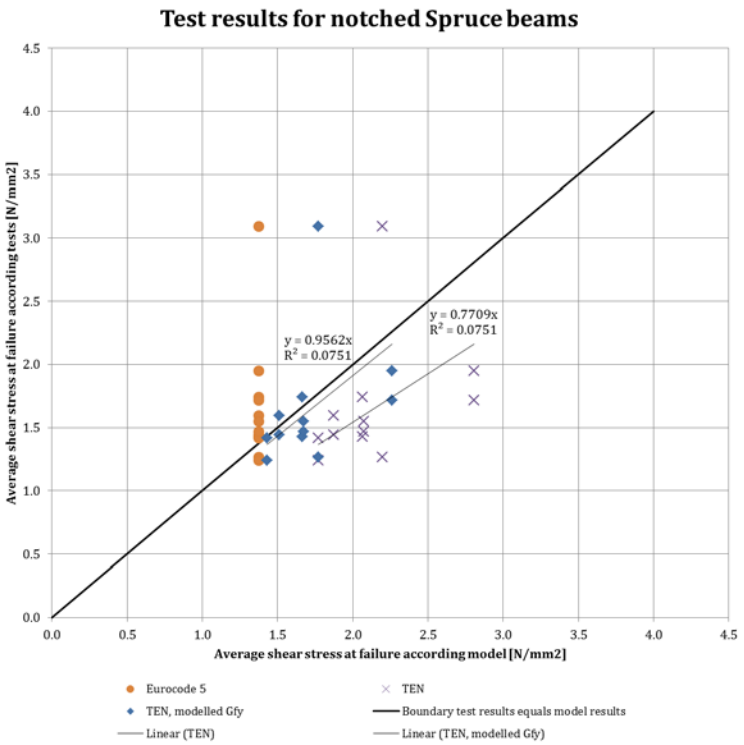

Figure 98 (Test data originates from Vermeij, 2011)

8.2 TEST RESULTS FOR TENONNED SPRUCE BEAMS

The rough test data for tenonned Spruce beams originates from Vermeij (2011) and is analysed again for this research. For these beams the material parameters are known but which effect the tenon geometry has on the results is not. In Figure 99 and Table 12 the results are reported.

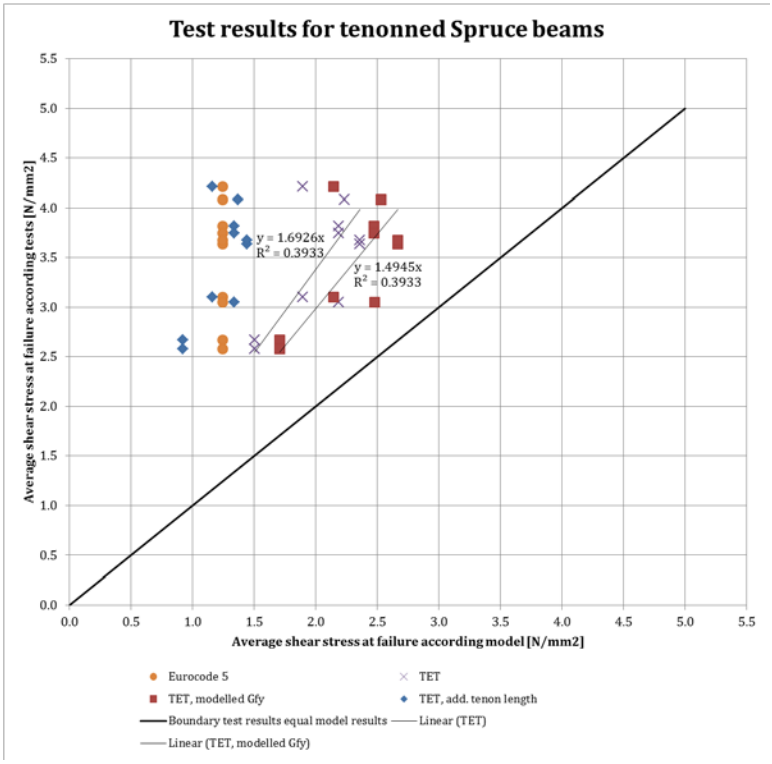

Figure 99 (Test data originates from Vermeij, 2011)

From the graph it is clear the Eurocode 5 expression returns conservative results. The characteristic value is more than a factor 2 smaller than the 5th percentile value tests indicate. The ratio Eurocode 5 / test results for the 5th percentile values tenonned Spruce beams is 0.47. TET returns results which correspond better to the test results. However, the development of stresses after the discontinuity is still neglected. Approximating this phenomenon by fictively extending the tenon results in a worse approximation than the Eurocode 5 expression assuming the ratios are constant between 5th percentile and average values.

Table 12: Average shear stress at failure for tenonned Spruce beams [N/mm²]

	Average	COV	5th percentile
Tests	3.46	0.16	2.62
TEN	2.06	0.14	
TET	2.89	0.14	
TET, modelled $G_{f,y}$	2.33	0.14	
TET, additional tenon length	1.26	0.14	
Eurocode 5 expression			1.24

Although TET returns the best results, still a about factor 0.84 separates the average values of TET and tests.

8.3 Test results for notched Azobé beams

The rough test data for notched Azobé beams originates from Vermeij (2011) and is analysed again for this research. For these beams TEN describes the effect of geometry well, but the value of the fracture energy for the material is uncertain. In Figure 100 and Table 13 the results are reported.

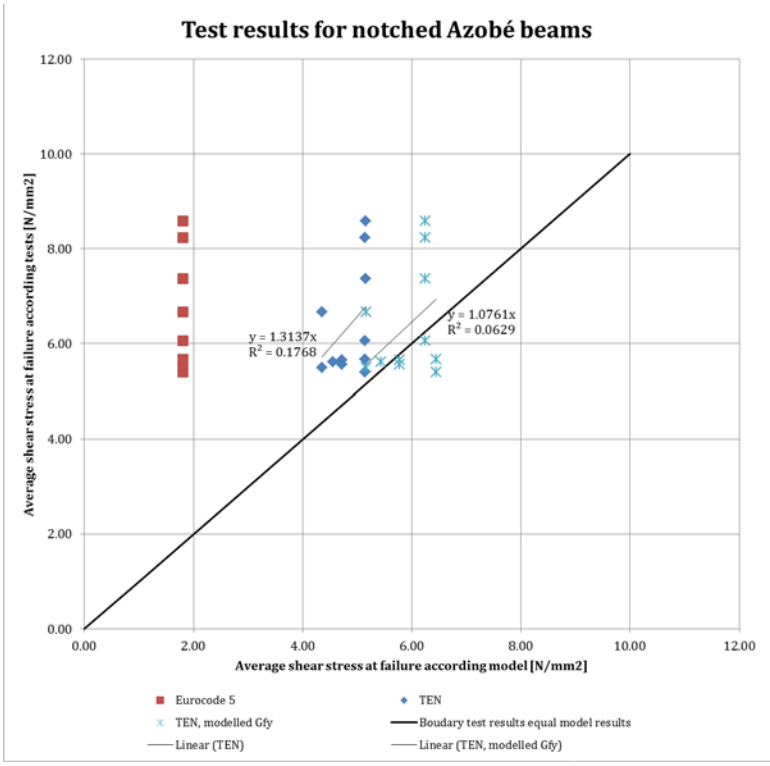

Figure 100 (Test data originates from Vermeij, 2011)

From the results it is striking the Eurocode 5 expression returns very conservative results. The characteristic value is a factor 3 smaller than the 5th percentile value tests indicate. The ratio Eurocode 5 / test results for the 5th percentile values is 0.33. TEN, not fitted on material parameters of softwoods, but using the regression line to determine the fracture energy, delivers much better results. The graph indicates the result is safe, but not too conservatively. Notched Azobé beams are therefore better approximated by TEN than by the Eurocode 5 expression assuming ratios are constant between 5th percentile and average values. The ratio of TEN / test results for average values is 0.76.

Table 13: Average shear stress at failure for notched Azobé beams [N/mm²]

	Average	COV	5th percentile
Tests	6.39	0.17	5.45
TEN	4.84	0.07	
TET, modelled $G_{f,y}$	5.89	0.08	
Eurocode 5 expression			1.81

The 'solve' function within Excel came up with the following formula for the fracture energy:

$$G_{f,y} = 5.36373 \cdot 10^{-4} \cdot \rho + 4.1504 \cdot 10^{-5} \cdot E_0$$

TEN, using the adapted relation for the fracture energy, returns values closer to the test results than when the relation according literature is used. The ratio TEN / test value for average values is 0.76, which can be improved by modelling the fracture energy to a ratio of 0.92. Note ρ and E_0 vary little between test pieces, which influences the utility of the relation. The fracture energy of hardwoods needs further research.

8.4 Test results for tenonned Azobé beams

For tenonned Azobé beams both the effect of geometry as the material parameter fracture energy is uncertain. In Figure 101 to Figure 105 and Table 14 to Table 15 the results are reported.

8.4.1 Comparison test results Vermeij (2011) with model formulas

The rough test data for tenonned Azobé beams originates from Vermeij (2011) and is analysed again for this research. First the test results are analysed by comparing them with the result of the model formulas, as is done in the previous paragraphs.

First referring to Figure 101 and Table 14, again the Eurocode 5 expression returns a very conservative result. A factor 0.23 separates the two characteristic values. When TET is combined with the modelled fracture energy, average values are still separated by a large difference with a ratio TET / test results of 0.48.

As can be seen from the graph the scatter of the test results is large with a COV of 0.27 which is completely opposite to the resulting COV of the model formulas. Due to the lack of data per test piece (more elaborately discussed at the end of paragraph 7.1) it is impossible to determine the cause of the scatter. On the one hand the scatter could be caused by material related phenomena, on the other hand the lack of specific data per test piece could be the cause. The additional tests are therefore viewed as necessary.

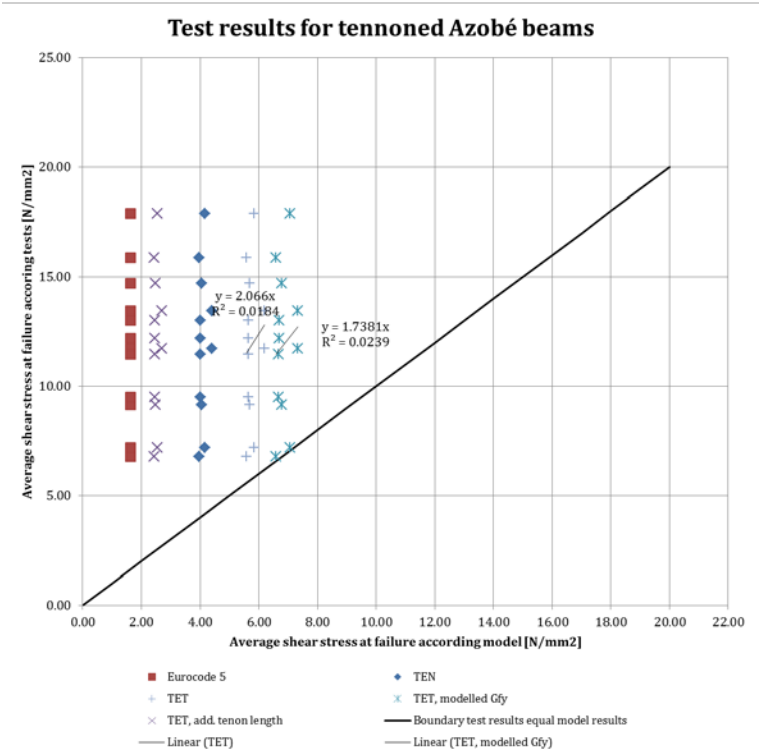

Figure 101 (Test data originates from Vermeij, 2011. Regression lines are forced through 0,0.)

Table 14: Average shear stress at failure for tenonned Azobé beams [N/mm²] (Test results from Vermeij, 2011)

	Average	COV	5th percentile
Tests	11.91	0.27	7.01
TEN	4.10	0.04	3.97
TET	5.77	0.04	5.58
TET, modelled $G_{f,y}$	6.87	0.04	6.61
TET, additional tenon length	2.51	0.04	2.43
Eurocode 5 expression			1.64

8.4.2 Comparison test results Van Otterloo (2013) with model formulas

For this research additional test on tenonned beams are performed. All data per test piece and test is reported in Appendix D. The test results for the additional tests are depicted in several graphs to make the results more clear. In the following it is referred to Figure 102 to Figure 105 and Table 15 to Table 17.

The first remarkable result is that compared to the results from Figure 101 the stresses are much smaller in value, even though the test pieces originate from the same batch of timber and geometry 1 is similar to the test pieces from Figure 101. Only the test set-up was different, but this should not influence the result at this extend, as the combination of shear force and bending moment in the tenon should be equal.

For tenonned Azobé beams again conservative results are obtained when the expression for the strength of notched beams from Eurocode 5 is applied. The ratio Eurocode 5 / test results for the 5th percentile values averagely 0.24 for the tested geometries.

From Figure 102 four clouds can be distinguished which represent the four test set-ups. For comparison of the four test set-ups TET is used. Per test set-up the scatter is normal with an average COV of 0.14.

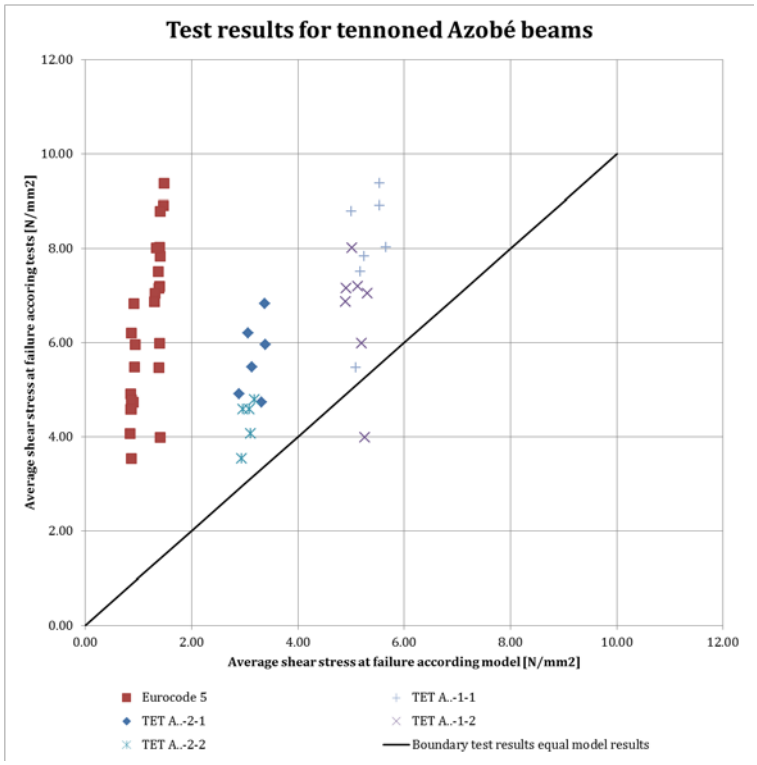

Figure 102 (From tests within this research (Van Otterloo, 2013))

In Table 15 the average results for the four test set-ups and their ratios are reported. Both the Eurocode 5 expression as TET return about the same ratios as the test results indicate when the tenon cantilever length is varied. The ratio of the test results for short and long tenon cantilever length are 1.40 and 1.53 for tenon geometry 1 and 2 which corresponds with the ratio which TET returns which is for both tenon geometries 1.67. Varying the tenon cantilever length is well described by both the Eurocode as TET.

When geometry is varied the test results indicate the average result changes significantly, but for both the Eurocode as TET little change of result is obtained. The ratio of the test results for tenon geometry 1 and 2 are 1.21 and 1.32 for short and long tenon cantilever length which does not correspond with the ratio which TET returns which is for both tenon cantilever lengths 1.04. It is remarkable the formula takes the tenon cantilever length into account very well, but tenon geometry does not significantly influence the model formula's values.

The fact that the factor c, which introduces the influence of the tenon geometry on stresses and strains near the transition from tenon to beam, is set to a value of zero; most probably is the cause of the bad representation of tenon geometry by TET.

When both tenon cantilever lengths are combined for both tenon geometries, its regression line fits well, which is depicted in Figure 103. The slope of the regression lines are almost equal to one, which means that for both populations a multiplication factor can make the average values of tests and formula equal. However, it is again evident the influence of geometry is not described well, as the possible multiplication factors will not have the same value.

Table 15: Ratios average results of the four test set-ups (From tests within this research (Van Otterloo, 2013))

Test results		Tenon cantilever length		
		Short	Long	
Geometry	1	7.99	5.69	*1.40*
	2	6.61	4.32	*1.53*
		1.21	*1.32*	

Eurocode 5		Tenon cantilever length		
		Short	Long	
Geometry	1	1.41	0.92	*1.53*
	2	1.40	0.86	*1.63*
		1.01	*1.07*	

TET		Tenon cantilever length		
		Short	Long	
Geometry	1	5.32	3.20	*1.66*
	2	5.10	3.06	*1.67*
		1.04	*1.05*	

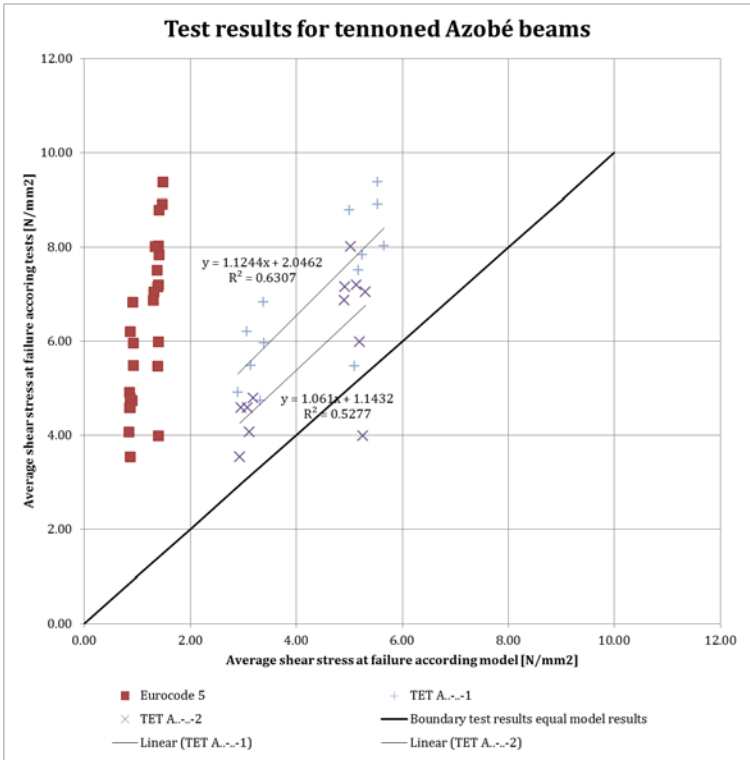

Figure 103 (From tests within this research (Van Otterloo, 2013))

Figure 104 shows TET comes closer to the test results and has a better corresponding slope than TEN. However, as the effect of geometry is not taking into account by TET yet, the conclusion is uncertain yet. For the test set-ups for tenonned Azobé beams A..1-1, A..-2-1, A..-1-2 and A..-2-2 TET returns average values near the test results'. Ratios of TET / test results for the respective test set-ups are 0.67, 0.56, 0.77 and 0.71 according Table 16.

In Figure 105 two variations of TET are depicted. Using the fictively extended tenon worse results are obtained than when the actual tenon cantilever length is used. Note that the

additional length for tenon geometry 2 is estimated to be 60 mm, as the geometry is not researched by FEM. Using the modelled fracture energy leads to good results.

According Table 16 the following ratios are found: modelling the fracture energy gives ratios of TET / test results for average values of 0.80, 0.68, 0.93 and 0.86 for respectively the test set-ups A..1-1, A..-2-1, A..-1-2 and A..-2-2. The approximation thus improves the expression. Approximating the development of stresses near the transition of tenon to full-size beam, ratios of TET / test results for average values of 0.31, 0.32, 0.49 and 0.51 are obtained for respectively the test set-ups A..1-1, A..-2-1, A..-1-2 and A..-2-2. The approximation thus does not improve the expression.

Table 16: Average shear stress at failure for tenonned Azobé beams [N/mm²]. Test results per combination of geometry and tenon cantilever length from tests within this research. (From tests within this research (Van Otterloo, 2013))

		A..-1-1	A..-2-1	A..-1-2	A..-2-2
Tests	Average	7.99	5.69	6.61	4.32
	COV	0.15	0.13	0.18	0.11
	5th percentile	6.08	4.78	4.59	3.64
TEN	Average	3.77	2.42	3.61	2.31
	COV	0.04	0.05	0.03	0.03
TET	Average	5.32	3.20	5.10	3.06
	COV	0.04	0.06	0.03	0.03
TET, modelled $G_{f,y}$	Average	6.40	3.86	6.14	3.70
	COV	0.06	0.06	0.04	0.04
TET, additional tenon length	Average	2.46	1.82	3.25	2.22
	COV	0.04	0.05	0.03	0.03
Eurocode 5 expression	5th percentile	1.41	0.92	1.40	0.86

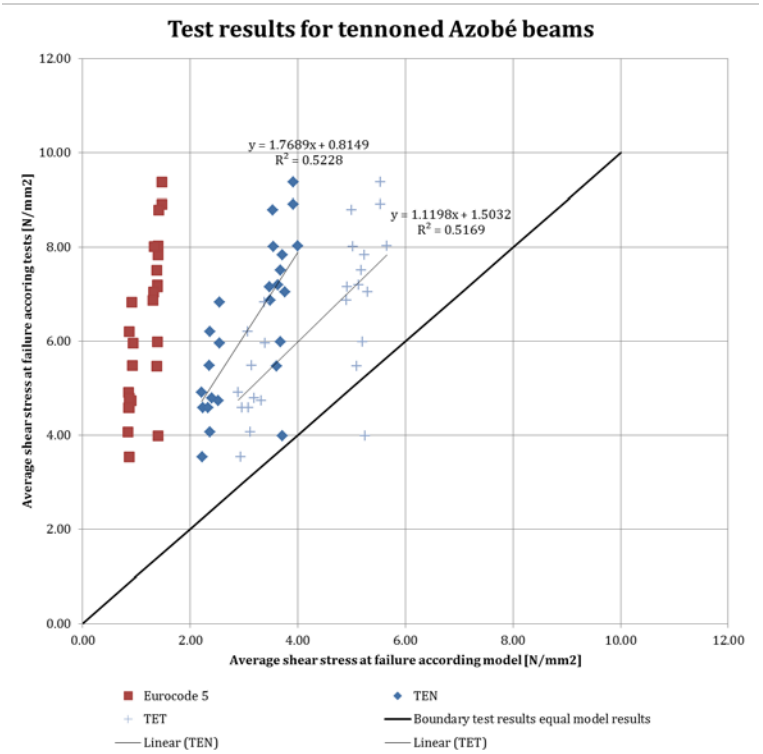

Figure 104 (From tests within this research (Van Otterloo, 2013))

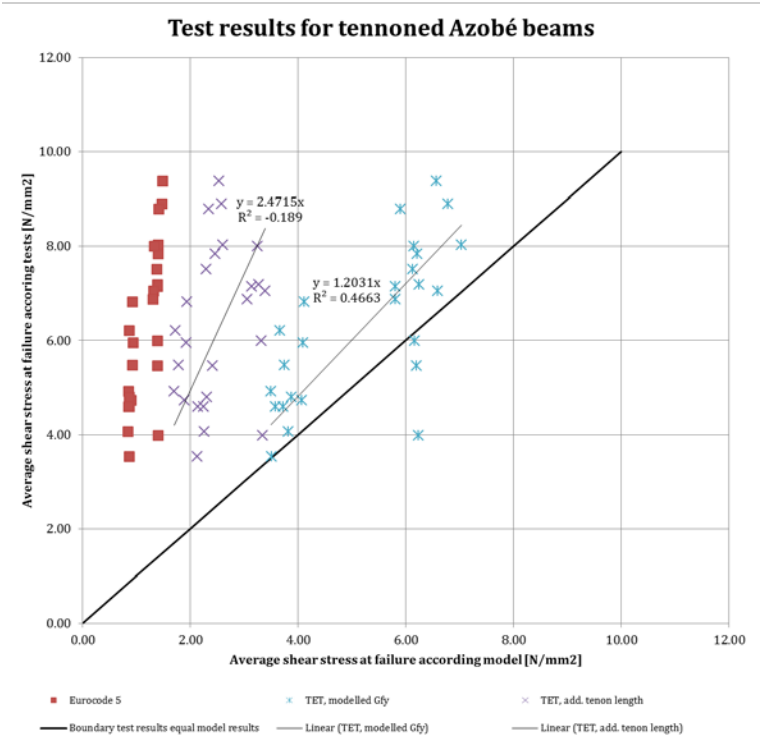

Figure 105 (From tests within this research (Van Otterloo, 2013))

In Table 17 the results for all four test set-ups are combined and as the geometry parameters vary, the COV is rather high.

Table 17: Average shear stress at failure for tenonned Azobé beams [N/mm²]. All test results combined from tests within this research. (From tests within this research (Van Otterloo, 2013))

	Average	COV	5th percentile
Tests	6.31	0.26	4.00
TEN	3.11	0.22	
TET	4.30	0.24	
TET, modelled $G_{f,y}$	5.18	0.24	
TET, additional tenon length	2.48	0.22	

In the journal of the test series (Appendix D) the angle of the crack with the beam's axis is reported. For all tests the crack was carefully investigated. After analysis of the results no correlation between the angle of the grain with the beam's axis and the test results could be found. Tests where cracks with large angles had developed often higher loads were reached than small angled cracks and vice versa. The largest angle of the crack with the beam's axis found was 12 degrees and only for 4 of 26 test pieces the angle of the crack with the beam's axis was larger than 5 degrees. The deviation of test pieces' grains with the beam's axis thus was not very large.

8.4.3 INDICATIVE ANALYSIS OF FAILURE MECHANISMS

During testing it was observed in all test pieces a crack developed, but not all of them finally failed due to the crack. Bending failure of the tenon and of the remaining beam was observed in many cases.

Four failure mechanisms are distinguished, after a period of stable crack growth:

- unstable crack growth leads to failure;
- bending failure of the tenon occurs;
- bending failure of the remaining beam occurs;
- shear failure of the tenon occurs.

Table 18 reports the observed failure mechanism per test piece. Note the indicative analysis performed in this paragraph is valid for the test set-up used for this research.

Table 18: Failure mechanism per test piece (From tests within this research (Van Otterloo, 2013))

	A..-1-1		A..-2-1		A..-1-2		A..-2-2	
	Failure mechanism / Reaction force at failure [kN]							
A1-..-..	Cracking	7.4	Bending tenon	6.1	Bending remaining beam	11.6	Cracking	6.9
A2-..-..	Bending tenon	12.1	Bending tenon	7.6	Cracking	6.3	Bending remaining beam	7.0
A2-..-..	Bending tenon	9.9	Cracking	7.3	Cracking	9.2	Cracking	6.2
A3-..-..	Bending remaining beam	12.0			Bending remaining beam	12.8		
A4-..-..	Bending tenon	10.9	Bending tenon	6.9	Bending remaining beam	10.7	Bending remaining beam	5.4
A5-..-..	Bending tenon	9.5	Bending tenon	5.6	Cracking	10.4	Cracking	6.0
A6-..-..	Bending tenon	8.2	Shear failure tenon	5.8	Cracking	9.8		

Average values at which the failure mechanisms occur according theory, are calculated the following way:

Assuming a Gaussian distribution, from the characteristic value for the strength class D70 the mean value can be calculated:

$$f_{m,mean} = \frac{f_{m,k}}{1 - a \cdot COV} = \frac{70}{1 - 1.645 \cdot 0.25} = 119\ N/mm^2$$

where $f_{m,mean}$ is the mean bending strength, $f_{m,k}$ is the characteristic bending strength, a is a multiplication factor on the standard deviation with which a 5 to 95 % interval is created and COV is the coefficient of variation.

The maximum bending moment is calculated by:

$$M_{mean} = W \cdot f_{m,mean}$$

where

$W = \frac{1}{6} b d_t^2$ for bending failure at the tenon and

$W = \frac{1}{6} b d_{rb}^2$ for bending failure at the remaining beam (Figure 106).

The reaction force at which failure occurs then becomes:

$R_t = M_{mean}/x$ for bending failure at the tenon and

$R_{rb} = M_{mean}/b$ for bending failure at the remaining beam (Figure 106).

The reaction force at which cracking develops is calculated with TET where x is taken as a variable. In Figure 107 the calculated values are depicted for the four test set-ups.

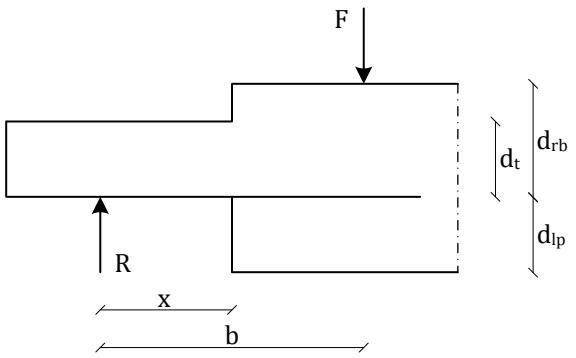

Figure 106: Cracked tenonned beam

It can be seen from Figure 107 that when the load increases a crack appears at an early stage, as was observed during testing. For many of the test pieces a period of stable crack growth followed during which the crack increased steadily under increasing load. At some point failure occurred, either by unstable crack growth where the crack extended "with a bang" or bending failure occurred at the tenon or at the remaining beam. When bending failure occurred first plastic compression failure in the upper part developed after which tension failure occurred at the lower part of the failing section.

Table 19: Number of failure mechanisms occurring per test set-up

	A..-1-1	A..-2-1	A..-1-2	A..-2-2
Cracking	1	1	4	3
Bending tenon	5	4		
Bending remaining beam	1		3	2
Shear failure tenon		1		

Referring to Table 19, for A..-1-1, A..-2-1 and A..-1-2 when bending failure occurred, the location of failure corresponds with the indicative location according Figure 107. For A..-2-2 the two bending failure mechanisms lie close together and therefore it is not remarkable the indicative bending failure mechanism did not occur. It is remarkable however, that all test results' values, when bending failure occurred, are about half the values obtained by calculation.

For the tests with short tenon cantilever length A..-1-.. the failure loads, when cracking was the final failure mechanism, correspond very well with the result of TET with an average ratio of 1.09. For tests with geometry 2 and long tenon cantilever length A..-2-2 the results correspond well too with a ratio of 1.33. Only for tests with geometry 1 and long tenon cantilever length A..-2-1 the results when cracking was the final failure mechanism deviate significantly with a ratio of 1.83.

The following phenomenon is suggested. When the load, and accompanying shear force, increases at some point a crack starts to grow. For some test pieces unstable crack growth follows quickly due to the specific material parameters of the cracking area concerned. For other test pieces the load is able to grow further while the crack length increases

proportional to the decline of strength according TET, as illustrated by the dashed line in Figure 107. For these test pieces either unstable crack growth still leads to failure or when the dashed line would cross the bending failure load, failure is induced by bending. When a calculation rule for standards is prepared, it could be considered to note that cracking in the ultimate limit state is accepted but it needs to be prevented in the serviceability state.

It is noted the above explained sequence of failure is only estimated on the basis of Figure 107 and observation during testing. No conclusions can be drawn from the amplification yet. For instance, the relative larger stiffness of the remaining beam above the crack need to be taken into account in the analysis.

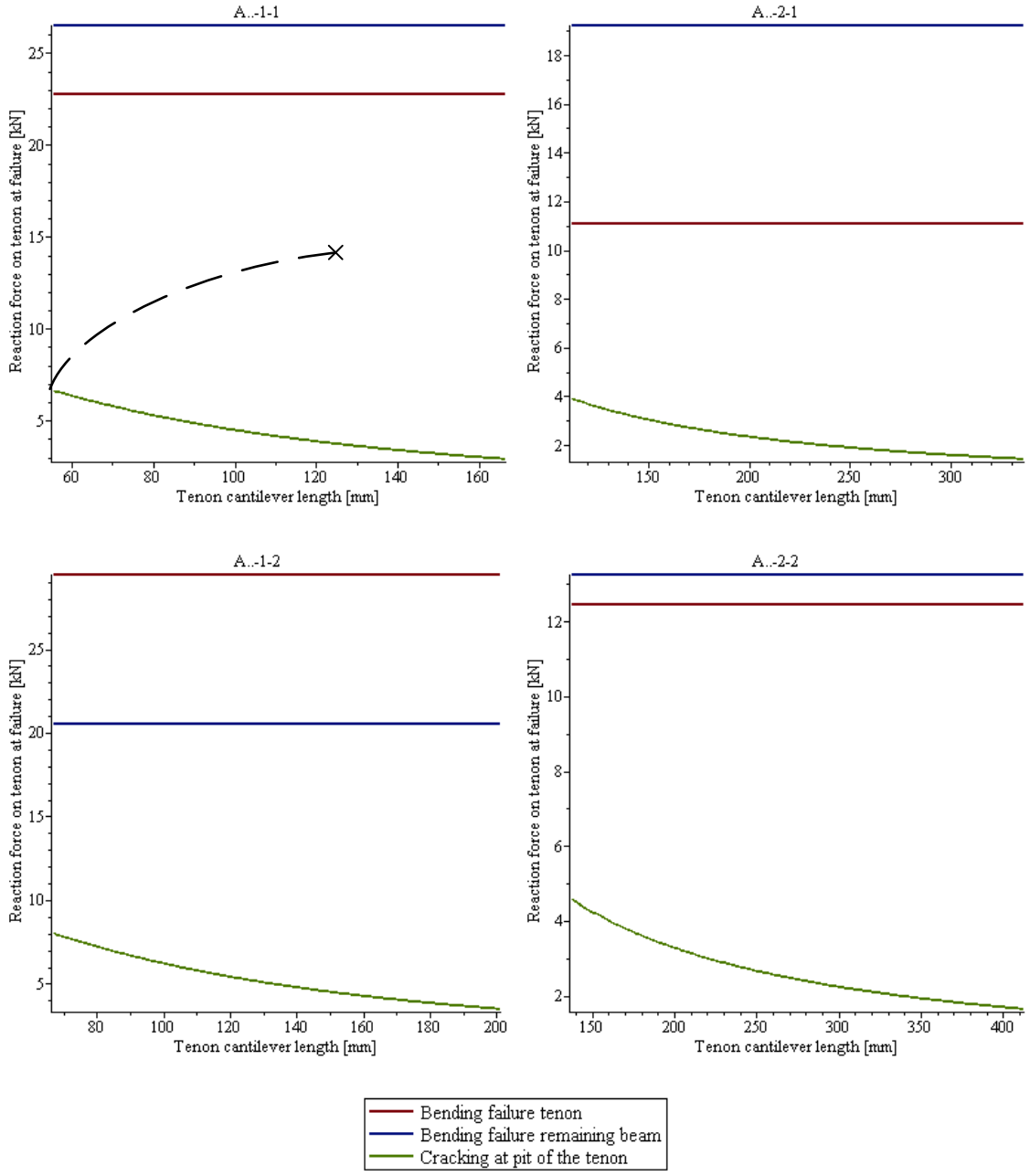

Figure 107: Reaction force at failure for three failure mechanisms for the four test set-ups. Possible load – deflection curve indicated in the first graph with a dashed line.

In Figure 108 the test results are depicted for the tests where cracking is the final failure mechanism. The adapted theoretical expression approximates the test results well and on the safe side. A ratio of TET / test results for average values of 0.77 is obtained.

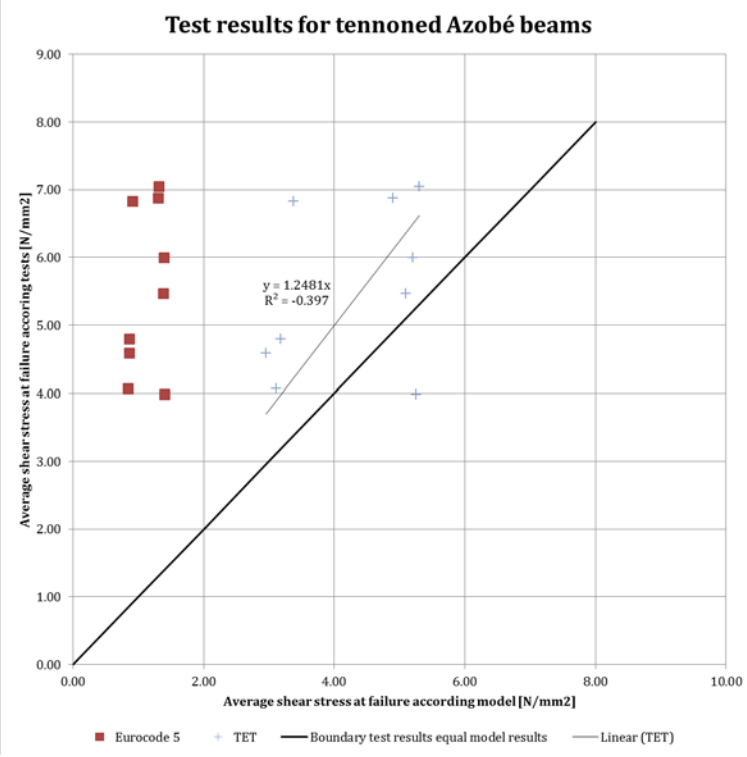

Figure 108: Test results for tests with failure mechanism cracking (From tests within this research (Van Otterloo, 2013))

8.5 Conclusions on test results

For notched and tenonned beams the following conclusions relating to today's standards can be made:

- The Eurocode 5 expression for the strength of notched beams, paragraph 6.5.2 from NEN-EN 1995-1-1 (2005), is confirmed for notched Spruce beams by tests.

- For notched Azobé beams and tenonned Spruce or Azobé beams conservative results are obtained when the expression for the strength of notched beams from Eurocode 5 is applied. The ratio Eurocode 5 / test results for the 5th percentile values for notched Azobé beams and tenonned Spruce and Azobé beams are respectively 0.33, 0.47 and averagely 0.24 for the tested geometries.

For notched beams the following conclusions relating to their strength can be made:

- The theoretical basic expression for notched beams (TEN) returns good results for notched Spruce beams, the ratio TEN / test results for average values is 1.28. Modelling the fracture energy in pure tensile spitting perpendicular to the grain according Larsen and Gustafsson (1992) the ratio becomes 1.03.

- Notched Azobé beams are better approximated by TEN than by the Eurocode 5 expression assuming ratios are constant between 5th percentile and average values. The ratio of TEN / test results for average values is 0.76.

- Applying the least squares method to approximate the fracture energy the ratio of average values TEN / test results can be improved to 1.08. The resulting fracture energy is: $G_{f,y}$ [N/mm] $= 5.36373 \cdot 10^{-4} \cdot \rho$ [kg/m^3] $+ 4.1504 \cdot 10^{-5} \cdot E_0$ [N/mm^2]. Note ρ and E_0 vary little between test pieces, which influences the utility of the relation.

For tenonned beams the following conclusions relating to their strength can be made:

- For tenonned Spruce beams the theoretical basic expression for tenonned beams (TET) returns better results than TEN. The ratio TEN or TET / test results for average values is improved from 0.60 for TEN to 0.84 for TET.

- Approximating the distribution of stresses near the discontinuity in the beam by fictively extending the tenon within TET for Spruce beams, the result is a ratio of 0.36 which is a worse approximation than for the Eurocode 5 expression assuming ratios are constant between 5th percentile and average values.

- For the test set-ups for tenonned Azobé beams A..1-1, A..-2-1, A..-1-2 and A..-2-2 TET returns average values near the test results'. Ratios of TET / test results for the respective test set-ups are 0.67, 0.56, 0.77 and 0.71.

- Approximating the fracture energy with $G_{f,y} = 5.36373 \cdot 10^{-4} \cdot \rho + 4.1504 \cdot 10^{-5} \cdot E_0$, ratios of TET / test results for average values of 0.80, 0.68, 0.93 and 0.86 are obtained for respectively the test set-ups A..1-1, A..-2-1, A..-1-2 and A..-2-2. The approximation thus improves the expression.

- Approximating the development of stresses near the transition of tenon to full-size beam, ratios of TET / test results for average values of 0.31, 0.32, 0.49 and 0.51 are obtained for respectively the test set-ups A..1-1, A..-2-1, A..-1-2 and A..-2-2. The approximation thus does not improve the expression.

- The ratio of the test results for short and long tenon cantilever length are 1.40 and 1.53 for tenon geometry 1 and 2 which corresponds with the ratio which TET returns which is for both tenon geometries 1.67.

- The ratio of the test results for tenon geometry 1 and 2 are 1.21 and 1.32 for short and long tenon cantilever length which does not correspond with the ratio which TET returns which is for both tenon cantilever lengths 1.04.

- Considering the test results for the two tenon geometries separately and approximating them with TET, the result are two regression lines with slopes of 1.12 and 1.06 for tenon geometry 1 and 2. As the slopes are almost equal to 1.0, TET does approximate the trend of strength increase well.

- No correlation between the angle of the grain with the beam's axis and the test results could be found. The largest angle of the crack with the beam's axis found was 12 degrees and only for 4 of 26 test pieces the angle of the crack with the beam's axis was larger than 5 degrees.

9 CONCLUSIONS AND RECOMMENDATIONS

The strength of the mortise and tenon joint in a wooden mitre gate is much higher than formerly assumed in calculations. Not only experience from practice shows this fact, but also calculations can confirm this. Former assumptions on the force distribution within the gate and joint and the used calculation rules are conservative or even not applicable for this case. In the following more detailed conclusions are drawn on the two main issues researched within this thesis: the force distribution in the mortise and tenon joint and the strength of a hardwood tenon.

CONCLUSIONS RELATING TO THE FORCE DISTRIBUTION

For a wooden mitre gate designed according traditional design the following conclusions relating to the force distribution in the mortise and tenon joint can be made:

- The shear force from the crossbeam is transferred to the rear post for the largest part through the tenon. Friction on the square contact surfaces between the crossbeam and the rear post contribute only little, even when a high friction coefficient is applied.

- A 3D effect is present in the joint whereby a large part of the shear force from the tenon is transferred to the sides of the mortise after which the force is then transferred to the seal strip via the full section of the rear post (Figure 109).

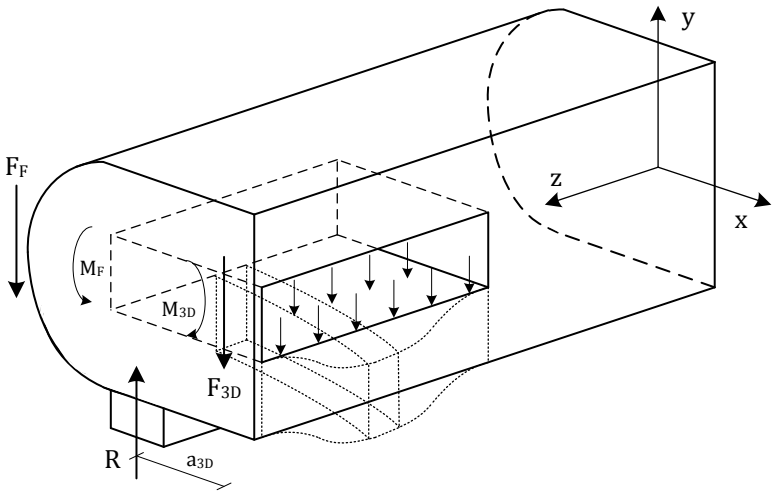

Figure 109: A negative moment in the rear post must develop when (a part of) the shear force from the crossbeam is not transferred from the tenon to the rear post at the line of action of the seal strip support (Note this figure is copied from Figure 48)

- Due to the 3D effect the line of action of the reaction force on the tenon lies closer to the pit of the tenon than the line of action of the reaction force at the seal strip support does.

- The reaction force from the tenon introduces a negative moment in the rear post as its line of action does not coincide with the line of action of the reaction force at the seal strip support. The tenon is clamped into the mortise and at the back of the rear post a frictional force at the concave support counteracts the negative moment.

- The compression force from the crossbeam is transferred through the upper and lower parts of the rear post to the back of the rear post in a straight line. The ratio of the magnitudes of the two internal compression forces are equal to the ratio of sectional surfaces. Therefore, compression stresses' values are equal in both parts.

- Ignoring singular effects near discontinuities within the finite element model's results, appearing stresses throughout the joint satisfy design strength values.

- The following critical areas are identified:
  - behind the mortise high tension stresses have developed as the clamped tenon presses upwards on the rear post.
  - at the lower back side of the rear post high shear stresses develop due to the transfer of compression forces on a concave shape.

  Due to expected 3D effects, the small size of the critical locations and the limited extend in which design strength values are exceeded the critical areas are determined to satisfy strength requirements.

CONCLUSIONS RELATING TO THE STRENGTH OF NOTCHED AND TENONNED BEAMS

For notched and tenonned beams the following conclusions relating to today's standards can be made:

- The Eurocode 5 expression for the strength of notched beams, given in paragraph 6.5.2 from NEN-EN 1995-1-1 (2005), is specifically derived for notched softwood beams as geometry - and material parameters are included in the factor k_n.

- The shear strength parameter $f_{v,k}$, present in the Eurocode 5 expression for the strength of notched beams, is not related to the strength of notched beams. This strength parameter is added to the expression to obtain a practical unity check, useful for engineers in practise.

- The Eurocode 5 expression for the strength of notched beams, paragraph 6.5.2 from NEN-EN 1995-1-1 (2005), is confirmed for notched Spruce beams by tests.

- For notched Azobé beams and tenonned Spruce or Azobé beams conservative results are obtained when the expression for the strength of notched beams from Eurocode 5 is applied. The ratio Eurocode 5 / test results for the 5th percentile values for notched Azobé beams and tenonned Spruce and Azobé beams are respectively 0.33, 0.47 and averagely 0.24 for the tested geometries.

For notched beams the following conclusions relating to their strength can be made:

- The strength of a notched beam is described by the theoretical basic expression for notched beams (TEN) which is derived by Gustafsson (1988):

$$\frac{V_f}{b\alpha d} = \frac{\sqrt{\frac{G_{f,y}}{d}}}{\sqrt{\frac{0.6(\alpha-\alpha^2)}{G_{xy}}} + \beta\sqrt{\frac{6\left(\frac{1}{\alpha}-\alpha^2\right)}{E_x}}}$$

  where V_f [N] is the shear force, b [m] is the width of the beam, $G_{f,y}$ [N/m] is the fracture energy in pure tensile spitting perpendicular to the grain, G_{xy} [N/m^2] is the shear modulus and E_x [N/m^2] is the modulus of elasticity parallel to the grain. In Figure 110 α [-], β [-] and d [m] are indicated.

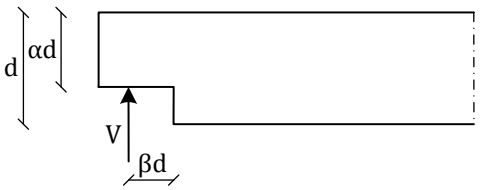

Figure 110: Variables notched beams

- TEN is not applicable to determine the strength of tenonned beams.
- TEN returns good results for notched Spruce beams, the ratio TEN / test results for average values is 1.28. Modelling the fracture energy as is done in the derivation of the Eurocode 5 expression the ratio becomes 1.03. Reformulating the expression and introducing material parameters for softwood the Eurocode 5 expression is obtained.
- Notched Azobé beams are better approximated by TEN than by the Eurocode 5 expression assuming ratios are constant between 5th percentile and average values. The ratio of TEN / test results for average values is 0.76.
- Applying the least squares method to approximate the fracture energy, the ratio of average values TEN / test results can be improved to 1.08. The resulting fracture energy is: $G_{f,y}$ [N/mm] $= 5.36373 \cdot 10^{-4} \cdot \rho$ [kg/m^3] $+ 4.1504 \cdot 10^{-5} \cdot E_0$ [N/mm^2]. Note ρ and E_0 vary little between test pieces, which influences the utility of the relation.

For tenonned beams the following conclusions relating to their strength can be made:

- The strength of a tenonned beam is described by the theoretical basic expression for tenonned beams (TEN) which is derived within this thesis:

$$\frac{V_f}{b\alpha d} = \sqrt{2}\sqrt{\frac{G_{f,y}}{b\alpha^2 d\left(\frac{1.2\left(\frac{1}{b\alpha}-\frac{1}{b}\right)}{G} + 2c\beta d^2 + \frac{12\beta^2\left(\frac{1}{\alpha^3}-1\right)}{Eb}\right)}}$$

where V_f [N] is the shear force, b [m] is the width of the beam, c is a factor which introduces the influence of the tenon geometry on stresses and strains near the transition from tenon to beam, $G_{f,y}$ [N/m] is the fracture energy in pure tensile spitting perpendicular to the grain, G [N/m^2] is the shear modulus and E [N/m^2] is the modulus of elasticity parallel to the grain. In Figure 111 α [-], β [-] and d [m] are indicated.

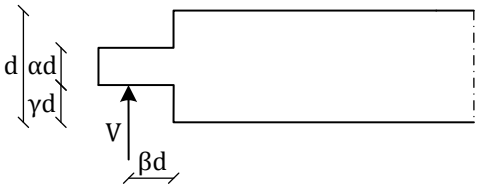

Figure 111: Variables tenonned beam

- Indicative material properties for the strength of a tenonned beam are:
  - Fracture energy
  - Modulus of elasticity
  - Shear modulus

- The factor *c* introduces the influence of the tenon geometry on stresses and strains near the transition from tenon to beam. The factor *c* depends on α, γ, E and G. For a tenon no analytical expression could be obtained.

- For tenonned Spruce beams TET returns better results than TEN. The ratio TEN or TET / test results for average values is improved from 0.60 for TEN to 0.84 for TET.

- For four different test set-ups for tenonned Azobé beams TET returns average values near the test results'. Ratios of TET / test results obtained are 0.67, 0.56, 0.77 and 0.71.

- TET can determine the influence of tenon cantilever length on the strength but the influence of different tenon geometries, present in test results, is not taken into account by TET.

- Considering the test results for the two tenon geometries separately and approximating them with TET, two regression lines are obtained with slopes of 1.12 and 1.06 for tenon geometry 1 and 2. As the slopes are almost equal to 1.0, TET does approximate the trend of strength increase well.

- No correlation between the angle of the grain with the beam's axis and the test results could be found.

RECOMMENDATIONS FOR CONTINUATION OF RESEARCH

The following recommendations are made with relation to the force distribution:

- Statements on the force distribution and appearing stresses should be confirmed for joints designed according traditional design but which have larger thicknesses.

- A three dimensional finite element model of the mortise and tenon joint should be built to confirm or adapt the statements on the 3D effect and accompanying negative moment in the rear post.

- Using a material model within FEM, as developed by Sandhaas (2012), the failure behaviour of tenonned beams could be researched.

- A parameter research should be performed to investigate the influence of dimensions and their ratios with each other to be able to answer the main questions on the force distribution for a broad set of designs.

The following recommendations are made with relation to notch and tenon strength:

- As the Eurocode 5 expression is only valid for notched Spruce beams, firstly the paragraph concerned should mention this fact and secondly expressions valid for notched hardwood beams and tenonned softwood and hardwood beams should be added.

- Performing more tests is an important requirement to confirm the conclusions on the test results on tenonned beams. The test series performed within this research is too small to make definite conclusions. Material, tenon geometry and tenon cantilever length should be varied to research tenon strength.

- It would be valuable when an analytical expression is derived for the factor c, which introduces the influence of the tenon geometry on stresses and strains near the transition from tenon to beam. TET would then theoretically be completely correct.

The background of the factor c for notched beams, given by Gustafsson (1988), should then also be researched to fully describe the phenomenon.

- In addition to the previous recommendation; another option could be to obtain an approximation of the influence of the tenon geometry on stresses and strains near the transition from tenon to beam. E.g. an equivalent fictive additional tenon length could be determined for common combinations of tenon geometry and tenon cantilever length.

- Different failure mechanisms where observed during testing. A theoretical analysis of possible (successive) failure mechanisms should be performed for varying tenon geometry and tenon cantilever length.

- The fracture energy in pure tensile spitting perpendicular to the grain, in pure parallel splitting to the grain and their combination should be researched for hardwoods. This material parameter is not only of much importance for the resistance to splitting of a tenonned beam, but also for many other applications such as for the strength of joints using steel dowels between hardwood parts.

REFERENCES

Literature, standards and websites:

Blass, H. J., & Görlacher, R. (2000). Rolling shear in structural bonded timber elements (pp. 327–337). Stuttgart: Universität Stuttgart.

Ehlbeck, J., & Kromer, M. (1995). Carpentry joints. In H. J. Blass, et al., (Ed.), *Timber Engineering STEP 1* (pp. C12/15 - C12/17). Almere: Centrum Hout.

Engineer's Handbook. (2006). Reference Tables -- Coefficient of Friction. Retrieved 7 July 2012, from http://www.engineershandbook.com/Tables/frictioncoefficients.htm

Forest Products Laboratory. (2010). *Wood handbook - Wood as an engineering material. General Technical Report FPL-GTR-190.* Madison: WI: U.S. Department of Agriculture, Forest Service, Forest Products Laboratory.

Gustafsson, P. J. (1988). *A study of strength of notched beams*. Paper presented at the CIB-W18 Timber Structures, Parksville, Vancouver Island, Canada.

Larsen, H. J., & Gustaffson, P. J. (1990). *The fracture energy of wood in tension perpendicular to the grain. Results from a joint testing project.* Paper presented at the CIB-W18 Timber Structures, Lisbon, Portugal.

Larsen, H. J., & Gustafsson, P. J. (1992). *Annex to paper CIB-W18/25-102-1. Eurocode 5 - Design of notched beams.* Paper presented at the CIB-W18 Timber Structures, Åhus, Sweden.

NEN-EN 338. (2009). Structural timber - Strength classes. Delft: Nederlands Normalisatie-instituut.

NEN-EN 384. (2010). Structural Timber - Determination of characteristic values of mechanical properties and density. Delft: Nederlands Normalisatie-instituut.

NEN-EN 408. (2010). Timber structures - Structural timber and glued laminated timber - determination of some physical and mechanical properties. Delft: Nederlands Normalisatie-instituut.

NEN-EN 1995-1-1. (2005). Eurocode 5 - Design of timber structures - Part 1-1: General - Common rules and rules for buildings. Delft: Nederlands Normalisatie-instituut.

NEN-EN 13183-1. (2002). Moisture content of a piece of sawn timber - Part 1: Determination by oven dry method. Delft: Nederlands Normalisatie-Instituut.

Raadschelders, V. L. (2012). Pen/gat verbinding in regels van sluisdeuren. Spaarndam: Raadschelders Bouwadvies b.v.

Sandhaas, S. (2012). *Mechanical behavior of timber joints with slotted-in steel plates.* Technische Universiteit Delft, Zutphen.

Van de Kuilen, J. W. G., & Blass, H. J. (2005). Mechanical properties of azobé (Lophira alata). *European journal of wood and wood products, 63*(1), 1-10. doi: 10.1007/s00107-004-0533-7

Van de Kuilen, J. W. G., & Leijten, A. J. M. (2002). Schuifsterkte bepaling van zeven houtsoorten voor de toepassing in verkeersbruggen: Report 2001-4/HE43, Sectie Staal- & Houtconstructies, Technische Universiteit Delft.

Van Leusen, B. (1991). *Duikers en sluizen*. Culemborg: Educaboek BV.

Vermeij, D. A. A. N. (2011). *De pen-gat verbinding in houten sluisdeuren: een onderzoek naar de bruikbaarheid van de rekenregels voor nokken uit de eurocode.* BSc Thesis, TU Delft, Delft.

Wijma Kampen B.V. (2012a). Foto's bouw, montage en eindresultaat sluisdeuren. Kampen.

Wijma Kampen B.V. (2012b). Projecten Wijma. Retrieved 31 May 2012, from http://www.wijma.com/producten-en-diensten/projecten/5/1

Wijma Kampen B.V. (2012c). Technische tekeningen sluisdeuren: 'Onbekend' en 'Sluisdeuren Prins Bernard Sluis'. Kampen.

Personal contact:

Banning, M. (2012). *E-mail contact met Rijkswaterstaat Dienst Infrastructuur.*
Hakkers, J. (2012). *Mondeling en schriftelijk contact met Wijma Kampen B.V..*
Plokkaar, H. (2012). S*chriftelijk contact met Wetterskip Fryslân.*
Van Dongen, L (2012). *E-mail contact met Waterschap Brabantse Delta.*

APPENDICES

Appendices accompanying the concept report of the Master's Thesis 'Force distribution and connection strength in timber lock gates'.

J.R. van Otterloo
20 March 2013

TU Delft

[Continuation in separate file]